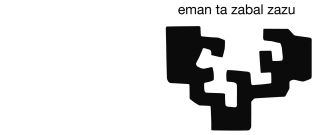

Embedding Quantum Simulators

Roberto Di Candia

Supervisor:

Prof. Enrique Solano

Departamento de Química Física
Facultad de Ciencia y Tecnología
Universidad del País Vasco UPV/EHU

Leioa, June 2015

Any sufficiently advanced technology is indistinguishable from magic.

Arthur C. Clarke

Abstract

Quantum simulations consist in the reproduction of the dynamics of a quantum system on a controllable platform, with the goal of capturing an interesting feature of the considered model. It is broadly believed that the advent of quantum simulators will represent a technological revolution, as they promise to solve several problems which are considered intractable in a classical computer. Although there are strong theoretical bases confirming this claim, several aspects of quantum simulators have still to be studied, in order to faithfully prove their feasibility. Moreover, the general question on which features of the considered models are simulatable is an attractive research topic, whose study would help to define the limits of a quantum simulator.

In this Thesis, we develop several algorithms, which are able to catch relevant properties of the simulated quantum model. The proposed protocols follow a new concept named *embedding quantum simulator*, in which the simulated Schrödinger equation is mapped onto an enlarged Hilbert space in a nontrivial way. Via this embedding, we are able to retrieve, by measuring few observables, quantities that generally require full tomography in order to be evaluated. Moreover, we pay a special attention to the experimental feasibility, defining mappings which are space efficient, and do not require the implementation of challenging Hamiltonians. The presented algorithms are general, and they may be implemented in several quantum platforms, e.g. photonics, trapped ions, circuit QED, among others.

First, we propose a protocol which simulate the dynamics of an embedded Hamiltonian, allowing for the efficient extraction of a class of entanglement monotones. This is done using an embedding that is able to implement unphysical operations, as is the case of complex conjugation. The analysis is accompanied with a study of feasibility in a trapped-ion setup, which can be generalised to other platforms following similar computational models. Second, we propose an algorithm to measure n-time correlation functions of spinorial, fermionic, and bosonic operators, by considerably improving previous versions of the same result. We apply this protocol to the computation of magnetic susceptibilities, as well as to the simulation of Markovian and non-Markovian dissipative processes in a novel way, without the necessity of engineering any bath. All the proposed protocols are designed with a single ancillary qubit, minimising the needed experimental resources.

We believe that embedding quantum simulators have a potential to become a powerful tool in the quantum simulation theory, since they pave the way for improving the flexibility of a quantum simulator in different experimental contexts.

Resumen

En esta Tesis, introducimos el concepto de “Embedding Quantum Simulator” (EQS), un paradigma que nos permite capturar características especificas de un modelo cuántico, cuya medida típicamente supone un desafío en un simulador cuántico estándar (“one-to-one quantum simulator”), donde la dinámica se implementa directamente. El “Embedding Quantum Simulator” consiste en la codificación adecuada de la dinámica simulada en un espacio de Hilbert ampliado. De esta manera, cantidades físicas interesantes están convenientemente mapeadas a observables físicos, superando la necesidad de tomografía cuántica y ganando en términos de eficiencia. Los protocolos propuestos son muy generales, en el sentido que pueden ser implementados en plataformas cuánticas que siguen modelos computacionales típicos. De hecho, una característica del “Embedding Quantum Simulator” es que puede ser aplicado a modelos cuánticos generales, con un pequeño coste en términos de recursos experimentales adicionales. En concreto, hemos diseñado mapeos capaces de capturar la dinámica de medidas de entrelazamiento y para medir las funciones de correlación temporales en sistemas bosónicos y fermiónicos. En el caso de las medidas de entrelazamiento, hemos proporcionado una propuesta de implementación realista en plataformas basadas en iones atrapados, teniendo en cuenta del ruido típico de estos sistemas. A su vez, el protocolo para calcular funciones de correlación ha sido aplicado a la computación de susceptibilidades magnéticas, y en general al calculo de funciones de respuesta lineales y no lineales. Por otra parte, hemos propuesto un nuevo algoritmo para simular sistemas disipativos sin necesidad de hacer ingeniería de baños. Esto nos ha permitido introducir un nuevo concepto de simulador cuántico, donde no queremos crear el estado final bajo una dinámica dada, sino que apuntamos directamente al valor esperado de un observable. Por tanto el EQS es

potencialmente útil en varios campos, como la materia condensada, química cuántica, óptica cuántica, etc.

Esta Tesis contiene un Capitulo introductorio, seguido de cuatro Capítulos. Cada uno contiene ejemplos de aplicaciones del "Embedding Quantum Simulator". Concluimos con una sección de Apéndices, que contiene las demostraciones técnicas de las afirmaciones de la parte principal.

En los Capítulos 2 y 3, hemos estudiado un protocolo para simular la dinámica de una clase de medidas de entrelazamiento en sistemas de qubits. El mapeo propuesto puede ser implementado en una plataforma cuántica añadiendo un solo qubit, y la longitud de interacción de la dinámica se incrementa en uno. Todo el sistema tiene que interactuar con el qubit auxiliar, y eso puede dar lugar a interacciones no locales. Hemos mostrado como resolver este problema, mediante la definición de un qubit lógico a costa de eficiencia espacial, es decir del numero de partículas. Por último, generalizamos los resultados al caso de matrices densidad, discutiendo un algoritmo híbrido clásico-cuántico. Aunque hemos tratado el caso de las medidas de entrelazamiento, es importante mencionar que el protocolo propuesto es capaz de simular operadores antilineales generales, que no se pueden medir en un "one-to-one quantum simulator". En el Capitulo 3, hemos propuesto una de estas ideas implementación en plataformas basadas en iones atrapados. Este Capitulo proporciona también un protocolo para medir un producto tensorial arbitrario de matrices de Pauli, mediante su codificación en un observable de un qubit auxiliar. El análisis vale en general para plataformas cuánticas donde puertas de Mølmer-Sørensen pueden implementarse de manera eficiente, como es el caso de la óptica lineal.

Una futura investigación interesante de estos resultados sería el estudio de las propiedades del mapeo propuesto, con el fin de aumentar la flexibilidad de un simulador cuántico. De hecho, si no estamos limitados a un solo qubit auxiliar, mapeos arbitrarios a espacio de Hilbert más grandes podrían simular otras cantidades no físicamente accesible en un "one-to-one quantum simulator". Otra cuestión es cómo el entorno afecta a los resultados finales de la dinámica

unitaria simulada. Aquí, el “Embedding Quantum Simulator” podría conducir a una mejora de la estabilidad frente al ruido. Estas preguntas se quedan abiertas, y requieren de mas análisis para se bien entendida.

Un experimento de primeros principios basado en estas ideas se está ejecutando en este momento en el grupo del Prof. Andrew White de la Universidad de Queensland (Brisbane, Australia). La implementación es en una plataforma de fotónica, y consiste en realizar medidas de entrelazamiento entre dos qubits que evolucionan bajo una dinámica específica. El experimento se realiza con tres qubits, cada uno de ellos correspondiente a una polarización de la señal óptica que se propaga. Todas las operaciones se implementan con dispositivos estándar de óptica cuántica, por ejemplo divisores de haz, rotaciones de qubits y puertas NOT controladas. Resultados preliminares muestran que la medida de entrelazamiento elegida posee una alta fidelidad, y eso puede llevar a implementaciones similares en otras plataformas basadas en iones atrapados o circuitos superconductores.

En el Capitulo 4, hemos desarrollado un protocolo para computar funciones de correlación temporal de operadores generales en un simulador cuántico. También en este caso, hemos mapeado a una ecuación de Schrödinger en un espacio de Hilbert de dimensión doble. El mapeo tiene la misma estructura que el caso de los operadores antilineales, discutido en los Capitulos 2 y 3, y esto es un indicio que otras aplicaciones no triviales son posibles. Hemos discutido cómo aplicar el protocolo en los casos espinorial, fermionico y bosónicos, mostrando que el método es eficiente en términos de tiempo y de espacio. El algoritmo propuesto no requiere la implementación de Hamiltonianos controlados, que puede ser un problema complicado para la mayoría de modelos interesante desde el punto de vista físico. Este aspecto, en comparación con los protocolos anteriores, conlleva una ganancia enorme a nivel experimental, y es posible que pronto veamos experimentos de primeros principios donde se aplica este protocolo. También en este caso necesitamos que el sistema interactúe a nivel no local con un qubit auxiliar. Este problema se puede resolver de la misma manera que en el Capitulo 1, codificando el qubit auxiliar en una serie de qubits lógicos.

Como aplicación típica, hemos considerado la simulación cuántica de susceptibilidades magnéticas y de funciones de respuesta lineales y no-lineales. Este protocolo es suficientemente simple para permitir una implementación experimental con la tecnología actual o en un futuro próximo, dependiendo de la plataforma.

En el Capitulo 5, hemos estudiado un protocolo original para simular procesos disipativos Markovianos y no Markovianos. La potencia del método propuesto reside en que no requieres ninguna ingeniería de baños. En su lugar, desarrollamos perturbativamente con respecto a los parámetros disipativos, computando de forma efectiva los términos de corrección a la dinámica unitaria. La evaluación de cada termino consiste en medir funciones de correlación temporal del observable que queremos simular y de los operadores de Lindblad. Para lograr esto, aplicamos el protocolo discutido en el Capitulo 4. El método propuesto es una alternativa a las técnicas basadas en descomposición de Trotter y puede ser implementado en sistemas donde el algoritmo del Capitulo 4 puede aplicarse, incluyendo plataformas cuánticas analógicas donde puertas especificas son viables. La principal novedad de este algoritmo consiste en un nuevo tipo de simulador, en el que no estamos interesados en alcanzar el estado final del modelo simulado, sino en el valor esperado del observable que queremos medir. Por esta razón, hemos llamado este tipo de protocolos "Algorithmic Quantum Simulation".

Vale la pena mencionar que con nuestro método podemos simular ecuaciones maestra tipo Lindblad locales en el tiempo, que pueden ser no Markovianas si los parámetros disipativos toman valores negativos durante ciertos intervalos de tiempo. Seria interesante extender resultados a ecuaciones maestras no Markovianas mas generales, que no sean locales en el tiempo. Esto es actualmente objecto de estudio, y puede dar lugar a un avance claro con respecto otros métodos, que no pueden manejar dinámicas no Markovianas de este tipo. Por otra parte, hay posibilidades que nuestro algoritmo obtenga mejores resultados en términos de eficiencia. De hecho, ya se ha demostrado que un simulador cuántico basado en la expansión de Taylor es optimo en términos de

precisión. Este resultado debería ser traslado al caso disipativo, posiblemente considerando modelos computacionales mas generales.

En los Apéndices, hemos proporcionado detalles técnicos de varias afirmaciones del texto principal. En los Apéndices A y B demostramos que el algoritmo de funciones de correlaciones es eficiente, y comparamos nuestro método con los protocolos previos. Los Apendices C, D, E y F están centradas a probar los resultados de la simulación cuántica de procesos disipativos, dando fórmulas explícitas que describen la eficiencia del protocolo. En particular, en el Apéndice F hemos discutido la simulación cuántica de Hamiltonianos no Hermiticos, de la misma manera del caso disipativo.

En definitiva, esta Tesis trata sobre cuán flexible puede ser un simulador cuántico. Nuestro "Embedding Quantum Simulator" tiene como objetivo principal la mejora de la clases de operaciones que un simulador cuántico puede llevar a cabo. Buscar algoritmos que codifican cantidades generales utilizando la teoría cuántica es un campo de investigación atractivo, y en esta Tesis hemos tratado de seguir una línea original en este tema. Sin embargo, hay varias preguntas teóricas que necesitan una respuesta si queremos demostrar la ventaja de un simulador cuántico respecto a uno clásico. Por ejemplo, no está claro si es posible demostrar que el resultado de un simulador cuántico es correcto. Protocolos de certificación pueden ser adaptados de los computadores cuántico universales, donde algoritmos de corrección de errores son teóricamente disponibles. Pero estos métodos funcionan solo para simuladores cuánticos digitales, y pueden llevar a una tremenda perdida de eficiencia en los métodos basados en descomposición de Trotter. Por otro lado, los simuladores cuánticos analógicos necesitan un tratamiento totalmente diferente y novedoso porque, en este caso, el error no se puede digitalizar. Una cuestión relacionada es sobre la eficiencia de los simuladores cuánticos. Las definiciones actuales de eficiencia pueden perder sentido cuando las condiciones experimentales entran en juego. Esto nos puede llevar hacia definiciones novedosas de clases de complejidad, capturando las versiones con ruido de los simuladores analógicos y digitales sin correcciones de errores. Concluyendo, en esta Tesis hemos tratado

el importante cuestión de encontrar el límite de lo que se puede simular en un simulado cuántico. Le comprensión de este problema, junto con una respuesta a las últimas preguntas presentadas, nos ayudaría en la comprensión de los aspectos fundamentales de las simulaciones cuánticas y, en general, de la mecánica cuántica.

Acknowledgements

I would like to thank Prof. Enrique Solano for his guidance through all these years. As advisor, he helped me settle the way to approach academic research and to enter the scientific community. The achievements done in this Thesis are the result of a constant commitment and interest, and I am grateful to him for having pushed me into this direction.

I would also like to thanks all researchers that have been in the QUTIS group, during these years, for the invaluable discussions and the time spent together. Special thanks to my direct QUTIS collaborators, with whom I have regularly discussed about physics, looking for the Truth. In particular, I thank Dr. Daniel Ballester for introducing me in the propagating quantum microwave world; Dr. Jorge Casanova and M.Sc. Julen Pedernales, with whom I have achieved and understood the main results of this Thesis; and, last but not least, Dr. Mikel Sanz, which has guided me in a more abstract side of quantum physics.

I thank all the members of the CCQED European Project, where I have been involved for the first three years of my PhD. This project has allowed me to be in touch and discuss with several scientists from the European elite, and it has been a pleasure to share the experience with other Early Stage Researchers coming from different parts of the world.

I thank the Qubit Group of the Walther Meißner Institute, for having hosted me several times and for the instructive discussions and collaborations. In particular, I would like to thank Prof. Rudolf Gross and Dr. Achim Marx for supervising our several works together, and Dr. Frank Deppe, Dr. Edwin P. Menzel, Dr. Kirill G. Fedorov and M.Sc. Ling Zhong: We have had good time trying to understand both the experimental and theoretical detailes of the propagating quantum microwave experiments.

During my four years of PhD, I have travelled a lot, and I have enjoyed the interaction with several scientists. Among them, I would like to mention Prof. Adolfo del Campo (University of Massachusetts, Boston), for our nice work done together, and Prof. Markus Hennrich, Dr. Thomas Monz and Dr. Philipp Schindler from University of Innsbruck, for the enlightened discussion on the trapped ion implementation of the results of my Thesis. I would like to thank Prof. Yasunobu Nakamura and people from his group for inviting me in their lab at University of Tokyo, and Prof. Franco Nori for the invitation at RIKEN Institute in Tokyo. During my visit in USA, I have profited from conversations with the top scientists of superconducting circuits: Many thanks go to to Prof. Steve Girvin (Yale University), Prof. Andrew Houck and Prof. Hakan

Türeci (Princeton University) for giving me this possibility. I also acknowledge fruitful discussions with Dr. Salvatore Mandrá and Dr. Gian Giacomo Guarreschi during my visit in the group of Prof. Alán Aspuru-Guzik at Harvard University. Special thanks go to Prof. Jens Eisert (Freie Universität Berlin), for sharing with me his very interesting views and ideas on the future of quantum simulations.

My warmest thanks go to my friends and to my family, for their invaluable support given through my academic career. Without it, I probably would not be here writing this.

Contents

List of Figures

List of publications

I) **The results of this Thesis are based on the following articles**

Published Articles

1. R. Di Candia, B. Mejia, H. Castillo, J. S. Pedernales, J. Casanova, and E. Solano
Embedding Quantum Simulators for Quantum Computation of Entanglement
Phys. Rev. Lett. **111**, 240502 (2013).

2. J. S. Pedernales, R. Di Candia, P. Schindler, T. Monz, M. Hennrich, J. Casanova, and E. Solano
Entanglement Measures in Ion-Trap Quantum Simulators without Full Tomography
Phys. Rev. A **90**, 012327 (2014).

3. J. S. Pedernales, R. Di Candia, I. L. Egusquiza, J. Casanova, and E. Solano
Efficient Quantum Algorithm for Computing n-time Correlation Functions
Phys. Rev. Lett. **113**, 020505 (2014).

4. R. Di Candia, J. S. Pedernales, A. del Campo, E. Solano, and J. Casanova
Quantum Simulation of Dissipative Processes without Reservoir Engineering
arXiv:1406.2592 (2014), accepted in Scientific Reports

In Preparation

5. J. C. Loredo, M. de Almeida, R. Di Candia, J. S. Pedernales, J. Casanova, E. Solano, and A. G. White
Embedding Quantum Simulators with Photons

6. U. Alvarez-Rodrigues, R. Di Candia, J. Casanova, M. Sanz, and E. Solano
Algorithmic Quantum Simulation of Non-Markovian Dynamics

II) **Other articles produced during the Thesis period but not included**

Published Articles

7. E. P. Menzel, R. Di Candia, F. Deppe, P. Eder, L. Zhong, M. Ihmig, M. Haeberlein, A. Baust, E. Hoffmann, D. Ballester, K. Inomata, T. Yamamoto, Y. Nakamura, E. Solano, A. Marx, and R. Gross
Path Entanglement of Continuous-Variable Quantum Microwaves
Phys. Rev. Lett. **109**, 250502 (2012).

8. J. S. Pedernales, R. Di Candia, D. Ballester, and E. Solano
Quantum Simulations of Relativistic Quantum Physics in Circuit QED
New J. Phys. **15**, 055008 (2013).

9. L. Zhong, E. P. Menzel, R. Di Candia, P. Eder, M. Ihmig, A. Baust, M. Haeberlein, E. Hoffmann, K. Inomata, T. Yamamoto, Y. Nakamura, E. Solano, F. Deppe, A. Marx, and R. Gross
Squeezing with a Flux-Driven Josephson Parametric Amplifier
New J. Phys. **15**, 125013 (2013).

10. R. Di Candia, E. P. Menzel, L. Zhong, F. Deppe, A. Marx, R. Gross, and E. Solano
Dual-Path Methods for Propagating Quantum Microwaves
New J. Phys. **16**, 015001 (2014).

Submitted Articles

11. M. Sanz, I. L. Egusquiza, R. Di Candia, H. Saberi, L. Lamata, and E. Solano
Entanglement Classification with Matrix Product States
arXiv:1504.07524 (2015), submitted for publication.

12. R. Di Candia, K. G. Fedorov, L. Zhong, S. Felicetti, E. P. Menzel, M. Sanz, F. Deppe, A. Marx, R. Gross, and E. Solano
Quantum Teleportation of Propagating Quantum Microwaves
submitted for publication.

Chapter 1

Introduction

Nature isn't classical, dammit, and if you want to make a simulation of nature, you'd better make it quantum mechanical, and by golly it's a wonderful problem, because it doesn't look so easy.

Richard Feynman

1.1 Introduction to quantum simulations

A *quantum simulation* [1, 2] consists in the reproduction of the dynamics of a quantum system on a controllable platform, called *quantum simulator*, with the goal of capturing an interesting feature of the considered model. Based on the intuition of Richard Feynman [3], who first envisioned that the degrees of freedom of a quantum system may be used as a computation resource, the field of quantum simulations has seen an increasing interest among physicists in recent years. Indeed, quantum simulations are considered the most promising candidates for overpassing the computational capabilities of a classical computer. In fact, it is broadly believed that simulating a quantum system is in a sense "hard". This is tought to be due to the exponential growth of the needed storage with the number of particles, even in the fortunate case in which there exists an efficient classical algorithm solving a particular problem [4]. This means that quantum mechanical models, even if apparently simple, are arduous to analyse without an adequate support. If we want to overcome this problem, a device following itself the quantum mechanical laws is thus a natural choice.

A quantum simulation can be seen as a specific problem that can be solved by a quantum computer, by decomposing the corresponding unitary operation in universal quantum gates. In fact, it has been shown that qubit-based quantum computer can be

used as a universal quantum simulator. However, not any Hamiltonian can be simulated in this way with polynomial resources, and this approach may be not practical. Therefore, one may think about a dedicated machine performing a quantum simulation more efficiently. As this machine is thought to be simpler, it is believed that practical quantum simulations will become a reality well before full-fledged quantum computers. Indeed, we are witnessing several advancements in coherently controlling quantum systems with larger fidelities, which brought to the first proof of principle experiments, e.g. in photonic [5], trapped ions [6], cold atoms [7], and, very recently, in circuit QED [8]. However, there are difficulties in finding a good compromise between scalability and individual control and readout of the system. For instance, typical platforms based on trapped ions and superconducting qubits have achieved a high level of controllability, but they still need to face the problem of an efficient scalability. Research on this line is very active, and it involves also large companies as Google, D-wave, IBM, among several others, indicating that in a near future quantum simulations, and novel quantum technologies in general, will appear very likely in the daily routines of people.

From the theoretical point of view, there are still several questions to answer. During the last years, we have witnessed tremendous progress in finding quantum algorithms for simulating specific dynamics in different quantum platforms. These proposals consist generally in a direct implementation of the dynamics of interest, which implies a one-to-one correspondence between the Hilbert space dimensions of the simulated system and the simulating architecture. Key examples of this approach involve the quantum simulation of black holes in Bose-Einstein condensates [9], relativistic quantum mechanical problems [10, 11] and quantum phase transitions [12] in optical lattices, many-body systems with Rydberg atoms [13], the quantum Rabi model [14] and quantum relativistic dynamics [15] in superconducting circuits. Similar efforts have been invested in trapped-ion technologies for simulating spin models [16–20], relativistic scattering processes [21–26], and interacting fermionic and bosonic theories including quantum chemistry problems [27–30]. However, the one-to-one approach may lead to a lost of flexibility of the quantum simulation. Defining the actual capabilities of a quantum simulator is one of the open theoretical questions, and it will be discussed in this Thesis. Indeed, one of our goals is to merge the concepts of quantum algorithms and quantum simulations, resulting in the ability of catching efficiently nontrivial features of the simulated dynamics.

1.2 Quantum simulation techniques

All kinds of quantum simulations consist in encoding a specific problem, typically quantum, in a Schrödinger equation

$$i\partial_t|\psi(t)\rangle = H|\psi(t)\rangle, \tag{1.1}$$

where $\hbar = 1$, H is the Hamiltonian, and $|\psi(t)\rangle$ is the state of the simulating system at time t. A quantum simulation consists basically in three steps: initialisation of the system at the state $|\psi(0)\rangle$, implementation of the dynamics H, and measurements of one or more observables, depending on the specific encoding. Each of these steps have to be made efficiently, in order to achieve a gain with respect a classical simulation. Let us briefly review each of these steps.

1.2.1 Initialisation

Preparing efficiently an arbitrary quantum state is, in general, not possible. However, efficient algorithms to prepare specific classes of quantum states are already available. Among others, we can mention the generation states encoding the antisymmetric many-particle states of fermions with polynomial resources [31] and realistic quantum states on a lattice [32]. Moreover, ground states of Hamiltonians can be prepared by coupling the system to a thermal bath at zero temperature. There is not a general method and each case has to be tackled individually.

1.2.2 Hamiltonian implementation

There are two ways of implementing an Hamiltonian H: digital and analog methods. Let us consider a Hamiltonian of the kind $H = \sum_i H_i$, where each term H_i may not commute with the others. A digital quantum simulation consists in implementing in small time steps each of the H_i's. This technique is justified by the Trotter decomposition

$$e^{-iHt} = \lim_{\Delta t \to 0} \left(\prod_i e^{-iH_i \Delta t} \right)^{t/\Delta t}. \tag{1.2}$$

This method has been proven to be efficient, in the sense that the time needed to implement the dynamics at time t scales mostly polynomially with the number of particles and with the error done by considering a finite time step Δt. A drawback of this approach is that a good approximation of the target dynamics comes with a small Δt. However, this requires a large number of quantum gates, which may be a cumbersome

problem if we want to implement them in its fall tolerant version [33]. The analogue quantum simulation is aimed to implement the dynamics directly, without any approximation technique. This version of the quantum simulation is useful if one is looking for qualitative answers. For instance, if we want to know whether a phase transition is happening in a particular model, we can retrieve this information even in presence of environmental noise and errors in the control parameters. The drawback of this method is that error correction is not currently available, so quantitative answers are quite hard to be trusted.

1.2.3 Measurement

After bringing the system to the final state $|\psi(t)\rangle$, approximately or not, we need to measure the observables whose results gives us the desired information. Generally, we would like to have a full-knowledge of the final state, in order to process classically all the needed information. However, full tomography techniques scale exponentially with the number of particles, unless we are restricted to a corner of the Hilbert space [34, 35]. This scaling is a problem if one needs to measure many observables, as for quantities requiring full tomography, and it may limit the capability of a quantum simulator. This issue can be solved by a careful encoding of the simulated dynamics, which bring us to the concept of embedding quantum simulator (EQS).

1.3 This Thesis

In this Thesis, we introduce the concept of *embedding quantum simulators* [36], a paradigm allowing to efficiently catch specific features of a quantum model, typically challenging to measure in a one-to-one quantum simulation. It consists in the suitable encoding of a simulated dynamics in the enlarged Hilbert space of an embedding quantum system. In this manner, typical interesting physical quantities are conveniently mapped onto physical observables, overcoming the necessity of full tomography and reducing drastically the experimental requirements. Therefore, the main goal of the embedding quantum simulator is to enhance the class of operations and features that a quantum simulator can carry out.

The proposed protocols are quite general, in the sense that can be implemented in quantum platforms following typical computational models. Indeed, a general feature of embedding quantum simulators is that it can be applied to general quantum models, with a small overhead of experimental resources, see Fig. 1.1. In particular, we have designed the structure of the enlarged Hilbert space able to catch the dynamics of specific

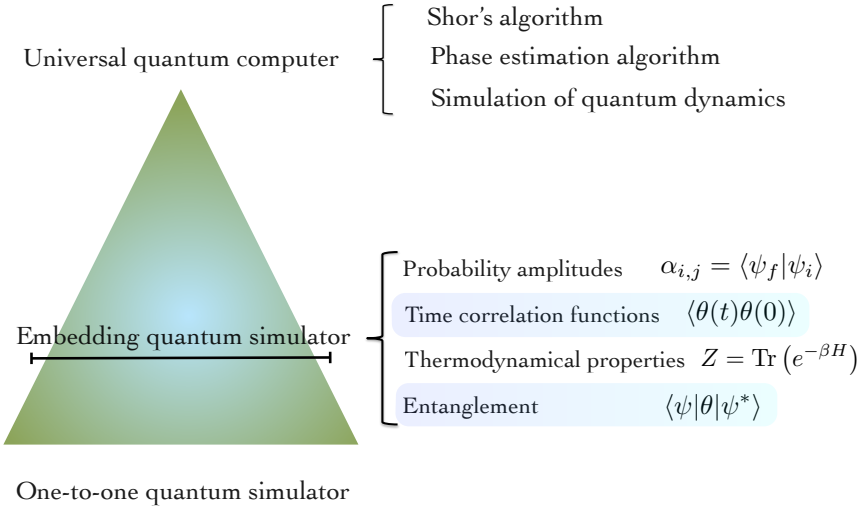

FIGURE 1.1: Complexity hierarchy of quantum simulators: the embedding quantum simulator is placed between the one-to-one and the universal quantum simulator. The embedding quantum simulator increases slightly the experimental complexity, in order to read quantities otherwise unreachable in a one-to-one quantum simulator. However, the complexity of an embedding quantum simulator is far from the one of the universal quantum computer. The highlighted parts correspond to the cases studied in this Thesis.

entanglement monotones, and to measure n-time correlation functions in a bosonic and fermionic systems. Regarding the entanglement monotones case, we have provided with a realistic implementation proposal in trapped ions, taking into account of typical noise sources. Instead, the proposed n-time correlation function protocol has been applied to compute magnetic susceptibilities, and in general to the computation of linear and non-linear response functions. Moreover, we have been able to create a novel algorithm to simulate dissipative systems without the needed of engineering any reservoir. This has allowed us to define the new concept of *algorithmic quantum simulation*, where we are not aimed to create the final state under a given dynamics, but we directly target the approximated expectation value of a given observable. Embedding quantum simulators is a powerful tool in quantum simulation theory, and it is potentially useful in several area as condensed matter, quantum chemistry, quantum optics, etc.

This Thesis contains an introductory Chapter 1, followed by four Chapters, each of them containing examples of physical quantities that can be simulated in an embedding quantum simulator. We conclude with an Appendix part, where we provide with technical proofs of those claims in the main part:

I **Quantum computation of entaglement monotones**

In Chapter 1 of this Thesis, we show how the dynamics of entanglement monotones can be simulated in an embedding quantum simulator. This is done by an appropriate encoding of the initial state, the dynamics and the final measurement onto an equivalent in a doubled Hilbert space. This mapping can be implemented by adding one qubit to the system. This results in a small overhead in the experimental resources, and a huge gain in the flexibility of the quantum simulation. In fact, we have that a wide class of entanglement monotones for spin system can be retrieved via the measurement of few observables instead of full tomography. We also consider the case of mixed states evolving under a unitary dynamics, by considering a classical-quantum hybrid algorithm. In this case the quantum simulation is able to enhance the classical algorithm in the time-evolution step. Finally, we show how to keep the simulating dynamics local by defining the ancillary qubit in a logical way, using the stabilizer formalism.

II **Trapped-ion embedding quantum simulator**

In Chapter 2 of this Thesis, we propose an implementation of the results of Chapter 1 in a trapped-ion setup [37]. Although we put a particular emphasis on trapped ions, the analysis holds for all quantum platforms where Mølmer-Sørensen gates are available. We provide with a statistical analysis taking into account typical noise arising in these setups, i.e. depolarising noise. Moreover, we present numerical examples where the simulating dynamics is implemented with Trotter techniques, and where we show how a typical entanglement monotone as the 3-tangle is simulated. We also provide with a novel measurement protocol, which encodes in a single-ion measurement general Pauli-operator correlations between the spinorial degrees of freedom of the ions.

III **Quantum Algorithm for computing n-time correlation functions**

In Chapter 3 of this Thesis, we propose a novel protocol to compute n-time correlation functions, when the system is evolving under a general dynamics [38]. On the one hand, this kind of quantities, although they can be cast as Hermitian operators, do not correspond to easy observables. On the other hand, n-time correlation functions are relevant for computing susceptibilities, and, in general, the response functions derived in perturbation theory. Moreover, they are interesting for studying Lieb-Robison bounds, which bound the propagation velocity of the information in a general system. It is already known how to measure this kind of quantities for propagating signals. The problem is more challenging if we are interested in the spinorial, fermionic and bosonic degrees of freedom of *massive* particles. Previous proposed protocols relies on operations which are considered

challenging to implement in a realistic experiment. Our method is space efficient and it requires only specific controlled operations, corresponding to the particular observables that we want to measure. Also in this case, the simulated system is embedded in a doubled Hilbert space that can be implemented by adding one qubit. The resulting interaction with the ancillary qubit can be cast to be local, by defining it in a logical way. Here, we have a huge benefit in experimental terms, as in general will happen with an embedding quantum simulator.

IV **Quantum simulation of dissipative processes**

In Chapter 4 of this Thesis, we propose an original method to simulate dissipative systems, Markovian and non-Markovian, without engineering the reservoir [39]. Dissipative systems are modelled through a Lindblad master equation, that is derived by coupling the system with a bath, and tracing out its degrees of freedom. Standard techniques are based on the actual implementation of the bath, or on engineering the resulting effective master equation, and they may not be practical in some cases. Instead, quantum simulation methods based in Trotter techniques are proved to be efficient, but they are not applicable on analogue quantum simulators. Our method is based on the expansion with respect the dissipative parameters, and it is aimed to give the expectation value of the chosen observable at a given time. Each perturbative term is computed using the protocol presented in Chapter 4. In this Chapter, we present the method, and we discuss its efficiency by calculating specific bounds.

V **Appendix**

The Appendix part of this Thesis, containing Appendices A, B, C, D, E, F, we present specific proofs of the claims in the main part of the Thesis. Appendices A and B are aimed to describe the efficiency of the n-time correlation algorithm, and its comparison with previous existing protocols. Instead, the rest of the Appendices are focused on proving the results regarding the quantum simulation of dissipative processes, by giving explicit bounds describing the efficiency of the protocol. Moreover, in Appendix F we give the details of how to apply the protocol to simulate non-Hermitian Hamiltonian in the same fashion as in the dissipative case.

Chapter 2

Quantum computation of entanglement monotones

In this Chapter, we introduce the concept of *embedding quantum simulator* [36], and we apply it to the efficient quantum computation of a class of bipartite and multipartite entanglement monotones. It consists in the suitable encoding of a simulated quantum dynamics in the enlarged Hilbert space of an embedding quantum simulator. In this manner, entanglement monotones are conveniently mapped onto physical observables, overcoming the necessity of full tomography and reducing drastically the experimental requirements. This method is directly applicable to pure states and, assisted by classical algorithms, to the mixed-state case.

2.1 Introduction

Entanglement is considered one of the most remarkable features of quantum mechanics [40, 41], stemming from bipartite or multipartite correlations without classical counterpart. Firstly revealed by Einstein, Podolsky, and Rosen as a possible drawback of quantum theory [42], entanglement was subsequently identified as a fundamental resource for quantum communication [43, 44] and quantum computing purposes [45, 46]. Beyond considering entanglement as a purely theoretical feature, the development of quantum technologies has allowed us to create, manipulate, and detect entangled states in different quantum platforms. Among them, we can mention trapped ions, where eight-qubit W and fourteen-qubit GHZ states have been created [47, 48], circuit QED (cQED) where seven superconducting elements have been entangled [49], superconducting circuits where continuous-variable entanglement has been realized in propagating quantum

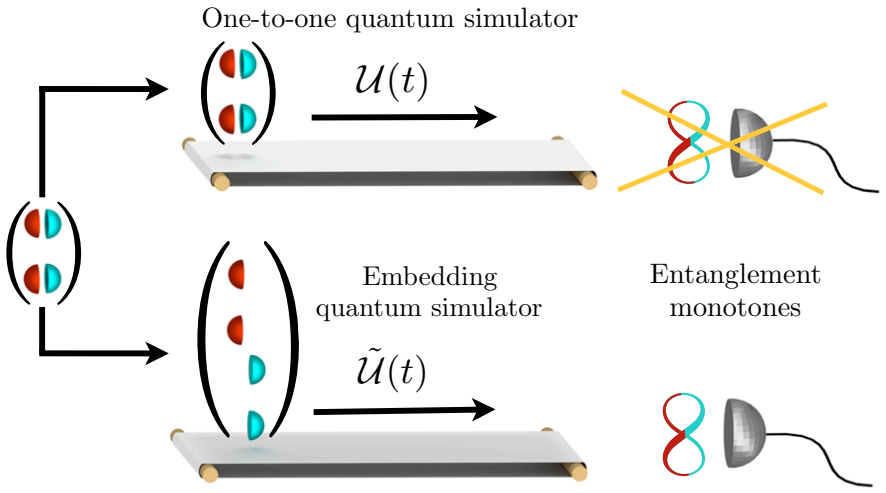

FIGURE 2.1: One-to-one quantum simulator versus embedding quantum simulator. The conveyor belts represent the dynamical evolution of the quantum simulators. The real (red) and imaginary (blue) parts of the simulated wave vector components are split in the embedding quantum simulator, allowing the efficient computation of entanglement monotones.

microwaves [50], and bulk-optic based setups where entanglement between eight photons has been achieved [51].

Quantifying entanglement is considered a particularly difficult task, both from theoretical and experimental viewpoints. In fact, it is challenging to define entanglement measures for an arbitrary number of parties [52, 53]. Moreover, the existing entanglement monotones [54] do not correspond directly to the expectation value of a Hermitian operator [55]. Accordingly, the computation of many entanglement measures, see Ref. [56] for lower bound estimations, requires previously the reconstruction of the full quantum state, which could be a cumbersome problem if the size of the associated Hilbert space is large. If we consider, for instance, an N-qubit system, quantum tomography techniques become already experimentally unfeasible for $N \sim 10$ qubits. This is because the dimension of the Hilbert space grows exponentially with N, and the number of observables needed to reconstruct the quantum state scales as $2^{2N} - 1$.

From a general point of view, a *standard quantum simulation* is meant to be implemented in a *one-to-one quantum simulator* where, for example, a two-level system in the simulated dynamics is directly represented by another two-level system in the simulator. In this Chapter, we show how to compute efficiently a wide class of entanglement monotones [54] in a spin system. This method can be applied at any time of the evolution of a simulated bipartite or multipartite system, with the prior knowledge of the Hamiltonian H and the corresponding initial state $|\psi_0\rangle$. The efficiency of the protocol lies in

the fact that, unlike standard quantum simulations, the evolution of the state $|\psi_0\rangle$ is embedded in an *enlarged Hilbert space* dynamics (see Fig. 2.1). In our case, antilinear operators associated with a certain class of entanglement monotones can be efficiently encoded into physical observables, overcoming the necessity of full state reconstruction. The simulating quantum dynamics, which embeds the desired quantum simulation, may be implemented in different quantum technologies with analog and digital simulation methods.

2.2 Complex conjugation and entanglement monotones

An entanglement monotone is a function of the quantum state, which is zero for all separable states and does not increase on average under local quantum operations and classical communication [54]. There are several functions satisfying these basic properties, as concurrence [55] or three-tangle [60], extracting information about a specific feature of entanglement. For pure states, an entanglement monotone $E(|\psi\rangle)$ can be defined univocally, while the standard approach for mixed states requires the computation of the convex roof

$$E(\rho) = \min_{\{p_i,|\psi_i\rangle\}} \sum_i p_i E(|\psi_i\rangle). \tag{2.1}$$

Here, $\rho = \sum_i p_i |\psi_i\rangle\langle\psi_i|$ is the density matrix describing the system, and the minimum in Eq. (2.1) is taken over all possible pure-state decompositions [41].

A systematic procedure to define entanglement monotones for pure states involves the complex-conjugation operator K [61, 62]. For instance, the concurrence for two-qubit pure states [55] can be written as

$$C(|\psi\rangle) \equiv |\langle\psi|\sigma_y \otimes \sigma_y K|\psi\rangle|. \tag{2.2}$$

Note that $\sigma_y \otimes \sigma_y K$, where $K|\psi\rangle \equiv |\psi^*\rangle$, is an antilinear operator that cannot be associated with a physical observable. In general, we can construct entanglement monotones for N-qubit systems combining three operational building blocks: K, σ_y, and $g^{\mu\nu}\sigma_\mu\sigma_\nu$, with $g^{\mu\nu} = \mathrm{diag}\{-1,1,0,1\}$, $\sigma_0 = \mathbb{I}_2$, $\sigma_1 = \sigma_x$, $\sigma_2 = \sigma_y$, $\sigma_3 = \sigma_z$, where we assume the repeated index summation convention [62]. For a two-qubit system, $N = 2$, we can define $|\langle\psi|\sigma_y \otimes \sigma_y K|\psi\rangle|$ and $|g^{\mu\nu}g^{\lambda\tau}\langle\psi|\sigma_\mu \otimes \sigma_\lambda K|\psi\rangle\langle\psi|\sigma_\nu \otimes \sigma_\tau K|\psi\rangle|$ as entanglement monotones. The first expression corresponds to the concurrence and the second one is a second-order monotone defined in Ref. [62]. For $N = 3$ we have $|g^{\mu\nu}\langle\psi|\sigma_\mu \otimes \sigma_y \otimes \sigma_y K|\psi\rangle\langle\psi|\sigma_\nu \otimes \sigma_y \otimes \sigma_y K|\psi\rangle|$, corresponding to the 3-tangle [60], and so on.

To evaluate the above class of entanglement monotones in a one-to-one quantum simulator, we would need to perform full tomography on the system. This is because terms like $\langle\psi|OK|\psi\rangle \equiv \langle\psi|O|\psi^*\rangle$, with O Hermitian, do not correspond to the expectation value of a physical observable, and they have to be computed classically once each complex component of $|\psi\rangle$ is known. We will explain now how to compute efficiently quantities as $\langle\psi|OK|\psi\rangle$ in our proposed embedding quantum simulator, via the measurement of a reduced number of observables.

Consider a pure quantum state $|\psi\rangle$ of an N-qubit system $\in \mathbb{C}_{2^N}$, whose evolution is governed by the Hamiltonian H via the Schrödinger equation ($\hbar = 1$)

$$(i\partial_t - H)|\psi(t)\rangle = 0. \tag{2.3}$$

The quantum dynamics associated with the Hamiltonian H can be implemented in a one-to-one quantum simulator [1, 3] or, alternatively, it can be encoded in an embedding quantum simulator, where K may become a physical quantum operation [63]. The latter can be achieved according to the following rules.

2.3 Embedding quantum simulation

We define a mapping $\mathcal{M} : \mathbb{C}_{2^N} \to \mathbb{R}_{2^{N+1}}$ in the following way:

$$|\psi\rangle = \begin{pmatrix} \psi^1_{\rm re} + i\psi^1_{\rm im} \\ \psi^2_{\rm re} + i\psi^2_{\rm im} \\ \psi^3_{\rm re} + i\psi^3_{\rm im} \\ \vdots \end{pmatrix} \xrightarrow{\mathcal{M}} |\tilde{\psi}\rangle = \begin{pmatrix} \psi^1_{\rm re} \\ \psi^2_{\rm re} \\ \psi^3_{\rm re} \\ \vdots \\ \psi^1_{\rm im} \\ \psi^2_{\rm im} \\ \psi^3_{\rm im} \\ \vdots \end{pmatrix}. \tag{2.4}$$

Hereafter, we will call $\mathbb{C}_{2^N}$ the *simulated space* and $\mathbb{R}_{2^{N+1}}$ the *simulating space* or the *enlarged space*. We note that the resulting vector $|\tilde{\psi}\rangle$ has only real components (see refs. [57–59] for other developments involving real Hilbert spaces), and that the reverse mapping is $|\psi\rangle = M|\tilde{\psi}\rangle$, with $M = (1\ ,\ i) \otimes \mathbb{I}_{2^N}$. It is noteworthy to mention that, for an unknown initial state, the mapping $\mathcal{M}$ is not physically implementable. However, according to Eq. (2.4), the knowledge of the initial state in the simulated space determines completely the possibility of initializing the state in the enlarged space. Furthermore, it

can be easily checked that the inverse mapping M can always be completed to form a unitary operation.

Now, we can write

$$K|\psi\rangle \equiv |\psi^*\rangle = M|\tilde{\psi}^*\rangle = M(\sigma_z \otimes \mathbb{I}_{2^N})|\tilde{\psi}\rangle \equiv M\tilde{K}|\tilde{\psi}\rangle, \tag{2.5}$$

which, despite its simple aspect, has important consequences. Basically, Eq. (2.5) tells us that while $|\psi\rangle$ and $|\psi^*\rangle$ are connected by the unphysical operation K in the simulated space, the relation between their images in the enlarged space, $|\tilde{\psi}\rangle$ and $|\tilde{\psi}^*\rangle$, is a physical quantum gate $\tilde{K} \equiv (\sigma_z \otimes \mathbb{I}_{2^N})$. In this way, we obtain that

$$\langle\psi|OK|\psi\rangle = \langle\tilde{\psi}|M^\dagger OM(\sigma_z \otimes \mathbb{I}_{2^N})|\tilde{\psi}\rangle, \tag{2.6}$$

where we can prove that

$$M^\dagger OM(\sigma_z \otimes \mathbb{I}_{2^N}) = (\sigma_z - i\sigma_x) \otimes O. \tag{2.7}$$

Note that $M^\dagger OM(\sigma_z \otimes \mathbb{I}_{2^N})$ is a linear combination of Hermitian operators $\sigma_z \otimes O$ and $\sigma_x \otimes O$. Hence, its expectation value can be efficiently computed via the measurement of these two observables in the enlarged space.

So far, we have found a mapping for quantum states and expectation values between the simulated space and the simulating space. If we also want to consider an associated quantum dynamics, we would need to map the Schrödinger equation (2.3) onto another one in the enlarged space. In this sense, we look for a wave equation

$$(i\partial_t - \tilde{H})|\tilde{\psi}(t)\rangle = 0, \tag{2.8}$$

whose solution respects $|\psi(t)\rangle = M|\tilde{\psi}(t)\rangle$ and $|\psi^*(t)\rangle = M\tilde{K}|\tilde{\psi}(t)\rangle$, thereby assuring that the complex conjugate operation can be applied at any time t with the same single qubit gate. If we define in the enlarged space a (Hermitian) Hamiltonian $\tilde{H}$ satisfying $M\tilde{H} = HM$, while applying M to both sides of Eq. (2.8), we arrive to equation $(i\partial_t - H)M|\tilde{\psi}(t)\rangle = 0$. It follows that if $|\tilde{\psi}(t)\rangle$ is the solution of Eq. (2.8) with the initial condition $|\tilde{\psi}_0\rangle$, then $M|\tilde{\psi}(t)\rangle$ is the solution of the original Schrödinger equation (2.3) with the initial condition $M|\tilde{\psi}_0\rangle$. Thus, if $|\psi_0\rangle = M|\tilde{\psi}_0\rangle$, then $|\psi(t)\rangle = M|\tilde{\psi}(t)\rangle$, as required. The Hamiltonian $\tilde{H}$ satisfying $HM = M\tilde{H}$ reads

$$\tilde{H} = \begin{pmatrix} iB & iA \\ -iA & iB \end{pmatrix} \equiv \big[i\mathbb{I}_2 \otimes B - \sigma_y \otimes A\big], \tag{2.9}$$

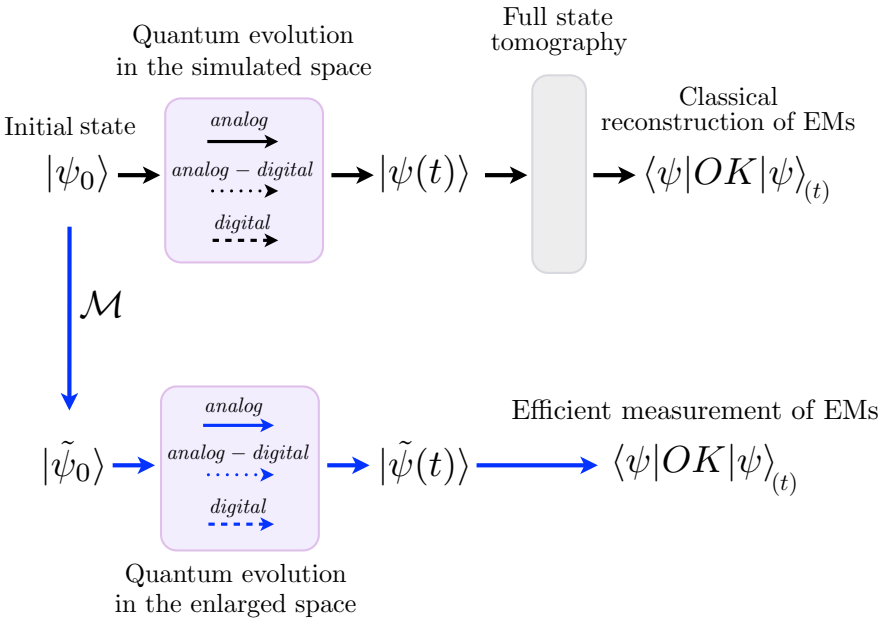

FIGURE 2.2: Protocol for computing entanglement monotones (EMs) using the enlarged space formalism (blue arrows), compared with the usual protocol (black arrows). For any initial state $|\psi_0\rangle$, we can construct throught the mapping $\mathcal{M}$ its image $|\tilde{\psi}_0\rangle$ in the enlarged space. The evolution will be implemented using analog or digital techniques giving rise to the state $|\tilde{\psi}(t)\rangle$. The subsequent measure of a reduced number of observables will provide us with the EMs.

where $H = A + iB$, with $A = A^\dagger$ and $B = -B^\dagger$ real matrices, corresponds to the original Hamiltonian in the simulated space. We note that $\tilde{H}$ is a Hermitian imaginary matrix, e.g. $H = \sigma_x \otimes \sigma_y + \sigma_x \otimes \sigma_z$ is mapped into $\tilde{H} = \mathbb{I}_2 \otimes \sigma_x \otimes \sigma_y - \sigma_y \otimes \sigma_x \otimes \sigma_z$ which is Hermitian and imaginary. In this sense, $|\tilde{\psi}_0\rangle$ with real entries implies the same character for $|\tilde{\psi}(t)\rangle$, given that the Schrödinger equation is a first order differential equation with real coefficients. In this way, the complex-conjugate operator in the enlarged space $\tilde{K} = \sigma_z \otimes \mathbb{I}_{2^N}$ is the same at any time t.

On one hand, the implementation of the dynamics of Eq. (2.8) in a quantum simulator will turn the computation of entanglement monotones into an efficient process, see Fig. 2.2. On the other hand, the evolution associated to Hamiltonian $\tilde{H}$ can be implemented efficiently in different quantum simulator platforms, as is the case of trapped ions or superconducting circuits [20, 64]. We want to point out that, in the most general case, the dynamics of a simulated system involving n-body interactions will require an embedding quantum simulator with $(n+1)$-body couplings. This represents, however, a small overhead of experimental resources. It is noteworthy to mention that the implementation of many-body spin interactions have already been realized experimentally in digital quantum simulators in trapped ions [20]. Concluding, quantum simulations in the enlarged space require the quantum control of *only one additional qubit*.

2.4 Preserving locality in multipartite systems

One important problem with the defined mapping is that the resulting Hamiltonian to implement may be not local. This turns out in a lost in implementability, if we consider that most of the operation that can be cast in a quantum platform are local. This issue can be overcome by carefully implementing the proposed mapping in a slightly alternative way. Indeed, let us consider the simulation of an array of qubits, and let us put an ancilla for each qubit. We can construct a two-dimensional subspace in the Hilbert space defined by all the ancillary qubits, in a way that the final simulating Hamiltonian is local [59]. Let us define the logical qubit

$$|\tilde{0}\rangle = \sqrt{\frac{1}{2^{N-1}}} \sum_{h(y)\,\text{even}} (-1)^{h(y)/2} |y\rangle \tag{2.10}$$

$$|\tilde{1}\rangle = \sqrt{\frac{1}{2^{N-1}}} \sum_{h(y)\,\text{odd}} (-1)^{(h(y)-1)/2} |y\rangle, \tag{2.11}$$

where N is the number of qubits, $y \in \{0,1\}^N$, and $h(y)$ is the number of ones in y. With this definition, it is easy to check that $\sigma_y^k|\tilde{0}\rangle = i|\tilde{1}\rangle$ and $\sigma_y^k|\tilde{1}\rangle = -i|\tilde{0}\rangle$, for all $1 \leq k \leq N$, meaning that applying a σ_y to any of the ancillary qubit is equivalent to apply $\tilde{\sigma}_y$ to the logical qubit. Consequently, in Eq. (2.9) we can change σ_y with a σ_y^k corresponding to an arbitrary ancillary qubit, and this choice can be done in the most convenient way. Lastly, regarding the observable in Eq. (2.7), we notice that measuring in the σ_z basis of the ancillary qubit in the nonlocal case, corresponds to measuring in the σ_z^k basis of each of the ancillary qubit in the local case. This correspondence is achieved by considering 0 as outcomes when we measure an even number of 1's, and 1 when we measure an odd number of 1's. A similar argument holds for σ_x measurement, and this keeps invariant the time efficiency of the method. As a result, locality is recovered at space efficiency cost, i.e. $2N$ qubits instead of $N+1$.

2.5 Efficient computation of entanglement monotones

A general entanglement monotone constructed with K, σ_y, and $g^{\mu\nu}\sigma_\mu\sigma_\nu$, contains at most 3^k terms of the form $\langle\psi|OK|\psi\rangle$, k being the number of times that $g^{\mu\nu}\sigma_\mu\sigma_\nu$ appears. Thus, to evaluate the most general set of entanglement monotones, we need to measure $2 \cdot 3^k$ observables, in contrast with the $2^{2N} - 1$ required for full tomography.

We present now examples showing how our protocol minimizes the required experimental resources.

i) The concurrence.— This two-qubit entanglement monotone defined in Eq. (2.2) is built using σ_y and K, and it can be evaluated with the measurement of 2 observables in the enlarged space, instead of the 15 required for full tomography. Suppose we know $|\psi_0\rangle$ and want to compute $C(|\psi(t)\rangle)$, where $|\psi(t)\rangle \equiv e^{-iHt}|\psi_0\rangle$. We first initialize the quantum simulator with the state $|\tilde{\psi}_0\rangle$ using the mapping of Eq. (2.4). Second, this state evolves according to Eq. (2.8) for a time t. Finally, following Eq. (2.6) with $O = \sigma_y \otimes \sigma_y$, we compute the quantity

$$\langle\tilde{\psi}(t)|\sigma_z \otimes \sigma_y \otimes \sigma_y - i\sigma_x \otimes \sigma_y \otimes \sigma_y|\tilde{\psi}(t)\rangle, \tag{2.12}$$

by measuring the observables $\sigma_z \otimes \sigma_y \otimes \sigma_y$ and $\sigma_x \otimes \sigma_y \otimes \sigma_y$ in the enlarged space.

ii) The 3*-tangle.*— The 3-tangle [60] is a 3-qubit entanglement monotone defined as $\tau_3(|\psi\rangle) = |g^{\mu\nu}\langle\psi|\sigma_\mu\otimes\sigma_y\otimes\sigma_y K|\psi\rangle\langle\psi|\sigma_\nu\otimes\sigma_y\otimes\sigma_y K|\psi\rangle|$. It is built using $g^{\mu\nu}\sigma_\mu\sigma_\nu$ and K, so the computation of τ_3 in the enlarged space requires 6 measurements instead of the 63 needed for full-tomography. The evaluation of $\tau_3(|\psi(t)\rangle)$ can be achieved following the same steps explained in the previous example, but now computing the quantity

$$\begin{aligned}
&\big| - \langle\tilde{\psi}(t)|\sigma_z \otimes \mathbb{I}_2 \otimes \sigma_y \otimes \sigma_y - i\sigma_x \otimes \mathbb{I}_2 \otimes \sigma_y \otimes \sigma_y|\tilde{\psi}(t)\rangle^2 + \\
&+\langle\tilde{\psi}(t)|\sigma_z \otimes \sigma_x \otimes \sigma_y \otimes \sigma_y - i\sigma_x \otimes \sigma_x \otimes \sigma_y \otimes \sigma_y|\tilde{\psi}(t)\rangle^2 + \\
&+\langle\tilde{\psi}(t)|\sigma_z \otimes \sigma_z \otimes \sigma_y \otimes \sigma_y - i\sigma_x \otimes \sigma_z \otimes \sigma_y \otimes \sigma_y|\tilde{\psi}(t)\rangle^2\big|,
\end{aligned} \tag{2.13}$$

with the corresponding measurement of observables in the enlarged space.

iii) N-qubit monotones.— In this case, the simplest entanglement monotone is $|\langle\psi|\sigma_y^{\otimes N}K|\psi\rangle|$ if N is even (expression that is identically zero if N is odd), and $|g^{\mu\nu}\langle\psi|\sigma_\mu\otimes\sigma_y^{\otimes N-1}K|\psi\rangle\langle\psi|\sigma_\nu\otimes\sigma_y^{\otimes N-1}K|\psi\rangle|$ if N is odd. The first entanglement monotone needs 2 measurements, while the second one needs 6. This minimal requirements have to be compared with the $2^{2N}-1$ observables required for full quantum tomography.

iv) The mixed-state case.— Once we have defined $E(|\psi\rangle)$ for the pure state case, we can extend our method to the mixed state case via the convex roof construction, see Eq. (2.1). Such a definition is needed because the possible pure state decompositions of ρ are infinite, and each of them brings a different value of $\sum_i p_i E(|\psi_i\rangle)$. By considering its minimal value, as in Eq. (2.1), we eliminate this ambiguity preserving the properties that define an entanglement monotone. To decide when $E(\rho)$ is zero is called *separability problem*, and it is proven to be NP-hard for states close enough to the border between

the sets of entangled and separable states [65, 66]. However, there exist useful classical algorithms [1] able to find an estimation of $E(\rho)$ up to a finite error [67, 68].

Our approach for mixed states involves a hybrid quantum-classical algorithm, working well in cases in which ρ is approximately a low-rank state. We restrict our study to the case of unitary evolutions acting on mixed-states, given that the inclusion of dissipative processes would require an independent development. Let us consider a state with rank r and assume that the pure state decomposition solving Eq. (2.1) has c additional terms. That is, $k = r + c$, with k being the number of terms in the optimal decomposition, while c is assumed to be low. An algorithm that solves Eq. (2.1) (see for example [67, 68]) evaluates at each step the quantity $\sum_{i=1}^{k} p_i E(|\psi_i\rangle)$ and, depending on the result, it changes $\{p_i, |\psi_i\rangle\}$ in order to find the minimum. Our method consists in inserting an embedded quantum simulation protocol in the evaluation of each $E(|\psi_i\rangle)$, which can be done with few measurements in the enlarged space. We gain in efficiency with respect to full tomography if $k \cdot l \cdot m < 2^{2N} - 1$, where l is the number of iterations of the algorithm and m is the number of measurements to evaluate the specific entanglement monotone. We note that m is a constant that can be low, depending on the choice of E, and, if ρ is low rank, k is a low constant too. With this approach, the performance of the computation of entanglement monotones, $E(\rho)$, can be cast in two parts: while the quantum computation of $\sum_{i=1}^{k} p_i E(|\psi_i\rangle)$ can be efficiently implemented, the subsequent minimization remains a difficult task.

2.6 Outlook

We have presented a paradigm for the efficient computation of a class of entanglement monotones requiring minimal experimental added resources. The proposed framework consists in the adequate embedding of a quantum dynamics in the degrees of freedom of an enlarged-space quantum simulator. In this manner, we have proposed novel concepts merging the fundamentals of quantum computation with those of quantum simulation. This is a first example of how nontrivial mapping between quantum systems, may bring to an excellent gain in efficiency for the quantum computation of physical interesting features, as it is the case of entanglement monotones. It is noteworthy to mention that the presented algorithm can be implement in most of the promising quantum platform, such as trapped ions, cQED, photonics etc.

At this point, some comments are needed. First of all, we have not taken into account the possible decoherence of a quantum platform. During the last years, we

[1] We stress that this is not equivalent to solving the separability problem, as the classical algorithm will always give a strict upper bound of $E(\rho)$.

have witnessed a tremendous improvement in the development of coherently controllable quantum platforms. However, the effects of dissipation and decoherence are still enough strong to simulate a many-body unitary quantum dynamics up to a small error. Robustness of the embedding quantum simulator under decoherence is still an open problem, and it needs further studies. Moreover, the question whether we can simulate more complicated quantities, such as entropies, norm-based entanglement measures, etc., and and the limit of what is simulatable with this approach, are also other open questions, which we try to answer, at least partially, in this Thesis.

Chapter 3

Trapped-ion embedding quantum simulator

In this Chapter, we provide an experimental quantum simulation recipe to efficiently compute entanglement monotones involving antilinear operations, developing the embedding quantum simulator concepts for an ion-trap based quantum platform [37]. The associated quantum algorithm is composed of two steps. First, we embed the N-qubit quantum dynamics of interest into a larger Hilbert space involving only one additional ion qubit and stroboscopic techniques. Second, we extract the corresponding entanglement monotones with a protocol requiring only the measurement of the additional single qubit. It is noteworthy to mention that, for the computation of the associated entanglement monotones, the embedding quantum simulator approach does not require full-state tomography. Finally, we show how to correct experimental imperfections induced by our quantum algorithm.

3.1 Introduction

Trapped-ion systems are among the most promising technologies for quantum computation and quantum simulation protocols [69]. In such systems, fidelities of state preparation, two-qubit gate generation, and qubit detection, exceed values of 99% [70]. With current technology, more than 140 quantum gates including many body interactions have been performed [20]. In this sense, the technology of trapped ions becomes a promising quantum platform to host the described embedded quantum algorithm. In the following analysis, we will rely only on a set of operations involving local rotations and global entangling Mølmer-Sørensen (MS) gates [70, 71]. Therefore, our method is not only applicable to trapped-ion systems. In general, it can be used in any platform

where MS gates, or other long-range entangling interactions, as well as local rotations and qubit decoupling are available. Among such systems, we can mention cQED [64] where an implementation of MS gates has been recently proposed [72], or quantum photonics where MS interactions are available after a decomposition in controlled NOT gates [73].

As already seen in Chapter 2, entanglement monotones are functionals of the quantum state of a system taking zero value when the state is separable, and do not increase under local operations and classical communication (LOCC). For pure states, a class of entanglement monotones can be defined as $E_\Psi(t) = |\langle\Psi|\Theta|\Psi^*\rangle| = |\langle\Psi|\Theta K|\Psi\rangle|$, where Θ is some Hermitian operator, and K is the complex-conjugation operation [62]; see, for example, the case of the two-qubit concurrence [74] where $\Theta = \sigma_y \otimes \sigma_y$. As a consequence, $E_\Psi(t)$ does not correspond to the the expectation value of a physical observable, thus it cannot be directly measured. Let us assume that we have an N-qubit system, represented by the wavefunction ψ, evolving under a Hamiltonian H. As described above, this system will be embedded in a larger one, requiring only one additional qubit, in such a way that K becomes a physical operation [25]. Let us briefly summarise the embedding procedure [36]. This is based on the following mapping

$$\begin{aligned} \psi \qquad &\longrightarrow \quad \Psi = \tfrac{1}{2}\begin{pmatrix} \psi + \psi^* \\ i\psi - i\psi^* \end{pmatrix}, \\ H = A + iB \quad &\longrightarrow \quad \tilde{H} = \left[i\mathbb{I}_2 \otimes B - \sigma^y \otimes A\right]. \end{aligned} \tag{3.1}$$

Here, $\psi \in \mathbb{C}^{2^N}$ and $H \in \mathbb{C}^{2^N} \times \mathbb{C}^{2^N}$ are the wavefunction and Hamiltonian (with A and B its real and imaginary parts) governing the dynamics of the N-qubit system in the simulated space, while Ψ and $\tilde{H}$ correspond to their images in the enlarged Hilbert space, these having a dimension of 2^{N+1} and $2^{N+1} \times 2^{N+1}$ respectively. The matrix $M = (1\ ,\ i) \otimes \mathbb{I}_{2^N}$, projects the states of the embedding quantum simulator onto the simulated space through the identity $\psi(t) = M\Psi(t)$. For example, for a single-qubit case where $\psi(t) = (\alpha(t), \beta(t))^T$, T being the transpose operation, the corresponding enlarged-wavefunction is $\Psi(t) = (\alpha_r(t), \beta_r(t), \alpha_i(t), \beta_i(t))^T$, with $\alpha_{r,i}(t)$, $\beta_{r,i}(t)$ the real and imaginary parts of $\alpha(t)$ and $\beta(t)$ respectively, and the M matrix is $M = \begin{pmatrix} 1 & 0 & i & 0 \\ 0 & 1 & 0 & i \end{pmatrix}$. Note that due to the property $M\tilde{H} = HM$, the previous relation is valid at any time t as long as the embedding quantum simulator is initialized such that $\psi(0) = M\Psi(0)$. Although this mapping from $\psi(0)$ to $\Psi(0)$ is nonphysical, the initial state $\Psi(0)$ can be directly generated from the ground state of the simulator. In the embedding quantum simulator, the physical quantum gate $\sigma^z \otimes \mathbb{I}_{2^N}$ applied to Ψ produces a quantum state corresponding to ψ^* in the simulated space, i.e. $M(\sigma_z \otimes \mathbb{I}_{2^N})\Psi(t) = \psi^*(t)$. This will

allow us to efficiently compute correlations between ψ and ψ^* in terms of standard expectation values in the enlarged space as follows

$$\begin{aligned}\langle\psi|\Theta|\psi^*\rangle &= \langle\Psi|M^\dagger\Theta M(\sigma^z\otimes\mathbb{I}_{2^N})|\Psi\rangle \\ &= \langle\Psi|(\sigma^z - i\sigma^x)\otimes\Theta|\Psi\rangle, \end{aligned} \tag{3.2}$$

with Θ being a Hermitian operator. In this way, the expectation value of the antilinear operator ΘK in the simulated space can be evaluated via the measurement of $\sigma^z\otimes\Theta$ and $\sigma^x\otimes\Theta$ in the enlarged Hilbert space.

3.2 Trapped-ion implementation

The embedded dynamics of an interacting-qubit system is governed by the Schrödinger equation $i\hbar\partial_t\Psi = \tilde{H}\Psi$, where the Hamiltonian $\tilde{H}$ is $\tilde{H} = \sum_j \tilde{H}_j$ and each $\tilde{H}_j$ operator corresponds to a tensorial product of Pauli matrices. In this way, an embedded N-qubit dynamics can be implemented in two steps. First, we decompose the evolution operator using standard Trotter techniques [1, 75],

$$U_t = e^{-\frac{i}{\hbar}\sum_j \tilde{H}_j t} \approx \left(\Pi_j e^{-i\tilde{H}_j t/n}\right)^n, \tag{3.3}$$

where n is the number of Trotter steps. Second, each exponential $e^{-\frac{i}{\hbar}\tilde{H}_j t/n}$ can be implemented with a sequence of two Mølmer-Sørensen gates [71] and a single qubit rotation between them [28, 76]. These three quantum gates generate the evolution operator

$$e^{i\varphi\sigma_1^z\otimes\sigma_2^x\otimes\sigma_3^x\ldots\otimes\sigma_N^x}, \tag{3.4}$$

where $\varphi = gt$, g being the coupling constant of the single qubit rotation [76]. In Eq. (3.4), subsequent local rotations will produce any combination of Pauli matrices. As it is the case of quantum models involving Pauli operators, there exist different representations of the same dynamics. For example, the physically equivalent Ising Hamiltonians, $H_1 = \omega_1\sigma_1^x + \omega_2\sigma_2^x + g\sigma_1^y\otimes\sigma_2^y$ and $H_2 = \omega_1\sigma_1^y + \omega_2\sigma_2^y + g\sigma_1^x\otimes\sigma_2^x$, are mapped onto the enlarged space as $\tilde{H}_1 = -\omega_1\sigma_0^y\otimes\sigma_1^x - \omega_2\sigma_0^y\otimes\sigma_2^x - g\sigma_0^y\otimes\sigma_1^y\otimes\sigma_2^y$ and $\tilde{H}_2 = \omega_1\sigma_1^y + \omega_2\sigma_2^y - g\sigma_0^y\otimes\sigma_1^x\otimes\sigma_2^x$. In principle, both Hamiltonians $\tilde{H}_1$ and $\tilde{H}_2$ can be implemented in trapped ions. However, while $\tilde{H}_1$ requires two- and three-body interactions, $\tilde{H}_2$ is implementable with a collective rotation applied to the ions 1 and 2 for the implementation of the free-energy terms, and MS gates for the interaction term. In this sense, $\tilde{H}_2$ requires less experimental resources for the implementation of the embedding quantum simulator

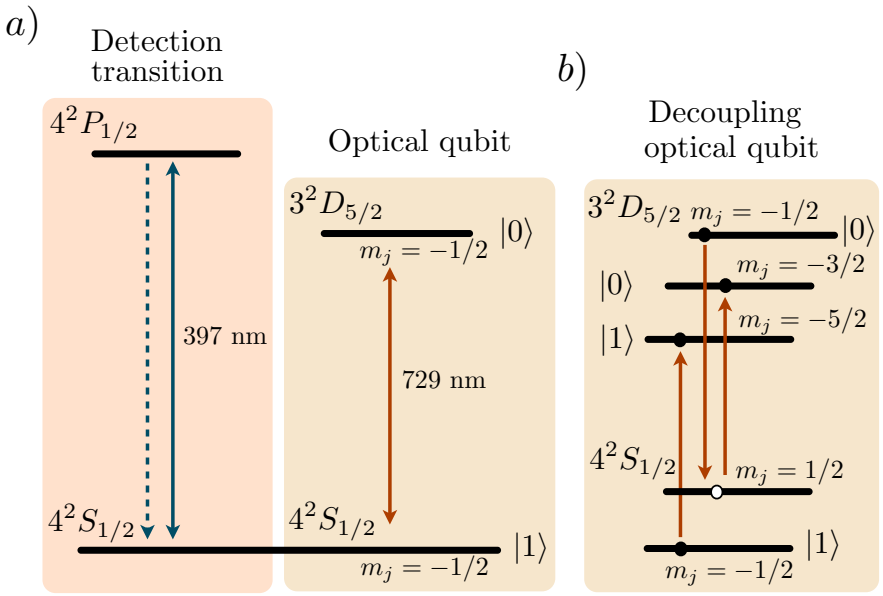

FIGURE 3.1: a) Level scheme of $^{40}Ca^+$ ions. The standard optical qubit is encoded in the $m_j = -1/2$ substates of the $3D_{5/2}$ and $4S_{1/2}$ states. The measurement is performed via fluorescence detection exciting the $4^2S_{1/2} \leftrightarrow 4^2P_{1/2}$ transition. b) The qubit can be spectroscopically decoupled from the evolution by shelving the information in the $m_j = -3/2, -5/2$ substates of the $3D_{5/2}$ state.

dynamics. Therefore, a suitable choice of the system representation can considerably enhance the performance of the simulator.

3.3 Measurement protocol

We want to measure correlations of the form appearing in Eq. (3.2), with Θ a linear combination of tensorial products of Pauli matrices and identity operators. This information can be encoded in the expectation value $\langle\sigma_a^\alpha\rangle$ of one of the ions in the chain after performing two evolutions of the form of Eq. (3.4). Let us consider the operators $U_1 = e^{-i\varphi_1(\sigma_1^i\otimes\sigma_2^j\otimes\sigma_3^k\ldots)}$ and $U_2 = e^{-i\varphi_2(\sigma_1^o\otimes\sigma_2^p\otimes\sigma_3^q\ldots)}$ and choose the Pauli matrices $\sigma_1^i, \sigma_2^j, \ldots$ and $\sigma_1^o, \sigma_2^p, \ldots$ such that U_1 and U_2 commute and both anticommute with the Pauli operator to be measured σ_a^α. In this manner, we have that

$$\begin{aligned}\langle\sigma_a^\alpha\rangle_{\varphi_1,\varphi_2=\frac{\pi}{4}} &= \langle U_1^\dagger(\frac{\pi}{4})U_2^\dagger(\frac{\pi}{4})\ \sigma_a^\alpha\ U_1(\frac{\pi}{4})U_2(\frac{\pi}{4})\rangle \\ &= \langle\sigma_1^i\sigma_1^o\otimes\sigma_2^j\sigma_2^p\otimes\ldots\otimes\sigma_a^\alpha\sigma_a^l\sigma_a^r\ldots\rangle. \end{aligned} \tag{3.5}$$

Then, a suitable choice of Pauli matrices will produce the desired correlation. Note that this protocol always results in a correlation of an odd number of Pauli matrices. In

order to access a correlation of an even number of qubits, we have to measure a two-qubit correlation $\sigma_a^\alpha \otimes \sigma_b^\beta$ instead of just σ_a^α. For the particular case of correlations of only Pauli matrices and no identity operators, evolution U_2 is not needed and no distinction between odd and even correlations has to be done. For instance, if one is interested in an even correlation like $\sigma_1^y \otimes \sigma_2^x \otimes \sigma_3^x \otimes \sigma_4^x \otimes \mathbb{I}_5 \otimes ... \otimes \mathbb{I}_N$, N being the number of ions of the system, then one would have to measure observable $\sigma_1^y \otimes \sigma_2^x$ after the evolutions $U_1 = e^{-i(\sigma_1^x \otimes \sigma_2^y \otimes \sigma_3^y \otimes \sigma_4^y \otimes \sigma_5^y \otimes ... \otimes \sigma_j^y \otimes ...)\varphi}$ and $U_2 = e^{-i(\sigma_1^x \otimes \sigma_2^y \otimes \sigma_3^z \otimes \sigma_4^z \otimes \sigma_5^y \otimes ... \otimes \sigma_j^y \otimes ...)\varphi}$. However, for the particular case of $N = 4$ a single evolution $U_1 = e^{-i(\sigma_1^x \otimes \sigma_2^x \otimes \sigma_3^x \otimes \sigma_4^x)\varphi}$ and subsequent measurement of $\langle \sigma_1^z \rangle$ is enough. Note that all the gates in the protocol, as they are of the type of Eq. (3.4), are implementable with single qubit and MS gates.

3.4 Examples

Consider the Ising Hamiltonian for two spins, $H = \hbar\omega_1\sigma_1^y + \omega_2\sigma_2^y + g\sigma_1^x \otimes \sigma_2^x$ whose image in the enlarged space corresponds to $\tilde{H} = \omega_1\sigma_1^y + \omega_2\sigma_2^y - g\sigma_0^y \otimes \sigma_1^x \otimes \sigma_1^x$. The evolution operator associated to this Hamiltonian can be implemented using the Trotter method from Eq. (3.3) with $(\tilde{H}_1, \tilde{H}_2, \tilde{H}_3) = (\omega_1\sigma_1^y, \omega_2\sigma_2^y, -g\sigma_0^y \otimes \sigma_1^x \otimes \sigma_2^x)$. While evolutions $e^{-\frac{i}{\hbar}\tilde{H}_1 t/n}$ and $e^{-\frac{i}{\hbar}\tilde{H}_2 t/n}$ can be implemented with single ion rotations, the evolution $e^{-\frac{i}{\hbar}\tilde{H}_3 t/n}$, which is of the kind described in Eq. (3.4), is implemented with two MS gates and a single ion rotation. This simple case allows us to compute directly quantities such as the concurrence measuring $\langle \sigma_0^z \sigma_1^y \sigma_2^y \rangle$ and $\langle \sigma_0^x \sigma_1^y \sigma_2^y \rangle$. According to the measurement method introduced above, to access these correlations we first evolve the system under the gate $U = e^{-i(\sigma_0^y \otimes \sigma_1^y \otimes \sigma_2^y)\varphi}$ for a time such that $\varphi = \frac{\pi}{2}$, and then measure $\langle \sigma_0^x \rangle$ for the first correlation and $\langle \sigma_0^z \rangle$ for the second one.

Based on the two-qubit example, one can think of implementing a three-qubit model as $H_{\text{GHZ}} = \omega_1\sigma_1^y + \omega_2\sigma_2^y + \omega_3\sigma_3^y + g\sigma_1^x \otimes \sigma_2^x \otimes \sigma_3^x$, which in the enlarged space corresponds to

$$\tilde{H}_{\text{GHZ}} = \omega_1\sigma_1^y + \omega_2\sigma_2^y + \omega_3\sigma_3^y - g\sigma_0^y \otimes \sigma_1^x \otimes \sigma_2^x \otimes \sigma_3^x. \tag{3.6}$$

This evolution results in GHZ kind states, which can be readily detected using the 3-tangle τ_3 [60]. This is an entanglement monotone of the general class of Eq. (3.2) that can be computed in the enlarged space by measuring $\big| - \langle\tilde{\psi}(t)|\sigma_z \otimes \mathbb{I}_2 \otimes \sigma_y \otimes \sigma_y - i\sigma_x \otimes \mathbb{I}_2 \otimes \sigma_y \otimes \sigma_y|\tilde{\psi}(t)\rangle^2 + \langle\tilde{\psi}(t)|\sigma_z \otimes \sigma_x \otimes \sigma_y \otimes \sigma_y - i\sigma_x \otimes \sigma_x \otimes \sigma_y \otimes \sigma_y|\tilde{\psi}(t)\rangle^2 + \langle\tilde{\psi}(t)|\sigma_z \otimes \sigma_z \otimes \sigma_y \otimes \sigma_y - i\sigma_x \otimes \sigma_z \otimes \sigma_y \otimes \sigma_y|\tilde{\psi}(t)\rangle^2\big|$. More complex Hamiltonians with interactions involving only three of the four particles can also be implemented. In this case, the required entangling operations acting only on a part of the entire register can be realized with the aid of splitting the MS operations into smaller parts and inserting refocusing pulses between them as shown in Ref. [76]. An alternative method is to

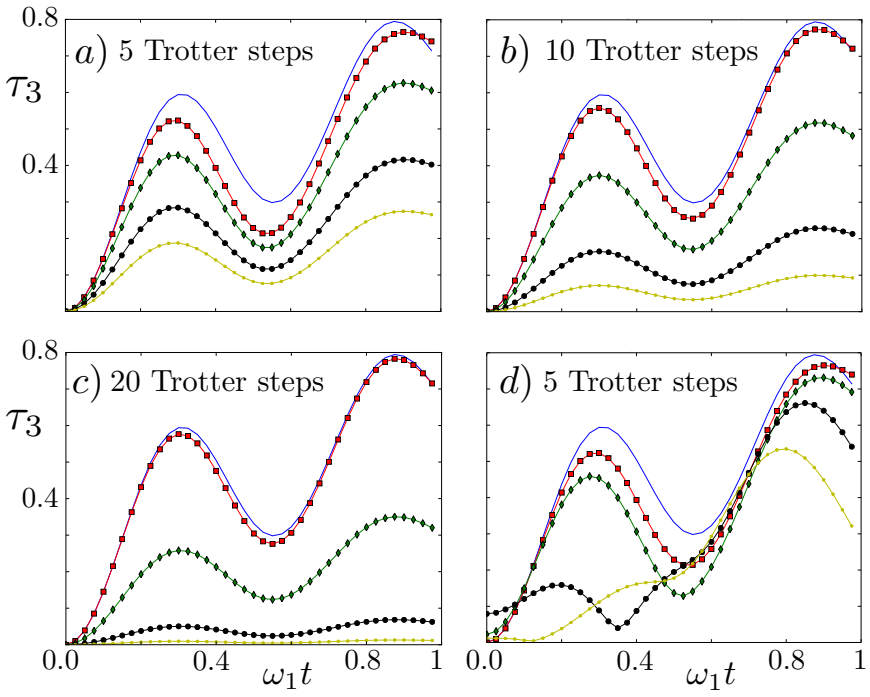

FIGURE 3.2: Numerical simulation of the 3-tangle evolving under Hamiltonian in Eq. (3.6) and assuming different error sources. In all the plots, the blue line shows the ideal evolution. In a), b), c) depolarizing noise is considered, with N=5,10 and 20 Trotter steps, respectively. Gate fidelities are $\epsilon = 1, 0.99$, 0.97, and 0.95 marked by red rectangles, green diamonds, black circles and yellow dots, respectively. In d) crosstalk between ions is added with strength $\Delta_0 = 0, 0.01$, 0.03, and 0.05 marked by red rectangles, green diamonds, black circles and yellow dots, respectively. All the simulations in d) were performed with 5 Trotter steps. In all the plots, we have used $\omega_1 = \omega_2 = \omega_3 = g/2 = 1$.

decouple the spectator ions from the laser light by shelving the quantum information into additional Zeeman substates of the ions as sketched in Fig. 3.1 for $^{40}Ca^{+}$ ions. This procedure has been successfully demonstrated in Ref. [77]. For systems composed of a larger number of qubits, for example $N > 10$, our method yields nontrivial results given that the standard computation of entanglement monotones of the kind $\langle\psi(t)|\Theta|\psi(t)^*\rangle$ requires the measurement of a number of observables that grows exponentially with N. For example, in the case of $\Theta = \sigma^y \otimes \sigma^y \otimes \cdots \otimes \sigma^y$ [62] our method requires the evaluation of 2 observables while the standard procedure based on state tomography requires, in general, the measurement of $2^{2N} - 1$ observables.

3.5 Experimental considerations

A crucial issue of a quantum simulation algorithm is its susceptibility to experimental imperfections. In order to investigate the deviations with respect to the ideal case, the system dynamics needs to be described by completely positive maps instead of unitary dynamics. Such a map is defined by the process matrix χ acting on a density operator ρ as follows: $\rho \to \sum_{i,j} \chi_{i,j} \sigma^i \rho \sigma^j$, where σ^i are the Pauli matrices spanning a basis of the operator space. In complex algorithms, errors can be modeled by adding a depolarizing process with a probability $1-\varepsilon$ to the ideal process χ^{id}

$$\rho \to \varepsilon \sum_{i,j} \chi^{id}_{i,j} \sigma^i \rho \sigma^j + (1-\varepsilon)\frac{\mathbb{I}}{2^N}. \tag{3.7}$$

In order to perform a numerical simulation including this error model, it is required to decompose the quantum simulation into an implementable gate sequence. Numerical simulations of the Hamiltonian in Eq. (3.6), including realistic values gate fidelity $\varepsilon = \{1, 0.99, 0.97, 0.95\}$ and for $\{5, 10, 20\}$ Trotter steps, are shown in Figs. 3.2 a), b), and c). Naturally, this analysis is only valid if the noise in the real system is close to depolarizing noise. However, recent analysis of entangling operations indicates that this noise model is accurate [70, 78]. According to Eq. (3.7), after n gate operations, we show that

$$\langle O \rangle_{\mathcal{E}_{id}(\rho)} = \frac{\langle O \rangle_{\mathcal{E}(\rho)}}{\varepsilon^n} - \frac{1-\varepsilon^n}{\varepsilon^n} \mathrm{Tr}\,(O), \tag{3.8}$$

where $\langle O \rangle_{\mathcal{E}_{id}(\rho)}$ corresponds to the ideal expectation value in the absence of decoherence, and $\langle O \rangle_{\mathcal{E}(\rho)}$ is the observable measured in the experiment. Given that we are working with observables composed of tensorial products of Pauli operators $\sigma_0^y \otimes \sigma_1^x ...$ with $\mathrm{Tr}\,(O) = 0$, Eq. (3.8) will simplify to $\langle O \rangle_{\mathcal{E}_{id}(\rho)} = \frac{\langle O \rangle_{\mathcal{E}(\rho)}}{\varepsilon^n}$. In order to retrieve with uncertainty k the expected value of an operator O, the experiment will need to be repeated $N_{emb} = \left(\frac{1}{k\epsilon^n}\right)^2$ times. Here, we have used $k \equiv \sigma^{\mathcal{E}(\rho)}_{\langle O \rangle} = \sigma^{\mathcal{E}(\rho)}_{O}/\sqrt{N}$ (for large N), and that the relation between the standard deviations of the ideal and experimental expectation values is $\sigma^{\mathcal{E}(\rho)}_{O} = \sigma^{\mathcal{E}_{id}(\rho)}_{O}/\varepsilon^n$. If we compare N_{emb} with the required number of repetitions to measure the same entanglement monotone to the same accuracy k in a one-to-one quantum simulator, $N_{oto} = 3^{N_{qubits}} \left(\frac{1}{k\delta^n}\right)^2$, we have

$$\frac{N_{emb}}{N_{oto}} = l \left(\frac{\delta}{\sqrt{3}\varepsilon}\right)^{2N_{qubit}}. \tag{3.9}$$

Here, l is the number of observables corresponding to a given entanglement monotone in the enlarged space, and δ is the gate fidelity in the one-to-one approach. We are also asuming that full state tomography of N_{qubits} qubits requires $3^{N_{qubit}}$ measurement settings for experiments exploiting single-qubit discrimination during the measurement

process [79]. Additionally, we assume the one-to-one quantum simulator to work under the same error model but with δ fidelity per gate. Finally, we expect that the number of gates grows linearly with the number of qubits, that is $n \sim N_{qubit}$, which is a fair assumption for a nearest-neighbour interaction model. In general, we can assume that δ is always bigger than ε as the embedding quantum simulator requires an additional qubit which naturally could increase the gate error rate. However, for realistic values of ε and δ, e.g. $\varepsilon = 0.97$ and $\delta = 0.98$ one can prove that $\frac{N_{emb}}{N_{oto}} \ll 1$. This condition is always fulfilled for large systems if $\frac{\delta}{\sqrt{3}\varepsilon} < 1$. The latter is a reasonable assumption given that in any quantum platform it is expected $\delta \approx \epsilon$ when the number of qubits grows, i.e. we expect the same gate fidelity for N and $N+1$ qubit systems when N is large. Note that this analysis assumes that the same amount of Trotter steps is required for the embedded and the one-to-one simulator. This is a realistic assumption if one considers the relation between H and $\tilde{H}$ in Eq. (3.1). A second type of imperfections are undesired unitary operations due to imperfect calibration of the applied gates or due to crosstalk between neighbouring qubits. This crosstalk occurs when performing operations on a single ion due to imperfect single site illumination [70]. Thus the operation $s_j^z(\theta) = \exp(-i\,\theta\,\sigma_j^z/2)$ needs to be written as $s_j^z(\theta) = \exp(-i\,\sum_k \epsilon_{k,j}\,\theta\sigma_k^z/2)$ where the crosstalk is characterized by the matrix Δ. For this analysis, we assume that the crosstalk affects only the nearest neighbours with strength Δ_0 leading to a matrix $\Delta = \delta_{k,j} + \Delta_0\,\delta_{k\pm1,j}$. In Fig. 3.2 d) simulations including crosstalk are shown. It can be seen, that simulations with increasing crosstalk show qualitatively different behavior of the 3-tangle, as in the simulation for $\Delta_0 = 0.05$ (yellow line) where the entire dynamics is distorted. This effect was not observed in the simulations including depolarizing noise and, therefore, we identify unitary crosstalk as a critical error in the embedding quantum simulator. It should be noted that, if accurately characterized, the described crosstalk can be completely compensated experimentally [70].

3.6 Outlook

We have discussed an embedded quantum algorithm for trapped-ion systems to efficiently compute entanglement monotones for N interacting qubits at any time of their evolution and without the need for full state tomography. Furthermore, we showed that the involved decoherence effects can be corrected if they are well characterised. We have given a first proof of principle theoretical experiment to predict how the method would perform in a real experiment. Although we have discussed the trapped-ion scheme, this analysis holds for whatever platforms in which Mølmer-Sørensen gates, or its decomposition in simpler gates, are available, making this analysis rather general. Experimental

verification of the embedding quantum simulator for entanglement monotones would open the way for studying quantum correlations in generic many-body systems.

Chapter 4

Quantum algorithm for computing n-time correlation functions

In this Chapter, we study an efficient quantum algorithm for computing general n-time correlation functions of an arbitrary quantum system, requiring only an initially added probe and control qubit [38]. Our method is applicable to a general class of interacting spinorial, bosonic, and fermionic systems, and it does not require the implementation of the controlled version of the evolution Hamiltonian. We provide examples of this protocol in the frame of the linear response theory, where n-time correlation functions are needed.

4.1 Introduction

According to quantum theory, all information about a system, its stationary states and its evolution, is encoded in the Hamiltonian. Nonetheless, for most cases, the extraction of this information may not be straightforward [80, 81]. Therefore, alternative strategies are needed to identify and obtain measurable quantities that characterize the relevant physical information [36, 37]. A case of particular importance is given by response functions and susceptibilities, which in the linear response theory are computed in terms of two-time correlation functions [82–84]. For example, the knowledge of two-time correlation functions of the form $\langle\Psi|A(t)B(0)|\Psi\rangle$, stemming from perturbation theory, provides us with a microscopic derivation of useful quantities such as conductivity and magnetization [85]. The reconstruction of time-correlation functions, however, need not be trivial at all, and could profit from quantum algorithm and simulation protocols

for their determination. The computation of time correlation functions for propagating signals is at the heart of quantum optical methods [86], including the case of propagating quantum microwaves [50, 87, 88]. However, these methods are not necessarily easy to export to the case of spinorial, fermionic and bosonic degrees of freedom of massive particles. In this sense, recent methods have been proposed for the case of two-time correlation functions associated to specific dynamics in optical lattices [89], as well as in setups where post-selection and cloning methods are available [90]. On the other hand, in quantum computer science the SWAP test [91] (see Appendix B) represents a standard way to access n-time correlation functions if a quantum register is available that is, at least, able to store two copies of a state, and to perform a generalized-controlled swap gate [92]. However, this could be demanding if the system of interest is large, for example, for an N-qubit system the SWAP test requires the quantum control of a system of more than $2N$ qubits. Another possibility corresponds to the Hadamard test [93] (see Appendix B) that requires controlled-time evolutions. The latter is demanding if the dynamics of interest involve many-body or time-dependent Hamiltonians. In contrast to this, here we present an *embedding* protocol that exploits the natural evolution of the system and that requires the addition of only one qubit.

Let us thus consider a two-time correlation function $\langle A(t)B(0)\rangle$ where $A(t) = U^\dagger(t)A(0)U(t)$, $U(t)$ being a given unitary operator, while $A(0)$ and $B(0)$ are both Hermitian. Remark that, generically, $A(t)B(0)$ will not be Hermitian. However, one can always construct two self-adjoint operators $C(t) = \frac{1}{2}\{A(t), B(0)\}$ and $D(t) = \frac{1}{2i}[A(t), B(0)]$ such that $\langle A(t)B(0)\rangle = \langle C(t)\rangle + i\langle D(t)\rangle$. According to the quantum mechanical postulates, there exist two measurement apparatus associated with observables $C(t)$ and $D(t)$. In this way, we may formally compute $\langle A(t)B(0)\rangle$ from the measured $\langle C(t)\rangle$ and $\langle D(t)\rangle$. However, the determination of $\langle C(t)\rangle$ and $\langle D(t)\rangle$ depends non trivially on the correlation times and on the complexity of the specific time evolution operator $U(t)$. Furthermore, we point out that the computation of n-time correlations, as $\langle\Psi|\Psi'\rangle = \langle\Psi|U^\dagger(t)AU(t)B|\Psi\rangle$, is not a trivial task even if one has access to full state tomography, due to the ambiguity of the global phase of state $|\Psi'\rangle = U^\dagger(t)AU(t)B|\Psi\rangle$. Therefore, we are confronted with a cumbersome problem: the design of measurement apparatus depending on the system evolution for determinating n-time correlations of a system whose evolution may not be accessible.

4.2 The protocol

The protocol works under the following two assumptions. First, we are provided with a controllable quantum system undergoing a given quantum evolution described by

the Schrödinger equation

$$i\hbar\partial_t|\phi\rangle = H|\phi\rangle. \tag{4.1}$$

And second, we require the ability to perform entangling operations, for example Mølmer-Sørensen [94] or equivalent controlled gates [40], between some part of the system and the ancillary qubit. More specifically, and as it is discussed in the Appendix A, we require a number of entangling gates that grows linearly with the order n of the n-time correlation function and that remains fixed with increasing system-size. This protocol will provide us with the efficient measurement of generalized n-time correlation functions of the form $\langle\phi|O_{n-1}(t_{n-1})O_{n-2}(t_{n-2})...O_1(t_1)O_0(t_0)|\phi\rangle$, where $O_{n-1}(t_{n-1})...O_0(t_0)$ are certain operators evaluated at different times, e.g. $O_k(t_k) = U^\dagger(t_k;t_0)O_k\ U(t_k;t_0)$, $U(t_k;t_0)$ being the unitary operator evolving the system from t_0 to t_k. For the case of dynamics governed by time-independent Hamiltonians, $U(t_k;t_0) = U(t_k - t_0) = e^{-\frac{i}{\hbar}H(t_k-t_0)}$. However, our method applies also to the case where $H = H(t)$, and can be sketched as follows. First, the ancillary qubit is prepared in state $\frac{1}{\sqrt{2}}(|\mathrm{e}\rangle + |\mathrm{g}\rangle)$ with $|\mathrm{g}\rangle$ its ground state, as in step 1 of Fig. 4.1, so that the whole ancilla-system quantum state is $\frac{1}{\sqrt{2}}(|\mathrm{e}\rangle + |\mathrm{g}\rangle) \otimes |\phi\rangle$, where $|\phi\rangle$ is the state of the system. Second, we apply the controlled quantum gate $U_c^0 = \exp\left(-\frac{i}{\hbar}|\mathrm{g}\rangle\langle\mathrm{g}| \otimes H_0\tau_0\right)$, where, as we will see below, H_0 is a Hamiltonian related to the operator O_0, and τ_0 is the gate time. As we point out in the Appendix A, this entangling gate can be implemented efficiently with Mølmer-Sørensen gates for operators O_0 that consist in a tensor product of Pauli matrices [94]. This operation entangles the ancilla with the system generating the state $\frac{1}{\sqrt{2}}(|\mathrm{e}\rangle \otimes |\phi\rangle + |\mathrm{g}\rangle \otimes \tilde{U}_c^0|\phi\rangle)$, with $\tilde{U}_c^0 = e^{-\frac{i}{\hbar}H_0\tau_0}$, step 2 in Fig. 4.1. Next, we switch on the dynamics of the system governed by Eq. (4.1). For the sake of simplicity let us assume $t_0 = 0$. The effect on the ancilla-system wavefunction is to produce the state $\frac{1}{\sqrt{2}}\left(|\mathrm{e}\rangle \otimes U(t_1;0)|\phi\rangle + |\mathrm{g}\rangle \otimes U(t_1;0)\tilde{U}_c^0|\phi\rangle\right)$, step 3 in Fig. 4.1. Note that, remarkably, this last step does not require an interaction between the system and the ancillary-qubit degrees of freedom nor any knowledge of the Hamiltonian H. These techniques, as will be evident below, will find a natural playground in the context of quantum simulations, preserving its analogue or digital character. If we iterate n times step 2 and step 3 with a suitable choice of gates and evolution times, we obtain the state $\Phi = \frac{1}{\sqrt{2}}(|\mathrm{e}\rangle \otimes U(t_{n-1};0)|\phi\rangle + |\mathrm{g}\rangle \otimes \tilde{U}_c^{n-1}U(t_{n-1};t_{n-2})...\ U(t_2;t_1)\tilde{U}_c^1U(t_1;0)\tilde{U}_c^0|\phi\rangle)$. Now, we target the quantity $\mathrm{Tr}(|\mathrm{e}\rangle\langle\mathrm{g}||\Phi\rangle\langle\Phi|)$ by measuring the $\langle\sigma_x\rangle$ and $\langle\sigma_y\rangle$ corresponding to the ancillary degrees of freedom. Simple algebra leads us to

$$\begin{aligned}\mathrm{Tr}(|\mathrm{e}\rangle\langle\mathrm{g}||\Phi\rangle\langle\Phi|) = \frac{1}{2}\left(\langle\Phi|\sigma_x|\Phi\rangle + i\langle\Phi|\sigma_y|\Phi\rangle\right) = \\ \frac{1}{2}\langle\phi|U^\dagger(t_{n-1};0)\tilde{U}_c^{n-1}U(t_{n-1};t_{n-2})...\ U(t_2;t_1)\tilde{U}_c^1U(t_1;0)\tilde{U}_c^0|\phi\rangle.\end{aligned} \tag{4.2}$$

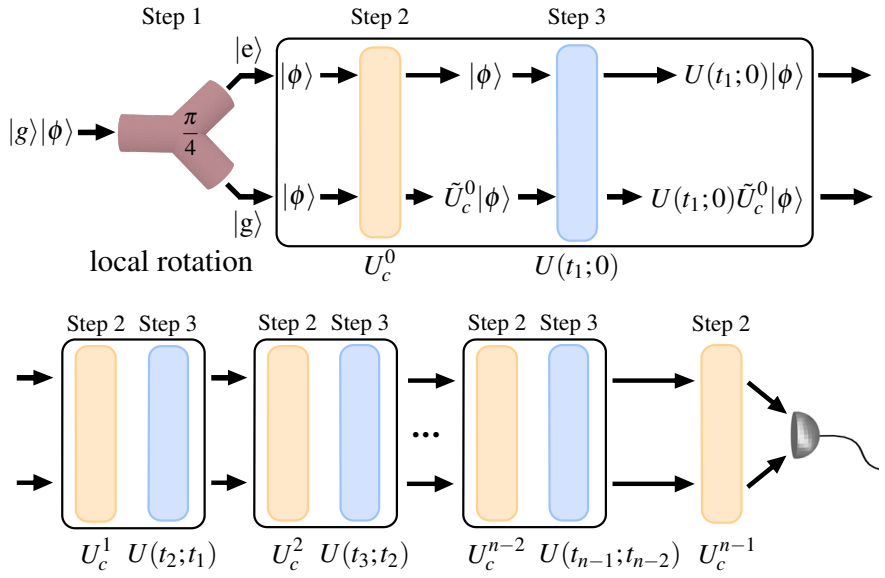

FIGURE 4.1: Quantum algorithm for computing n-time correlation functions. The ancilla state $\frac{1}{\sqrt{2}}(|\mathrm{e}\rangle + |\mathrm{g}\rangle)$ generates the $|\mathrm{e}\rangle$ and $|\mathrm{g}\rangle$ paths, step 1, for the ancilla-system coupling. After that, controlled gates U_c^m and unitary evolutions $U(t_m;t_{m-1})$ applied to our system, steps 2 and 3, produce the final state Φ. Finally, the measurement of the ancillary spin operators σ_x and σ_y leads us to n-time correlation functions.

It is easy to see that, by using the composition property $U(t_k;t_{k-1}) = U(t_k;0)U^\dagger(t_{k-1};0)$, Eq. (4.2) corresponds to a general construction relating n-time correlations of system operators $\tilde{U}_c^k$ with two one-time ancilla measurements. In order to explore its depth, we shall examine several classes of systems and suggest concrete realizations of the proposed algorithm. The crucial point is establishing a connection that associates the $\tilde{U}_c^k$ unitaries with O_k operators.

4.3 Preserving locality: stabilizer states

As in the simulation of entanglement monotones, also in this case we have the problem that we need the system to interact with an ancillary qubit. In most of the current platform, this means that we need to implement nonlocal operation to perform the protocol. We can fix this in the same way as in the second chapter, via the stabilizer formalism. First, we note that that all the operations in the protocol corresponds to Hamiltonian of the kind $\mathbb{I}\otimes H$, $\sigma_z \otimes H$ and their combinations, where H is an arbitrary system Hamiltonian. We consider an array of N ancillary qubits, where N can be chosen in the most convenient way. We want to find the subspace of their resulting Hilbert space, such that $\sigma_z^i\sigma_z^j|\phi\rangle = |\phi\rangle$, for an arbitrary state $|\phi\rangle$ of the N-qubit system.

This subspace is unique, and is spanned by the following vectors:

$$|\widetilde{-}\rangle = \sqrt{\frac{1}{2^{N-1}}} \sum_{h(y)\,\text{even}} |y\rangle \tag{4.3}$$

$$|\widetilde{+}\rangle = \sqrt{\frac{1}{2^{N-1}}} \sum_{h(y)\,\text{odd}} |y\rangle, \tag{4.4}$$

where $|\mp\rangle = \frac{1}{\sqrt{2}}(|e\rangle \mp |g\rangle)$, $y \in \{-,+\}^N$, and $h(y)$ is the number of $+$'s in y. If we define our logical ancillary qubit via Eqs. (4.3)-(4.4), we can substitute σ_z with σ_z^j, for any $1 \leq j \leq N$. Finally, the measurement of the logical σ_x corresponds to the parity of the $+$ outcomes of the N ancillary qubits, and a similar argument holds for the measurement of σ_y. In this way, while we have increased the space resources from 1 qubit more to N qubits more, the time efficiency is preserved.

4.4 Spinorial, fermionic and bosonic systems

So far, we have shown how to quantum compute n-time correlation functions of unitary operations. In the following, we show how to adapt these ideas for n-time correlation functions of Hermitian operators, in different kind of systems.

4.4.1 Spinorial systems

Starting with the discrete variable case, e.g. spin systems, and profiting from the fact that Pauli matrices are both Hermitian and unitary, it follows that

$$\tilde{U}_c^m\big|_{\Omega\tau_m=\pi/2} = \exp\left(-\frac{i}{\hbar} H_m \tau_m\right)\big|_{\Omega\tau_m=\pi/2} = -iO_m, \tag{4.5}$$

where $H_m = \hbar\Omega O_m$, Ω is a coupling constant, and O_m is a tensor product of Pauli matrices of the form $O_m = \sigma_{i_m} \otimes \sigma_{j_m} ... \sigma_{k_m}$ with $i_m, j_m, ..., k_m \in 0, x, y, z$, and $\sigma_0 = \mathbb{I}$. In consequence, the controlled quantum gates in step 2 correspond to $U_c^m\big|_{\Omega\tau_m=\pi/2} = \exp\left(-i|\mathrm{g}\rangle\langle\mathrm{g}| \otimes \Omega O_m \tau_m\right)$, which can be implemented efficiently, up to local rotations, with four Mølmer-Sørensen gates [20, 28, 76, 94]. In this way, we can write the second line of Eq. (4.2) as

$$(-i)^n \langle\phi| O_{n-1}(t_{n-1}) O_{n-2}(t_{n-2}) ... O_0(0) |\phi\rangle, \tag{4.6}$$

which amounts to the measured n-time correlation function of Hermitian and unitary operators O_k. We can also apply these ideas to the case of non-Hermitian operators,

independent of their unitary character, by considering linear superpositions of the Hermitian objects appearing in Eq. (4.6).

4.4.2 Fermionic systems

We show now how to apply this result to the case of fermionic systems. In principle, the previous proposed steps would apply straightforwardly if we had access to the corresponding fermionic operations. In the case of quantum simulations, a similar result is obtained via the Jordan-Wigner mapping of fermionic operators to tensorial products of Pauli matrices, $b_p^\dagger \rightarrow \Pi_{r=1}^{p-1}\sigma_+^p\sigma_z^r$ [95]. Here, $b_p^\dagger$ and b_q are creation and annihilation fermionic operators obeying anticommutation relations, $\{b_p^\dagger, b_q\} = \delta_{p,q}$. For trapped ions, a quantum algorithm for the efficient implementation of fermionic models has been recently proposed [28, 96, 97]. Then, we code $\langle b_p^\dagger(t)b_q(0)\rangle = \langle\Phi|(\sigma_+^p \otimes \sigma_z^{p-1}...\sigma_z^1)_t\ \sigma_-^q \otimes \sigma_z^{q-1}...\sigma_z^1|\Phi\rangle$, where $(\sigma_+^p \otimes \sigma_z^{p-1}...\sigma_z^1)_t = e^{\frac{i}{\hbar}Ht}\sigma_+^p \otimes \sigma_z^{p-1}...\sigma_z^1 e^{-\frac{i}{\hbar}Ht}$. Now, taking into account that $\sigma_\pm = \frac{1}{2}(\sigma_x \pm i\sigma_y)$, the fermionic correlator $\langle b_p^\dagger(t)b_q(0)\rangle$ can be written as the sum of four terms of the kind appearing in Eq. (4.6). This result extends naturally to multitime correlations of fermionic systems.

4.4.3 Bosonic systems

The case of bosonic n-time correlators requires a variant in the proposed method, due to the nonunitary character of the associated bosonic operators. In this sense, to reproduce a linearization similar to that of Eq. (4.5), we can write

$$\partial_{\Omega\tau_m}\tilde{U}_c^m\big|_{\Omega\tau_m=0} = \partial_{\Omega\tau_m}\exp\left(-\frac{i}{\hbar}H_m\tau_m\right)\big|_{\Omega\tau_m=0} = -iO_m\,, \tag{4.7}$$

with $H_m = \hbar\Omega O_m$. Consequently, it follows that

$$\begin{aligned}\partial_{\Omega\tau_j}...\partial_{\Omega\tau_k}\mathrm{Tr}(|\mathrm{e}\rangle\langle\mathrm{g}||\Phi\rangle\langle\Phi|)\big|_{\Omega(\tau_\alpha...\tau_\beta)=\frac{\pi}{2},\ \Omega(\tau_j...\tau_k)=0} = \\ (-i)^n\langle\phi|O_{n-1}(t_{n-1})O_{n-2}(t_{n-2})...O_0(0)|\phi\rangle\,,\end{aligned} \tag{4.8}$$

where the label $(\alpha, ..., \beta)$ corresponds to spin operators and $(j, ..., k)$ to spin-boson operators. The right hand side is a correlation of Hermitian operators, thus substantially extending our previous results. For example, O_m would include spin-boson couplings as $O_m = \sigma_{i_m} \otimes \sigma_{j_m}...\sigma_{k_m}(a + a^\dagger)$. The way of generating the associated evolution operator $\tilde{U}_c^m = \exp(-i\Omega O_m\tau_m)$ has been shown in [28, 29, 96], see also Appendix A. Note that, in general, dealing with discrete derivatives of experimental data is an involved task [98, 99]. However, recent experiments in trapped ions [22, 24, 100] have already

succeeded in the extraction of precise information from data associated to first and second-order derivatives.

4.4.4 Density matrix case

The method presented here works as well when the system is prepared in a mixed-state ρ_0, e.g. a state in thermal equilibrium [82, 83]. Accordingly, for the case of spin correlations, we have

$$\mathrm{Tr}(|\mathrm{e}\rangle\langle\mathrm{g}|\tilde{\rho}) = (-i)^n \mathrm{Tr}(O_{n-1}(t_{n-1})O_{n-2}(t_{n-2})...O_0(0)\rho_0), \tag{4.9}$$

with $\tilde{\rho} = \big(...U(t_2;t_1)U_c^1U(t_1;0)U_c^0\big)\tilde{\rho}_0\big(U_c^{0\dagger}U(t_1;0)^\dagger U_c^{1\dagger}U(t_2;t_1)^\dagger...\big)$ and $\tilde{\rho}_0 = \frac{1}{2}(|\mathrm{e}\rangle + |\mathrm{g}\rangle)(\langle\mathrm{e}| + \langle\mathrm{g}|) \otimes \rho_0$. If bosonic variables are involved, the analogue to Eq. (4.8) reads

$$\begin{aligned}\partial_{\Omega\tau_j}...\partial_{\Omega\tau_k}\mathrm{Tr}(|\mathrm{e}\rangle\langle\mathrm{g}|\tilde{\rho})\big|_{\Omega(\tau_\alpha...\tau_\beta)=\frac{\pi}{2},\ \Omega(\tau_j...\tau_k)=0} = \\ (-i)^n\mathrm{Tr}(O_{n-1}(t_{n-1})O_{n-2}(t_{n-2})...O_0(0)\rho_0).\end{aligned} \tag{4.10}$$

4.5 Example: magnetic susceptibility

We will now exemplify the introduced formalism with the case of quantum computing of spin-spin correlations of the form

$$\langle\sigma_i^k(t)\sigma_j^l(0)\rangle, \tag{4.11}$$

where $k, l = x, y, z$, and $i, j = 1, ..., N$, N being the number of spin-particles involved. In the context of spin lattices, where several quantum models can be simulated in different quantum platforms as trapped ions [17–19, 101–103], optical lattices [12, 104, 105], and circuit QED [106–109], correlations like (4.11) are a crucial element in the computation of, for example, the magnetic susceptibility [82–84]. In particular, with our protocol, we have access to the frequency-dependent susceptibility $\chi^\omega_{\sigma,\sigma}$ that quantifies the linear response of a spin-system when it is driven by a monochromatic field. This situation is described by the Schrödinger equation $i\hbar\partial_t|\psi\rangle = (H + f_\omega\sigma_j^l e^{i\omega t})|\psi\rangle$, where, for simplicity, we assume $H \neq H(t)$. With a perturbative approach, and following the Kubo relations [82, 83], one can calculate the first-order effect of a magnetic perturbation acting on the j-th spin in the polarization of the i-th spin as

$$\langle\sigma_i^k(t)\rangle = \langle\sigma_i^k(t)\rangle_0 + \chi^\omega_{\sigma,\sigma}f_\omega e^{i\omega t}. \tag{4.12}$$

Here, $\langle\sigma_i^k(t)\rangle_0$ corresponds to the value of the observable σ_i^k in the absence of perturbation, and the frequency-dependent susceptibility $\chi^{\omega}_{\sigma,\sigma}$ is

$$\chi^{\omega}_{\sigma,\sigma} = \int_0^t ds\ \phi_{\sigma,\sigma}(t-s)e^{i\omega(s-t)} \tag{4.13}$$

where $\phi_{\sigma,\sigma}(t-s)$ is called the response function, which can be written in terms of two-time correlation functions,

$$\phi_{\sigma,\sigma}(t-s) = \frac{i}{\hbar}\langle[\sigma_i^k(t-s),\sigma_j^l(0)]\rangle = \frac{i}{\hbar}\mathrm{Tr}\big([\sigma_i^k(t-s),\sigma_j^l(0)]\rho\big), \tag{4.14}$$

with $\rho = U(t)\rho_0 U^\dagger(t)$, ρ_0 being the initial state of the system and $U(t)$ the perturbation-free time-evolution operator [82]. Note that for thermal states or energy eigenstates, we have $\rho = \rho_0$. According to our proposed method, and assuming for the sake of simplicity $\rho = |\Phi\rangle\langle\Phi|$, the measurement of the commutator in Eq. (4.14), corresponding to the imaginary part of $\langle\sigma_i^k(t-s)\sigma_j^l(0)\rangle$, would require the following sequence of interactions: $|\Phi\rangle \to U_c^1 U(t-s)U_c^0|\Phi\rangle$, where $U_c^0 = e^{-i|\mathrm{g}\rangle\langle\mathrm{g}|\otimes\sigma_j^l\Omega\tau}$, $U(t-s) = e^{-\frac{i}{\hbar}H(t-s)}$, and $U_c^1 = e^{-i|\mathrm{g}\rangle\langle\mathrm{g}|\otimes\sigma_i^k\Omega\tau}$, for $\Omega\tau = \pi/2$. After such a gate sequence, the expected value in Eq. (4.14) corresponds to $-1/2\langle\Phi|\sigma_y|\Phi\rangle$. In the same way, Kubo relations allow the computation of higher order corrections of the perturbed dynamics in terms of higher order time correlation functions. In particular, second-order corrections to the linear response of Eq. (4.12) can be calculated through the computation of three-time correlation functions of the form $\langle\sigma_i^k(t_2)\sigma_j^l(t_1)\sigma_j^l(0)\rangle$. Using the method introduced in this paper, to measure such a three-time correlation function one should perform the evolution $|\Phi\rangle \to U_c^1 U(t_2-t_1)U_c^0 U(t_1)U_c^0|\Phi\rangle$, where $U_c^0 = e^{-i|\mathrm{g}\rangle\langle\mathrm{g}|\otimes\sigma_j^l\Omega\tau}$, $U(t) = e^{-\frac{i}{\hbar}Ht}$ and $U_c^1 = e^{-i|\mathrm{g}\rangle\langle\mathrm{g}|\otimes\sigma_i^k\Omega\tau}$ for $\Omega\tau = \pi/2$. The searched time correlation then corresponds to the quantity $1/2(i\langle\Phi|\sigma_x|\Phi\rangle - \langle\Phi|\sigma_y|\Phi\rangle)$.

Our method is not restricted to corrections of observables that involve the spinorial degree of freedom. Indeed, we can show how the method applies when one is interested in the effect of the perturbation onto the motional degrees of freedom of the involved particles. According to the linear response theory, corrections to observables involving the motional degree of freedom enter in the response function, $\phi_{a+a^\dagger,\sigma}(t-s)$, as time correlations of the type $\langle(a_i+a_i^\dagger)_{(t-s)}\sigma_j^l\rangle$, where $(a_i+a_i^\dagger)_{(t-s)} = e^{\frac{i}{\hbar}H(t-s)}(a_i+a_i^\dagger)e^{-\frac{i}{\hbar}H(t-s)}$. The response function can be written as in Eq. (4.14) but replacing the operator $\sigma_i^k(t-s)$ by $(a_i+a_i^\dagger)_{(t-s)}$. The corrected expectation value is now

$$\langle(a_i+a_i^\dagger)_t\rangle = \langle(a_i+a_i^\dagger)_t\rangle_0 + \chi^{\omega}_{a+a^\dagger,\sigma} f_\omega e^{i\omega t}. \tag{4.15}$$

In this case, the gate sequence for the measurement of the associated correlation function $\langle(a_i+a_i^\dagger)_{(t-s)}\sigma_j^l\rangle$ reads $|\Phi\rangle \to U_c^1 U(t-s)U_c^0|\Phi\rangle$, where $U_c^0 = e^{-i|\mathrm{g}\rangle\langle\mathrm{g}|\otimes\sigma_j^l\Omega_0\tau_0}$,

$U(t-s) = e^{-\frac{i}{\hbar}H(t-s)}$, and $U_c^1 = e^{-i|\mathrm{g}\rangle\langle\mathrm{g}|\otimes(a_i+a_i^\dagger)\Omega_1\tau_1}$, for $\Omega_0\tau_0 = \pi/2$. The time correlation is now obtained through the first derivative $-1/2\partial_{\Omega_1\tau_1}(\langle\Phi|\sigma_x|\Phi\rangle + i\langle\Phi|\sigma_y|\Phi\rangle)|_{\Omega_1\tau_1=0}$.

Equations (4.12) and (4.15) can be extended to describe the effect on the system of light pulses containing frequencies in a certain interval $(\omega_0, \omega_0+\delta)$. In this case, Eqs. (4.12) and (4.15) read

$$\langle\sigma_i^k(t)\rangle = \langle\sigma_i^k(t)\rangle_0 + \int_{\omega_0}^{\omega_0+\delta} \chi^{\omega}_{\sigma,\sigma} f_\omega e^{i\omega t} d\omega, \tag{4.16}$$

and

$$\langle(a_i + a_i^\dagger)_t\rangle = \langle(a_i + a_i^\dagger)_t\rangle_0 + \int_{\omega_0}^{\omega_0+\delta} \chi^{\omega}_{a+a^\dagger,\sigma} f_\omega e^{i\omega t} d\omega. \tag{4.17}$$

Note that despite the presence of many frequency components of the light field in the integrals of Eqs. (4.16, 4.17), the computation of the susceptibilities, $\chi^{\omega}_{\sigma,\sigma}$ and $\chi^{\omega}_{a+a^\dagger,\sigma}$, just requires the knowledge of the time correlation functions $\langle[\sigma_i^k(t-s), \sigma_j^l(0)]\rangle$ and $\langle[(a+a^\dagger)_{(t-s)}, \sigma_j^l(0)]\rangle$, which can be efficiently calculated with the protocol described in Fig 4.1. In this manner, we provide an efficient quantum algorithm to characterize the response of different quantum systems to external perturbations.

Lastly, our method may be related to the quantum computation of transition probabilities $|\alpha_{\mathrm{f,i}}(t)|^2 = |\langle\mathrm{f}|U(t)|\mathrm{i}\rangle|^2 = \langle\mathrm{i}|P_{\mathrm{f}}(t)|\mathrm{i}\rangle$, between initial and final states, $|\mathrm{i}\rangle$ and $|\mathrm{f}\rangle$, with $P_{\mathrm{f}}(t) = U(t)^\dagger|\mathrm{f}\rangle\langle\mathrm{f}|U(t)$, and to transition or decay rates $\partial_t|\alpha_{\mathrm{f,i}}(t)|^2$ in atomic ensembles. These questions are of general interest for evolutions perturbed by external driving fields or by interactions with other quantum particles.

4.6 Outlook

In this Chapter, we have presented an embedding quantum algorithm to efficiently compute arbitrary n-time correlation functions. The protocol requires the initial addition of a single probe and control qubit and is valid for arbitrary unitary evolutions. Furthermore, we have applied this method to interacting fermionic, spinorial, and bosonic systems, showing how to compute second-order effects beyond the linear response theory. Moreover, if used in a quantum simulation, the protocol preserves the analogue or digital character of the associated dynamics. This is a further example of encoding of a physical quantity, i.e. n-time correlation function, onto a larger Hilbert space, via a nontrivial mapping. It is noteworthy to mention that the complexity of the presented protocol relies only on the implementation of the considered Hamiltonian and of specific entangling gates. This makes the method a useful tool in quantum simulations, that can be used in a variety of situations. A further application is shown in the next Chapter.

Chapter 5

Quantum simulation of dissipative processes

In this Chapter, we introduce a quantum algorithm to simulate finite dimensional Lindblad master equations, corresponding to Markovian or non-Markovian processes [39]. Our protocol shows how to reconstruct, up to an arbitrary finite error, physical observables that evolve according to a dissipative dynamics, by evaluating multi-time correlation functions of its Lindblad operators. We show that the latter requires the implementation of the unitary part of the dynamics in a quantum simulator, without the necessity of physically engineering the system-environment interactions. Moreover, we demonstrate how these multi-time correlation functions can be computed with a reduced number of measurements. We further show that our method can be applied as well to the simulation of processes associated with non-Hermitian Hamiltonians. Finally, we provide specific error bounds to estimate the accuracy of our approach. The method presented in this Chapter falls under a class of simulation that we have called *algorithmic quantum simulation*, where we are not aimed to reproduce the state of the system, but we directly target the expected value of a given observable in an algorithmic way.

5.1 Introduction

While every physical system is indeed coupled to an environment [110, 111], modern quantum technologies have succeeded in isolating systems to an exquisite degree in a variety of platforms [64, 73, 112, 113]. In this sense, the last decade has witnessed great advances in testing and controlling the quantum features of these systems, spurring the quest for the development of quantum simulators [1–3, 114]. These efforts are guided by the early proposal of using a highly tunable quantum device to mimic the behavior

of another quantum system of interest, being the latter complex enough to render its description by classical means intractable. By now, a series of proof-of-principle experiments have successfully demonstrated the basic tenets of quantum simulations revealing quantum technologies as trapped ions [115], ultracold quantum gases [116], and superconducting circuits [117] as promising candidates to harbor quantum simulations beyond the computational capabilities of classical devices.

It was soon recognised that this endeavour should not be limited to simulating the dynamics of isolated complex quantum systems, but should more generally aim at the emulation of arbitrary physical processes, including the open quantum dynamics of a system coupled to an environment. Tailoring the complex nonequilibrium dynamics of an open system has the potential to uncover a plethora of technological and scientific applications. A remarkable instance results from the understanding of the role played by quantum effects in the open dynamics of photosynthetic processes in biological systems [118, 119], recently used in the design of artificial light-harvesting nanodevices [120–122]. At a more fundamental level, an open-dynamics quantum simulator would be invaluable to shed new light on core issues of foundations of physics, ranging from the quantum-to-classical transition and quantum measurement theory [123] to the characterization of Markovian and non-Markovian systems [124–126]. Further motivation arises at the forefront of quantum technologies. As the available resources increase, the verification with classical computers of quantum annealing devices [127, 128], possibly operating with a hybrid quantum-classical performance, becomes a daunting task. The comparison between different experimental implementations of quantum simulators is required to establish a confidence level, as customary with other quantum technologies, e.g., in the use of atomic clocks for time-frequency standards. In addition, the knowledge and control of dissipative processes can be used as well as a resource for quantum state engineering [129].

Facing the high dimensionality of the Hilbert space of the composite system made of a quantum device embedded in an environment, recent developments have been focused on the reduced dynamics of the system that emerges after tracing out the environmental degrees of freedom. The resulting nonunitary dynamics is governed by a dynamical map, or equivalently, by a master equation [110, 111]. In this respect, theoretical [130–132] and experimental [133] efforts in the simulation of open quantum systems have exploited the combination of coherent quantum operations with controlled dissipation. Notwithstanding, the experimental complexity required to simulate an arbitrary open quantum dynamics is recognised to substantially surpass that needed in the case of closed systems, where a smaller number of generators suffices to design a general time-evolution. Thus, the quantum simulation of open systems remains a challenging task.

5.2 The Lindblad form

Consider a quantum system coupled to an environment whose dynamics is described by the von Neumann equation $i\frac{d\bar{\rho}}{dt} = [\bar{H}, \bar{\rho}]$. Here, $\bar{\rho}$ is the system-environment density matrix, $\bar{H} = H_s + H_e + H_I$, where H_s and H_e are the system and environment Hamiltonians, while H_I corresponds to their interaction. Assuming weak coupling and short time-correlations between the system and the environment, after tracing out the environmental degrees of freedom we obtain the Markovian master equation

$$\frac{d\rho}{dt} = \mathcal{L}^t \rho, \tag{5.1}$$

being $\rho = \mathrm{Tr}_e(\bar{\rho})$ and $\mathcal{L}^t$ the time-dependent superoperator governing the dissipative dynamics [110, 111]. Notice that there are different ways to recover Eq. (5.1) [134]. Nevertheless, Eq. (5.1) is our starting point, and in the following we show how to simulate this equation regardless of its derivation. Indeed, our algorithm does not need control any of the approximations done to achieve this equation. We can decompose $\mathcal{L}^t$ into $\mathcal{L}^t = \mathcal{L}^t_H + \mathcal{L}^t_D$. Here, $\mathcal{L}^t_H$ corresponds to a unitary part, i.e. $\mathcal{L}^t_H \rho \equiv -i[H(t), \rho]$, where $H(t)$ is defined by H_s plus a term due to the lamb-shift effect and it may depend on time. Instead, $\mathcal{L}^t_D$ is the dissipative contribution and it follows the Lindblad form [135] $\mathcal{L}^t_D \rho \equiv \sum_{i=1}^{N} \gamma_i(t) \left(L_i \rho L_i^\dagger - \frac{1}{2}\{L_i^\dagger L_i, \rho\} \right)$, where L_i are the Lindblad operators modelling the effective interaction of the system with the bath that may depend on time, while $\gamma_i(t)$ are nonnegative parameters. Notice that, although the standard derivation of Eq. (5.1) requires the Markov approximation, a non-Markovian equation can have the same form. Indeed, it is known that if $\gamma_i(t) < 0$ for some t and $\int_0^t dt' \, \gamma_i(t') > 0$ for all t, then Eq. (5.1) corresponds to a completely positive non-Markovian channel [136]. Our approach can deal also with non-Markovian processes of this kind, keeping the same efficiency as the Markovian case. While we will consider the general case $\gamma_i = \gamma_i(t)$, whose sign distinguishes the Markovian processes by the non-Markovian ones, for the sake of simplicity we will consider the case $H \neq H(t)$ and $L_i \neq L_i(t)$ (in the following, we will denote $\mathcal{L}^t_H$ simply as $\mathcal{L}_H$). However, the inclusion in our formalism of time-dependent Hamiltonians and Lindblad operators is straightforward.

5.3 The protocol

One can integrate Eq. (5.1) obtaining a Volterra equation [137]

$$\rho(t) = e^{t\mathcal{L}_H} \rho(0) + \int_0^t ds \; e^{(t-s)\mathcal{L}_H} \mathcal{L}^s_D \; \rho(s), \tag{5.2}$$

where $e^{t\mathcal{L}_H} \equiv \sum_{k=0}^{\infty} t^k \mathcal{L}_H^k/k!$. The first term at the right-hand-side of Eq. (5.2) corresponds to the unitary evolution of $\rho(0)$ while the second term gives rise to the dissipative correction. Our goal is to find a perturbative expansion of Eq. (5.2) in the $\mathcal{L}_D^t$ term, and to provide with a protocol to measure the resulting expression in a unitary way. In order to do so, we consider the iterated solution of Eq. (5.2) obtaining

$$\rho(t) \equiv \sum_{i=0}^{\infty} \rho_i(t). \tag{5.3}$$

Here, $\rho_0(t) = e^{t\mathcal{L}_H}\rho(0)$, while, for $i \geq 1$, $\rho_i(t)$ has the following general structure: $\rho_i(t) = \Pi_{j=1}^{i}\Phi_j \; e^{s_i\mathcal{L}_H}\rho(0)$, Φ_j being a superoperator acting on an arbitrary matrix ξ as $\Phi_j\xi = \int_0^{s_{j-1}} ds_j \; e^{(s_{j-1}-s_j)\mathcal{L}_H}\mathcal{L}_D^{s_j}\,\xi$, where $s_0 \equiv t$. For instance, $\rho_2(t)$ can be written as

$$\begin{aligned}\rho_2(t) &= \Pi_{j=1}^{2}\Phi_j e^{s_2\mathcal{L}_H}\rho(0) = \Phi_1\Phi_2 \; e^{s_2\mathcal{L}_H}\rho(0) = \\ &= \int_0^t ds_1 e^{(t-s_1)\mathcal{L}_H}\mathcal{L}_D^{s_1}\int_0^{s_1} ds_2 e^{(s_1-s_2)\mathcal{L}_H}\mathcal{L}_D^{s_2}e^{s_2\mathcal{L}_H}\rho(0).\end{aligned} \tag{5.4}$$

In this way, Eq. (5.3) provides us with a general and useful expression of the solution of Eq. (5.1). Let us consider the truncated series in Eq. (5.3), that is $\tilde{\rho}_n(t) = e^{t\mathcal{L}_H}\rho(0) + \sum_{i=1}^{n}\rho_i(t)$, where n corresponds to the order of the approximation. We will prove that an expectation value $\langle O\rangle_{\rho(t)} \equiv \mathrm{Tr}\left[O\rho(t)\right]$ corresponding to a dissipative dynamics can be well approximated as

$$\langle O\rangle_{\rho(t)} \approx \mathrm{Tr}[Oe^{t\mathcal{L}_H}\rho(0)] + \sum_{i=1}^{n}\mathrm{Tr}[O\rho_i(t)]. \tag{5.5}$$

In the following, we will supply with a quantum algorithm based on single-shot random measurements to compute each of the terms appearing in Eq. (5.5), and we will derive specific upper-bounds quantifying the accuracy of our method. Notice that the first term at the right-hand-side of Eq. (5.5), i.e. $\mathrm{Tr}[Oe^{t\mathcal{L}_H}\rho(0)]$, corresponds to the expectation value of the operator O evolving under a unitary dynamics, thus it can be measured directly in a unitary quantum simulator where the dynamic associated with the Hamiltonian H is implementable. However, the successive terms of the considered series, i.e. $\mathrm{Tr}[O\rho_i(t)]$ with $i \geq 1$, require a specific development because they involve multi-time correlation functions of the Lindblad operators and the operator O.

Let us consider the first order term of the series in Eq. (5.5)

$$\begin{aligned}\langle O\rangle_{\rho_1(t)} &= \int_0^t ds_1 \; \mathrm{Tr}\left[Oe^{(t-s_1)\mathcal{L}_H}\mathcal{L}_D^{s_1}\rho_0(s_1)\right] = \\ &= \sum_{i=1}^{N}\int_0^t ds_1 \; \gamma_i(s_1)\left[\langle L_i^\dagger(s_1)O(t)L_i(s_1)\rangle - \frac{1}{2}\langle\Big\{O(t), L_i^\dagger L_i(s_1)\Big\}\rangle\right],\end{aligned} \tag{5.6}$$

where $\xi(s) \equiv e^{iHs}\xi e^{-iHs}$ for a general operator ξ and time s, and all the expectation values are computed in the state $\rho(0)$. Note that the average values appearing in the second and third lines of Eq. (5.6) correspond to time correlation functions of the operators O, L_i, $L_i^\dagger$, and $L_i^\dagger L_i$. In the following, we consider a basis $\{Q_j\}_{j=1}^{d^2}$, where d is the system dimension and Q_j are Pauli-kind operators, i.e. both unitary and Hermitian (see Appendix C for more details). The operators L_i and O can be decomposed as $L_i = \sum_{k=1}^{M_i} q_k^i Q_k^i$ and $O = \sum_{k=1}^{M_O} q_k^O Q_k^O$, with $q_k^{i,O} \in \mathbb{C}$, $Q_k^{i,O} \in \{Q_j\}_{j=1}^{d^2}$, and $M_i, M_O \leq d^2$. We obtain then

$$\langle L_i^\dagger(s_1) O(t) L_i(s_1)\rangle = \sum_{l=1}^{M_O}\sum_{k,k'=1}^{M_i} q_l^O q_k^{i*} q_{k'}^i \langle Q_k^i(s_1) Q_l^O(t) Q_{k'}^i(s_1)\rangle, \tag{5.7}$$

that is a sum of correlations of unitary operators. The same argument applies to the terms including $L_i^\dagger L_i$ in Eq. (5.6). Accordingly, we have seen that the problem of estimating the first-order correction is moved to the measurement of some specific multi-time correlation functions involving the $Q_k^{i,O}$ operators. The argument can be easily extended to higher-order corrections. Indeed, for the n-th order, we have to evaluate the quantity

$$\begin{aligned}\langle O\rangle_{\rho_n(t)} &= \int dV_n \, \mathrm{Tr}[O e^{(t-s_1)\mathcal{L}_H}\mathcal{L}_D^{s_1}\dots\mathcal{L}_D^{s_n} e^{s_n\mathcal{L}_H}\rho(0)] = \\ &= \sum_{i_1,\dots,i_n=1}^{N} \int dV_n \, \langle A_{[i_1,\cdots,i_n]}(\vec{s})\rangle. \end{aligned}\tag{5.8}$$

Here,

$$A_{[i_1,\dots,i_n]}(\vec{s}) \equiv e^{s_n\mathcal{L}_H^\dagger}\mathcal{L}_D^{s_n,i_n\dagger}\dots\mathcal{L}_D^{s_2,i_2\dagger} e^{(s_1-s_2)\mathcal{L}_H^\dagger}\mathcal{L}_D^{s_1,i_1\dagger} e^{(t-s_1)\mathcal{L}_H^\dagger} O, \tag{5.9}$$

where $\mathcal{L}_D^{s,i}\xi \equiv \gamma_i(s)\left(L_i\xi L_i^\dagger - \frac{1}{2}\{L_i^\dagger L_i, \xi\}\right)$, $\vec{s} = (s_1,\dots,s_n)$, $\int dV_n = \int_0^t \dots \int_0^{s_{n-1}} ds_1 \dots ds_n$, and $\mathcal{L}^\dagger\xi \equiv (\mathcal{L}\xi)^\dagger$ for a general superoperator $\mathcal{L}$. As in Eq. (5.6), the above expression contains multi-time correlation functions of the Lindblad operators $L_{i_1},\dots,L_{i_n}$ and the observable O, that have to be evaluated in order to compute each contribution in Eq. (5.5).

5.4 Computation of nth-order correction terms

Our next step is to provide a method to evaluate general terms as the one appearing in Eq. (5.8). The standard approach to estimate this kind of quantities corresponds to measuring the expected value $\langle A_{[i_1,\cdots,i_n]}(\vec{s})\rangle$ at different random times $\vec{s}$ in the integration domain, and then calculating the average. Nevertheless, this strategy involves a huge number of measurements, as we need to estimate an expectation value at each chosen

time. Our technique, instead, is based on single-shot random measurements and, as we will see below, it leads to an accurate estimate of Eq. (5.8). More specifically, we will prove that

$$\sum_{i_1,\ldots,i_n=1}^{N} \int dV_n \, \langle A_{[i_1,\cdots,i_n]}(\vec{s})\rangle \approx \frac{N^n |V_n|}{|\Omega_n|} \sum_{\Omega_n} \tilde{A}_{\vec{\omega}}(\vec{t}), \tag{5.10}$$

where $\tilde{A}_{\vec{\omega}}(\vec{t})$ corresponds to a single-shot measurement of $A_{\vec{\omega}}(\vec{t})$, being $[\vec{\omega},\vec{t}] \in \Omega_n \subset \{[\vec{\omega},\vec{t}] \mid \vec{\omega} = [i_1,\ldots,i_n], i_k \in [1,N], \vec{t} \in V_n\}$, $|\Omega_n|$ is the size of Ω_n, and $[\vec{\omega},\vec{t}]$ are sampled uniformly and independently. As already pointed out, the integrand in Eq. (5.8) involves multi-time correlation functions. In this respect, we can use the quantum algorithm introduced in Chapter 4, (see also Ref. [38]). Indeed, we have shown how, by adding only one ancillary qubit to the simulated system, general time-correlation functions are accessible by implementing only unitary evolutions of the kind $e^{t\mathcal{L}_H}$, together with entangling operations between the ancillary qubit and the system. It is noteworthy to mention that these operations have already experimentally demonstrated in quantum systems as trapped ions [20] or quantum optics [73], and have been recently proposed for cQED architectures [72]. Moreover, the same quantum algorithm allows us to measure single-shots of the real and imaginary part of these quantities providing, therefore, a way to compute the term at the right-hand-side of Eq. (5.10). Notice that the evaluation of each term $\langle A_{[i_1,\cdots,i_n]}(\vec{s})\rangle$ in Eq. (5.8), requires a number of measurements that depends on the observable decomposition, see Eq. (5.7). After specifying it, we measure the real and the imaginary part of the corresponding correlation function. Finally, in Appendix D we prove that

$$\left| \sum_{i_1,\ldots,i_n=1}^{N} \int dV_n \, \langle A_{[i_1,\cdots,i_n]}(\vec{s})\rangle - \frac{(Nt)^n}{n!|\Omega_n|} \sum_{\Omega_n} \tilde{A}_{\vec{\omega}}(\vec{t}) \right| \leq \delta_n \tag{5.11}$$

with probability higher than $1 - e^{-\beta}$, provided that $|\Omega_n| > \frac{36 M_O^2 (2+\beta)}{\delta_n^2} \frac{(2\bar{\gamma} M N t)^{2n}}{n!^2}$, where $\bar{\gamma} \equiv \max_{i,s\in[0,t]} |\gamma_i(s)|$ and $M \equiv \max_i M_i$. Equation (5.11) means that that the quantity in Eq. (5.8) can be estimated with arbitrary precision by random single-shot measurements of $A_{[i_1,\cdots,i_n]}(\vec{s})$, allowing, hence, to dramatically reduce the resources required by our quantum simulation algorithm. Notice that the required number of measurements to evaluate the order n is bounded by $3^n|\Omega_n|$, and the total number of measurements needed to compute the correction to the expected value of an observable up the order K is bounded by $\sum_{n=0}^{K} 3^n |\Omega_n|$.

So far, we have proved that we can compute, up to an arbitrary order in $\mathcal{L}_D^t$, expectation values corresponding to dissipative dynamics with a unitary quantum simulation. It is noteworthy that our method does not require to physically engineer the system-environment interaction. Instead, one only needs to implement the system Hamiltonian

H. In this way we are opening a new avenue for the quantum simulation of open quantum dynamics in situations where the complexity on the design of the dissipative terms excedes the capabilities of quantum platforms. This covers a wide range of physically relevant situations. One example corresponds to the case of fermionic theories where the encoding of the fermionic behavior in the degrees of freedom of the quantum simulator gives rise to highly delocalized operators [28, 95]. In this case a reliable dissipative term should act on these non-local operators instead of on the individual qubits of the system. Our protocol solves this problem because it avoids the necessity of implementing the Lindblad superoperator. Moreover, the scheme allows one to simulate at one time a class of master equations corresponding to the same Lindblad operators, but with different choices of γ_i, including the relevant case when only a part of the system is subjected to dissipation, i.e. $\gamma_i = 0$ for some values of i. Moreover, notice that this protocol does not really on achieving the final state of the dynamics of interest, but we directly target the expectation value of a given observable at a certain time, in an *algorithmic* way.

5.5 Error bounds and efficiency

We shall next quantify the quality of our method. In order to do so, we will find an error bound certifying how the truncated series in Eq. (5.3) is close to the solution of Eq. (5.1). This error bound will depend on the system parameters, i.e. the time t and the dissipative parameters γ_i. As figure of merit we choose the trace distance, defined by

$$D_1(\rho_1, \rho_2) \equiv \frac{\|\rho_1 - \rho_2\|_1}{2}, \tag{5.12}$$

where $\|A\|_1 \equiv \sum_i \sigma_i(A)$, being $\sigma_i(A)$ the singular values of A [148]. Our goal is to find a bound for $D_1(\rho(t), \tilde{\rho}_n(t))$, where $\tilde{\rho}_n(t) \equiv \sum_{i=0}^{n} \rho_i(t)$ is the series of Eq. (5.3) truncated at the n-th order. We note that the the following recursive relation holds

$$\tilde{\rho}_n(t) = e^{t\mathcal{L}_H}\rho(0) + \int_0^t ds\; e^{(t-s)\mathcal{L}_H}\mathcal{L}_D^s\,\tilde{\rho}_{n-1}(s). \tag{5.13}$$

From Eq. (5.13), it follows that

$$\begin{aligned} D_1(\rho(t), \tilde{\rho}_n(t)) &= \frac{1}{2}\left\| \int_0^t ds\; e^{(t-s)\mathcal{L}_H}\mathcal{L}_D^s(\rho(s) - \tilde{\rho}_{n-1}(s)) \right\|_1 \leq \\ &\leq \int_0^t ds\; \|\mathcal{L}_D^s\|_{1\to 1} D_1(\rho(s), \tilde{\rho}_{n-1}(s)), \end{aligned} \tag{5.14}$$

where we have introduced the induced superoperator norm $\|\mathcal{A}\|_{1\to 1} \equiv \sup_\sigma \frac{\|\mathcal{A}\sigma\|_1}{\|\sigma\|_1}$ [148]. For $n = 0$, i.e. for $\tilde{\rho}_n(t) \equiv \tilde{\rho}_0(t) = e^{t\mathcal{L}_H}\rho(0)$, we obtain the following bound

$$D_1(\rho(t), \tilde{\rho}_0(t)) \leq \frac{1}{2}\int_0^t ds\, \|\mathcal{L}_D^s\|_{1\to 1}\|\rho(s)\|_1 \leq \sum_{i=1}^{N} |\gamma_i(\epsilon_i)|\|L_i\|_\infty^2 t, \tag{5.15}$$

where $0 \leq \epsilon_i \leq t$ (see Appendix E), and $\|A\|_\infty \equiv \sup_i \sigma_i(A)$. Notice that, in finite dimension, one can always renormalize γ_i in order to have $\|L_i\|_\infty = 1$, i.e. if we transform $L_i \to L_i/\|L_i\|_\infty$, $\gamma_i \to \|L_i\|_\infty\gamma_i$, the master equation remains invariant. Using Eqs. (5.14)-(5.15), one can shown by induction that for the general n-th order the following bound holds (see Appendix E)

$$D_1(\rho(t), \tilde{\rho}_n(t)) \leq \prod_{k=0}^{n}\left[2\sum_{i_k=1}^{N}|\gamma_{i_k}(\epsilon_{i_k})|\right]\frac{t^{n+1}}{2(n+1)!} \leq \frac{(2\bar{\gamma}Nt)^{n+1}}{2(n+1)!}, \tag{5.16}$$

where $0 \leq \epsilon_{i_k} \leq t$ and we have set $\|L_i\|_\infty = 1$. From Eq. (5.16), it is clear that the series converges uniformly to the solution of Eq. (5.1) for every finite value of t and choices of γ_i. As a result, the number of measurements needed to simulate a certain dynamics at time t up to an error $\varepsilon < 1$ is $O\left(\left(\bar{t} + \log\frac{1}{\varepsilon}\right)^2 \frac{e^{12M\bar{t}}}{\varepsilon^2}\right)$, where $\bar{t} = \bar{\gamma}Nt$, see Appendix E. Here, a discussion on the efficiency of the method is needed. From the previous formula, we can say that our method performs well when M is low, i.e. in that case where each Lindblad operators can be decomposed in few Pauli-kind operators. Moreover, as our approach is perturbative in the dissipative parameters γ_i, it is reasonable that the method is more efficient when $|\gamma_i|$ are small. Notice that analytical perturbative techniques are not available in this case, because the solution of the unperturbed part is assumed to be not known. Lastly, it is evident that the algorithm is efficient for a certain choices of time, and the relevance of the simulation depends on the particular cases. For instance, a typical interesting situation is a strongly coupled Markovian system. Let us assume with site-independent couple parameter g and dissipative parameter γ. We have that $e^{12M\bar{t}} \leq 1 + 12eM\bar{t}$ if $t \leq \frac{1}{12M\gamma N} \equiv t_c$. In this period, the system oscillates typically $C \equiv gt_c = \frac{g/\gamma}{12MN}$ times, so the simulation can be considered efficient for $N \sim g/\gamma C$, which, in the strong coupling regime, can be of the order of $10^3/C$. Notice that, in most relevant physical cases, the number of Lindblad operators N is of the order of the number of system parties [131].

All in all, our method is aimed to simulate a different class of master equations with respect the previous approaches, including non-Markovian quantum dynamics, and it is efficient in the range of times where the exponential $e^{M\bar{t}}$ may be truncated at some low order. A similar result is achieved by the authors of Ref. [131], where they simulate a Lindblad equation via Trotter decomposition. They show that the Trotter error is

exponentially large in time, but this exponential can be truncated at some low order by choosing the Trotter time step Δt sufficiently small. Our method is qualitatively different, and it can be applied also to analogue quantum simulators where suitable entangled gates are available.

5.6 Non-Hermitian Hamiltonian case

Lastly, we note that this method is also appliable to simulate dynamics under a non-Hermitian Hamiltonian $J = H - i\Gamma$, with $H = H^\dagger$, $\Gamma = \Gamma^\dagger$. This type of generator emerges as an effective Hamiltonian in the Feshbach partitioning formalism [**?**], when one looks for the evolution of the density matrix projected onto a subspace. The new Schrödinger equation reads

$$\frac{d\rho}{dt} = -i[H, \rho] + \{\Gamma, \rho\}, \tag{5.17}$$

This kind of equation is useful in understanding several phenomena, e.g. scattering processes [139] and dissipative dynamics [140], or in the study of PT-symmetric Hamiltonian [141]. Our method consists in considering the non-Hermitian part as a perturbative term. As in the case previously discussed, similar bounds can be easily found (see Appendix F), and this proves that the method is reliable also in this situation.

5.7 Outlook

In this Chapter, we have introduced an algorithmic quantum simulation to compute expectation values of observables that evolve according to a general Lindblad master equation, requiring only the implementation of its unitary part. Through the quantum computation of n-time correlation functions of the Lindblad operators, we are able to reconstruct the corrections of the dissipative terms to the unitary quantum evolution without reservoir engineering techniques. We have provided with a complete recipe that combines quantum resources and specific theoretical developments to compute these corrections, and error-bounds quantifying the accuracy of the proposal and defining the cases when the proposed method is efficient. Our technique can be also applied, with small changes, to the quantum simulation of non-Hermitian Hamiltonians. The presented method provides a general strategy to perform quantum simulations of open systems, Markovian or not, in an algorithmic way.

Chapter 6

Conclusions

Technology is a gift of God. After the gift of life it is perhaps the greatest of God's gifts. It is the mother of civilizations, of arts and of sciences.

Freeman Dyson

This Thesis is focused on the development of quantum algorithms aimed to enhance the capability of quantum simulators based on controllable quantum technology. Specifically, we have shown how interesting physical quantities, such as entanglement and n-time correlation functions, can be efficiently computed in a quantum simulator. This brought us to define the new concept of *embedding quantum simulator*, which consists in specific mappings of the simulated dynamics onto a slightly larger Hilbert space. The embedding procedure allows us to retrieve, by measuring few observables, quantities that otherwise would need full tomography in order to be evaluated. Moreover, the space resources are comparable to the case of the one-to-one quantum simulator, where the target dynamics is directly implemented.

In Chapters 2 and 3, we have studied a protocol to simulate the dynamics of specific entanglement monotones in qubit systems [36, 37]. The proposed mapping can be implemented in a quantum platform by adding only one qubit, and interaction length of the dynamics is increased by one. The whole system have to interact with the ancillary qubit, which may lead to non-local interactions, e.g., in a linear array of qubits. We have shown how to overcome this problem, by defining a logical qubit at some space efficiency cost. Finally, we have extended the results in the density matrix case, by discussing a classical-quantum hybrid algorithm. While, we have discussed the entanglement monotone case, it is noteworthy to mention that the proposed protocol is able to simulate general antilinear operators, that cannot be measured in a one-to-one quantum simulators, and which may lead to other interesting applications. In Chapter 3, we

have discussed a trapped-ion implementation of en embedding quantum simulation for the quantum computation of entanglement monotones. Chapter 3 provides also with a protocol for measuring a general tensor product of Pauli operators, by encoding it in one ancilla observable. The analysis holds in general for quantum platform where Mølmer-Sørensen gates can be efficiently implemented, as it is also the case of linear optics.

An interesting follow up of these results is the study of the properties of the presented mapping, which can increase the flexibility of a quantum simulator. In fact, if we are not limited on one ancillary qubit, mapping on general Hilbert space dimensions may simulate other kinds of *unphysical* quantities. A further question is how the natural bath of the quantum simulator affects the final results of the unitary simulated dynamics. Here, the projective property of the embedding mapping may lead to an enhancement of the stability under the environmental noise. These questions are left as open, and they need further analysis in order to be well understood.

Based on these ideas, two proof of principle experiments on a photonics platform are currently running independently in the labs of Prof. Andrew White from University of Queensland (Brisbane, Australia) [142], where the author of this Thesis is a coauthor, and Prof. Jian-Wei Pan from University of Science and Technology of China (Hefei, China) [143]. The experiments are aimed to measure the concurrence between two qubits in an embedding quantum simulator, under a specific dynamics. They are performed with three qubits, each of them corresponding to the polarisation of the propagating optical signals. All operations are implemented with standard optical devices, i.e. polarising beamsplitters, single qubit rotations and control-NOTs. Preliminary results show that the concurrence is measured with high fidelity, which may bring to exciting sequels in other promising platform such as trapped ions and circuit QED.

In Chapter 4, we have developed a protocol to compute n-time correlation functions of general operators in a quantum simulator [38]. Also in this case, we have embedded the Schrödinger equation on a doubled Hilbert space. The mapping has the same structure as the antilinear operator case, discussed in Chapter 2, and this is a strong indication that further nontrivial mappings are possible. We have discussed how to apply the protocol to the spinorial, fermionic and bosonic cases, showing that the method is efficient in space and in time. The power of the proposed algorithm consists in the fact that we do not need to implement the controlled version of evolution Hamiltonian, which may be a cumbersome problem for most of the physically interesting models. This aspect, compared to the previous protocols, corresponds to a huge experimental gain, and we may see soon to the first proof of principle experiments. Also in this case, we need the system to interact non-locally with the ancillary qubit. This problem can be solved in

the same way as in the Chapter 1, by encoding the ancillary qubit logically in an array of qubits. As a typical application, we have considered the quantum simulation of magnetic susceptibilities, and in general linear and non-linear response functions. This protocol adheres with the scientific custom that an algorithm has to be the simpler possible, and experimental implementable nowadays or in the near future.

In Chapter 5, we have studied a novel protocol to simulate Markovian and non-Markovian dissipative processes [39]. The power of this proposed method is that it does not rely on any bath engineering. Instead, we perform perturbation theory with respect the dissipative parameters, and we compute the correction terms to the unitary dynamics. The computation of each perturbative term consists in measuring time correlation function of the desired observable and the Lindblad operators. To achieve this, we apply the embedding algorithm studied in Chapter 4. The presented method is a good alternative to the one based on Trotter decomposition [131], and it can be implemented in those platforms where the algorithm of Chapter 4 is available, e.g. analogue quantum simulators where specific gates are feasible. The main novelty of this algorithm results in a new kind of simulator, where we are not interested in achieving the final state of the simulated model, but we build the protocol depending on the final observable that we desire to measure. For this reason, we have named this kind of protocols as *algorithmic quantum simulations*.

It is noteworthy to mention that with our method, we are able to simulate time-local Lindblad equations, which are non-Markovian if the dissipative parameters takes negative values. It would be interesting to extend these results to more general non-Markovian master equations, e.g. of the kind

$$\partial_t \rho = \int_0^t d\tau k(t-\tau)\mathcal{L}\rho(\tau),$$

where $\mathcal{L}$ is the Lindblad superoperator and $k(t)$ is the kernel (note that $k(t) = 2\delta(t)$ corresponds to the Markovian case). This is currently subject of study [144], and it may lead to a clear cut with respect other methods, that cannot manage non-Markovian dynamics of this kind. Moreover, there are possibilities for our algorithm to get better in terms of efficiency. In fact, Taylor-based quantum simulator for unitary dynamics has been already proved to be optimal in the precision error [145]. These results should be translated in the dissipative case, possibly by considering more general computational model (see e.g. [146]).

In the Appendix, we have provided with several technical proofs and considerations for the claims in the main text. In particular, in Appendix F we have discussed the

quantum simulation of non-Hermitian Hamiltonian in the same fashion of the dissipative case.

All in all, this Thesis is about the actual capability of a quantum simulator. Looking for quantum algorithms that encode general quantities using quantum theory have always been an attractive research field, and we have provided with a breaking new direction in this line. However, there are several theoretical questions which need to be answered in order to prove the actual advantage of a quantum simulator over a classical one. Indeed, it is not clear whether it is possible to prove that the outcome of a quantum simulator is the right one. Certification protocols can be adapted from the universal quantum computer case, where error correction is theoretically available. However, this is not a solution at all, as it can work only for a digital quantum simulator, and in the methods based on Trotter decomposition this may bring to a tremendous lost of efficiency [33]. Therefore, new concepts for digital quantum simulation are welcome. On the other hand, analogue quantum simulators need a totally novel treatment, because in this case the error cannot be digitalised. A related question regards the efficiency of a quantum simulator. Current definitions of efficiency may become meaningless when realistic experimental conditions enter into the game. This may bring novel definitions of complexity classes, capturing noisy analogue and digital quantum simulation in the absence of quantum error correction. An answer to these general questions would help us in understanding fundamental aspects of quantum simulations, and, in general, of quantum mechanics.

Appendix A

Efficiency of the n-time correlation function protocol

In this Appendix, we provide with the efficiency of the n-time correlation function protocol presented in Chapter 4. Moreover, we show how to implement Hamiltonian consisting in general tensor Pauli operators using Mømer-Søredness gates and local gates.

A.1 Time and space efficiency

The embedding algorithm is conceived to be run in a setup composed of a system undergoing the evolution of interest and an ancillary qubit. Thus, the size of the setup where the algorithm is to be run is always that of the system plus one qubit, regardless of the order of the time correlation. For instance, if we are considering an N-qubit system then our method is performed in a setup composed of $N + 1$ qubits.

With respect to time-efficiency, our algorithm requires the performance of n controlled gates U_c^i and $n-1$ time-evolution operators $U(t_{j+1}; t_j)$, n being the order of the time-correlation function. If we assume that q gates are needed for the implementation of the system evolution and m gates are required per control operation, our algorithm employs $(m + q) * n - q$ gates. As m and q do not depend on the order of the time correlation we can state that our algorithm needs a number of gates that scales as a first-order polynomial with respect to the order n of the time-correlation function. The scaling of q with respect to the system size depends on the specific simulation under study. However, for most relevant cases it can be shown that this scaling is polynomial. For instance, in the case of an analogue quantum simulation of unitary dynamics, what it is usually called an always-on simulation, we have $q = 1$. For a model requiring digital

techniques q will scale polinomially if the number of terms in the Hamiltonian grows polinomially with the number of constituents, which is a physically-reasonable assumption [1, 28, 40]. In any case, we want to point out that the way in which q scales is a condition inherent to any quantum simulation process, and, hence, it is not an additional overhead introduced by our proposal. With respect to the number m, and as explained in the next section, this number does not depend on the system size, thus, from the point of view of efficiency it amounts to a constant factor.

In order to provide a complete runtime analysis of our protocol we study now the number of iterations needed to achieve a certain precision δ in the measurement of the time correlations. According to Bernstein's inequality [147] we have that

$$\Pr\left[\left|\frac{1}{L}\sum_{i=1}^{L} X_i - \langle X\rangle\right| > \delta\right] \leq 2\exp\left(\frac{-L\delta^2}{4\sigma_0^2}\right), \tag{A.1}$$

where X_i are independent random variables, and σ_0^2 is a bound on their variance. Interpreting X_i as a single observation of the real or imaginary part of the time-correlation function, we find the number of measurements needed to have a precision δ. Indeed, we have that $\left|\frac{1}{L}\sum_{i=1}^{L} X_i - \langle X\rangle\right| \leq \delta$ with probability $P \geq 1-e^{-c}$, provided that $L \geq \frac{4(1+c)}{\delta^2}$, where we have set $\sigma_0^2 \leq 1$, as we always measure Pauli observables. This implies that the number of gates that we need to implement to achieve a precision δ for the real or the imaginary part of the time-correlation function is $\frac{4(1+c)}{\delta^2}[(m+q)n-q]$. Again, c is a constant factor which does not depend nor on the order of the time correlation neither on the size of the system.

A.2 N-body interactions with Mølmer-Sørensen gates

Exponentials of tensor products of Pauli operators, $\exp[i\phi\sigma_1\otimes\sigma_2\otimes...\otimes\sigma_k]$, can be systematically constructed, up to local rotations, with a Mølmer-Sørensen gate applied over the k qubits, one local gate on one of the qubits, and the inverse Mølmer-Sørensen gate on the whole register. This can be schematized as follows,

$$U = U_{MS}(-\pi/2,0)U_{\sigma_z}(\phi)U_{MS}(\pi/2,0) = \exp[i\phi\sigma_1^z\otimes\sigma_2^x\otimes...\otimes\sigma_k^z], \tag{A.2}$$

where $U_{MS}(\theta,\phi) = \exp[-i\theta(\cos\phi S_x + \sin\phi S_y)^2/4]$, $S_{x,y} = \sum_{i=1}^{k}\sigma_i^{x,y}$ and $U_{\sigma_z}(\phi) = \exp(i\phi'\sigma_1^z)$ for odd k, where $\phi' = \phi$ for $k = 4n+1$, and $\phi' = -\phi$ for $k = 4n-1$, with positive integer n. For even k, $U_{\sigma_z}(\phi)$ is replaced by $U_{\sigma_y}(\phi) = \exp(i\phi'\sigma_1^y)$, where $\phi' = \phi$ for $k = 4n$, and $\phi' = \phi$ for $k = 4n-2$, with positive integer n. Subsequent local rotations will generate any combination of Pauli matrices in the exponential.

The replacement in the previous scheme of the central gate $U_{\sigma_z}(\phi)$ by an interaction containing a coupling with bosonic degrees of freedom, for example $U_{\sigma_z,(a+a^\dagger)}(\phi) = \exp[i\phi'\sigma_1^z(a+a^\dagger)]$, will directly provide us with

$$U = U_{MS}(-\pi/2,0)U_{\sigma_z,(a+a^\dagger)}(\phi)U_{MS}(\pi/2,0) = \exp[i\phi\sigma_1^z \otimes \sigma_2^x \otimes ... \otimes \sigma_k^z(a+a^\dagger)]. \quad \text{(A.3)}$$

In order to provide a complete recipe for systems where Mølmer-Sørensen interactions are not directly available, we want to comment that the kind of entangling quantum gates required by our algorithm, see the right hand side of Eq. (A.3) above, are always decomposable in a polynomial sequence of controlled-Z gates [40]. For example, in the case of a three-qubit system we have

$$CZ_{1,3}CZ_{1,2}e^{-i\phi\sigma_1^y}CZ_{1,2}CZ_{1,3} = \exp\left(-i\phi\sigma_1^y \otimes \sigma_2^z \otimes \sigma_3^z\right) \quad \text{(A.4)}$$

Here, $CZ_{i,j}$ is a controlled-Z gate between the i,j qubits and $e^{-i\phi\sigma_1^y}$ is local rotation applied on the first qubit. This result can be easily extended to n-qubit systems with the application of $2(n-1)$ controlled operations [40]. Therefore, it is demonstrated the polynomial character of our algorithm, and hence its efficiency, even if Mølmer-Sørensen gates are not available in our setup.

Appendix B

Embedding protocol Vs Hadamard and SWAP tests

In this Appendix, we compare the n-time correlation function protocol presented in Chapter 4 with respect previous existing methods: Hadamard test and SWAP test.

B.1 Hadamard test

Here, we describe the Hadamard test [93] to quantum compute the quantity $\langle\psi|U^\dagger V|\psi\rangle$, with U, V unitary operators and $|\psi\rangle$ the initial state of the system. The protocol can be generalised to n-time correlations functions very easily. Let us couple our system to a qubit ancilla, that is initially prepared in the state $\frac{1}{\sqrt{2}}(|e\rangle + |g\rangle)$. We perform in series a $|g\rangle$-control V gate and a $|e\rangle$-control U gate. The final state is $|\psi_f\rangle = \frac{1}{\sqrt{2}}[|e\rangle \otimes U|\psi\rangle + |g\rangle \otimes V|\psi\rangle]$. If we measure the ancilla operator $2|e\rangle\langle g| \equiv \sigma_x + i\sigma_y$, we recover the desired quantity.

The Hadamard test is performed in a setup consisting of the system of interest and a qubit, and thus in terms of space is as efficient as our algorithm. While the evolutions of the system of interest are not controlled in our protocol, the Hadamard test needs to perform control unitary operations which may not be trivial for many body Hamiltonians or Hamiltonians depending in time. In this sense our method supposes a significant step forward in simplicity and a notable reduction in the requirements of our setup. It is noteworthy to mention that our algorithm could access time correlations of systems that undergo non-unitary dynamics.

B.2 SWAP test

The SWAP test [91] allows to measure the quantity $|\langle\psi|U^\dagger V|\psi\rangle|^2$. We need two copies of the system, initially in the state $|\psi\rangle$, and a qubit ancilla, prepared in the state $\frac{1}{\sqrt{2}}(|e\rangle + |g\rangle)$, so that the initial state of the full system is $|\Psi\rangle = \frac{|e\rangle+|g\rangle}{\sqrt{2}} \otimes |\psi\rangle \otimes |\psi\rangle$. We first perform a U gate to one copy of the system, and a V gate to the other one, leading to the state $\frac{|e\rangle+|g\rangle}{\sqrt{2}} \otimes |\phi_1\rangle \otimes |\phi_2\rangle$, where we have defined $|\phi_1\rangle \equiv U|\psi\rangle$, $\phi_2\rangle \equiv V|\psi\rangle$. Then, we implement a controlled SWAP operation, which interchanges $\phi_1\rangle$ and $\phi_2\rangle$ only if the state of the ancillary qubit is $|e\rangle$. Finally we make a Hadamard rotation on the ancillary qubit. The final state is $|\psi_f\rangle = (|e\rangle [|\phi_1\rangle|\phi_2\rangle + |\phi_2\rangle|\phi_1\rangle] + |g\rangle [|\phi_1\rangle|\phi_2\rangle - |\phi_2\rangle|\phi_1\rangle])/2$. By measuring the ancillary operator σ_z, we retrieve the desired quantity.

Regarding the efficiency, while our protocol involves only one ancillary qubit, $N+1$, the SWAP test needs two copies of the system and the ancillary qubit which makes a total of $2N+1$ qubits in the N-qubit system case. This makes our protocol significantly more space saving.

Appendix C

Decomposition in Pauli Operators

In this Appendix, we discuss the decomposition of the Lindblad operators in Pauli-kind operators, which is useful in the implementation of the protocol discussed in Chapter 5. In order to implement the protocol of Chapter 4 to compute a general multitime correlation function, we need to decompose a general Lindblad operator L and observable O in Pauli-kind orthogonal matrices $\{Q_k\}_{k=1}^{d^2}$, where Q_k are both Hermitian and unitaries and d is the dimension of the system. If $d = 2^l$ for some integer l, then a basis of this kind is the one given by the tensor product of Pauli matrices. Otherwise, it is always possible to embed the problem in a larger Hilbert space, whose dimension is the closest power of 2 larger than d. Thus, we can set $\|Q_k\|_\infty = 1$ and $\|Q_k\|_2 = \sqrt{d}$, where $\|A\|_2 \equiv \sqrt{\mathrm{Tr}\,(A^\dagger A)}$ and we have redefined d as the embedding Hilbert space dimension. Here, we prove that if $\|L\|_\infty = 1$ and $L = \sum_{k=1}^M q_k Q_k$ with $M \leq d^2$, then (i) $\sum_{k=1}^M |q_k| \leq \sqrt{M}$. This relation is useful for the proofs in Appendix D. We first show that $\sum_{k=1}^M |q_k|^2 \leq 1$:

$$\sum_{k=1}^{M} |q_k|^2 = \frac{1}{d}\sum_{k=1}^{M} |q_k|^2 \|Q_k\|_2^2 = \frac{1}{d}\left\|\sum_{k=1}^{M} q_k Q_k\right\|_2^2 = \frac{1}{d}\|L\|_2^2 \leq \|L\|_\infty^2 = 1, \tag{C.1}$$

where we have used the orthogonality of the matrices Q_i, i.e. $\mathrm{Tr}\,(Q_i^\dagger Q_j) = \mathrm{Tr}\,(Q_i Q_j) = d\delta_{ij}$. The relation (i) follows simply from the norm inequality for a M-dimensional vector v: $\|v\|_1 \leq \sqrt{M}\|v\|_2$.

Appendix D

Simulation of dissipative systems: nth-order correction terms

In this Appendix, we provide a proof of Eq. (5.11) of the main text:

$$\left| \sum_{[i_1,\dots,i_n]=1}^{N} \int dV_n \, \langle A_{[i_1,\cdots,i_n]}(\vec{s})\rangle - \frac{(Nt)^n}{n!|\Omega_n|} \sum_{\Omega_n} \tilde{A}_{\vec{\omega}}(\vec{t}) \right| \leq \delta_n \tag{D.1}$$

with probability higher than $1-e^{-\beta}$, provided that $|\Omega_n| > \frac{36M_O^2(2+\beta)}{\delta_n^2}\frac{(2\bar{\gamma}MNt)^{2n}}{n!^2}$. Here, $\bar{\gamma} = \max_{i,s\in[0,t]}|\gamma_i(s)|$, $M = \max_i M_i$ where M_i is defined by the Pauli decomposition of the Lindblad operators $L_i = \sum_{k=1}^{M_i} q_k^i Q_k^i$, M_O is the Pauli decomposition of the observable O that we will to measure, $[\vec{\omega},\vec{t}] \in \Omega_n \subset \{[\vec{\omega},\vec{t}] \mid \vec{\omega} = [i_1,\dots,i_n], i_k \in [1,N], \vec{t} \in V_n\}$ and $[\vec{\omega},\vec{t}]$ are sampled uniformly and independently, $|\Omega_n|$ is the size of Ω_n, and $\tilde{A}_{\vec{\omega}}(\vec{t})$ corresponds to single-shot measurements of $A_{\vec{\omega}}(\vec{t})$. Notice that V_n is the integration volume corresponding to the n-th order term, and $|V_n| = t^n/n!$.

First, we write $\tilde{A}_{\vec{\omega}}(\vec{t}) = \langle A_{\vec{\omega}}(\vec{t})\rangle + \tilde{\epsilon}_{[\vec{\omega},\vec{t}]}$, where $\tilde{\epsilon}_{[\vec{\omega},\vec{t}]}$ is the shot-noise. Note that, due to the previous identity, $\langle \epsilon_{[\vec{\omega},\vec{t}]}\rangle = 0$. We have to bound the following quantity

$$\begin{aligned} &\left| \sum_{[i_1,\dots,i_n]=1}^{N} \int dV_n \, \langle A_{[i_1,\dots,i_n]}(\vec{s})\rangle - \frac{N^n|V_n|}{|\Omega_n|} \sum_{\Omega_n} \tilde{A}_{\vec{\omega}}(\vec{t}) \right| \leq \\ &\leq \left| \sum_{[i_1,\dots,i_n]=1}^{N} \int dV_n \, \langle A_{[i_1,\dots,i_n]}(\vec{s})\rangle - \frac{N^n|V_n|}{|\Omega_n|} \sum_{\Omega_n} \langle A_{\vec{\omega}}(\vec{t})\rangle \right| + \left| \frac{N^n|V_n|}{|\Omega_n|} \sum_{\Omega_n} \tilde{\epsilon}_{[\vec{\omega},\vec{t}]} \right|. \end{aligned} \tag{D.2}$$

The first term in the right side of Eq. (D.2) is basically the error bound in a Montecarlo integration, while the second term is small as the variance of ϵ is bounded. Indeed, both quantities can be bounded using the Bernstein inequality [147]:

Theorem (Bernstein Inequality [147]). Let $X_1, \ldots, X_m$ be independent zero-mean random variables. Suppose $\mathbb{E}[X_i^2] \leq \sigma_0^2$ and $|X_i| \leq c$. Then for any $\delta > 0$,

$$\Pr\left[\left|\sum_{i=1}^{m} X_i\right| > \delta\right] \leq 2\exp\left(\frac{-\delta^2}{4m\sigma_0^2}\right), \tag{D.3}$$

provided that $\delta \leq 2m\sigma_0^2/c$.

To compute the first term in the right-hand side of Eq. (D.2), we sample $[\vec{\omega}, \vec{t}]$ uniformly and independently in order to have that

$$\mathbb{E}\left[\frac{N^n|V_n|}{|\Omega_n|}\langle A_{\vec{\omega}}(\vec{t})\rangle\right] = \frac{1}{|\Omega_n|}\sum_{i_1,\ldots,i_n=1}^{N}\int dV_n\ \langle A_{[i_1,\ldots,i_n]}(\vec{s})\rangle. \tag{D.4}$$

We define the quantity $X_{[\vec{\omega},\vec{t}]} \equiv \frac{N^n|V_n|}{|\Omega_n|}\langle A_{\vec{\omega}}(\vec{t})\rangle - \frac{1}{|\Omega_n|}\sum_{i_1,\ldots,i_n=1}^{N}\int dV_n\ \langle A_{[i_1,\ldots,i_n]}(\vec{s})\rangle$, and look for an estimate $\left|\sum_{\Omega_n} X_{[\vec{\omega},\vec{t}]}\right|$, where $\mathbb{E}[X_{[\vec{\omega},\vec{t}]}] = 0$. We have that

$$\begin{aligned}\mathbb{E}\left[X^2_{[\vec{\omega},\vec{t}]}\right] &= \frac{1}{|\Omega_n|^2}N^{2n}|V_n|^2\mathbb{E}[\langle A_{\vec{\omega}}(\vec{t})\rangle^2] - \frac{1}{|\Omega_n|^2}\left(\sum_{[i_1,\ldots,i_n]=1}^{N}\int dV_n\ \langle A_{[i_1,\ldots,i_n]}(\vec{s})\rangle\right)^2 \leq \\ &\leq \frac{N^n|V_n|}{|\Omega_n|^2}\sum_{[i_1,\ldots,i_n]=1}^{N}\int dV_n\ \langle A_{[i_1,\ldots,i_n]}(\vec{s})\rangle^2 \leq \frac{N^{2n}|V_n|^2}{|\Omega_n|^2}\max_{[i_1,\ldots,i_n],\vec{s}}\langle A_{[i_1,\ldots,i_n]}(\vec{s})\rangle^2,\end{aligned} \tag{D.5}$$

where we have used the inequality $(\int dV\ f)^2 \leq |V|\int dV\ f^2$. Moreover, we have that

$$\begin{aligned}|X_{[\vec{\omega},\vec{t}]}| &= \frac{1}{|\Omega_n|}\left|N^n|V_n|\langle A_{\vec{\omega}}(\vec{t})\rangle - \sum_{[i_1,\ldots,i_n]=1}^{N}\int dV_n\ \langle A_{[i_1,\ldots,i_n]}(\vec{s})\rangle\right| \\ &\leq \frac{2N^n|V_n|}{|\Omega_n|}\max_{[i_1,\ldots,i_n],\vec{s}}|\langle A_{[i_1,\ldots,i_n]}(\vec{s})\rangle|,\end{aligned} \tag{D.6}$$

where we have used the inequality $|\sum_{i=1}^{N}\int dV\ f| \leq N|V|\max|f|$.
Now, recall that

$$A_{[i_1,\ldots,i_n]}(\vec{s}) \equiv e^{s_n\mathcal{L}^\dagger_{H_s}}\mathcal{L}_D^{s_n,i_n\dagger}\ldots\mathcal{L}_D^{s_2,i_2\dagger}e^{(s_1-s_2)\mathcal{L}^\dagger_{H_s}}\mathcal{L}_D^{s_1,i_1\dagger}e^{(t-s_1)\mathcal{L}^\dagger_{H_s}}O, \tag{D.7}$$

where $\mathcal{L}_D^{s,i}\xi \equiv \gamma_i(s)\left(L_i\xi L_i^\dagger - \frac{1}{2}\{L_i^\dagger L_i, \xi\}\right)$, and $\mathcal{L}^\dagger\xi \equiv (\mathcal{L}\xi)^\dagger$ for a general superoperator $\mathcal{L}$. It follows that $\max_{[i_1,\ldots,i_n],\vec{s}}\langle A_{[i_1,\ldots,i_n]}(\vec{s})\rangle^2 \leq (2\bar{\gamma})^{2n}\|O\|_\infty^2\prod_{k=1}^{n}\|L_{i_k}\|_\infty^4 = (2\bar{\gamma})^{2n}$, and $\max_{[i_1,\ldots,i_n],\vec{s}}|\langle A_{[i_1,\ldots,i_n]}(\vec{s})\rangle| \leq (2\bar{\gamma})^n$, where $\bar{\gamma} = \max_{i,s\in[0,t]}|\gamma_i(s)|$ and we have set $\|O\|_\infty = 1$ and $\|L_i\|_\infty = 1$. Here, we have used the fact that $\langle A_{[i_1,\ldots,i_n]}(\vec{s})\rangle$ is real, the inequality $|\mathrm{Tr}\,(AB)|^2 \leq \|A\|_\infty\|B\|_1$, and the result in Eq. (E.2) of the next Appendix.

Now, we can directly use the Bernstein inequality, obtaining

$$\Pr\left[\left|\sum_{\Omega_n} X_{[\vec{\omega},\vec{t}]}\right| > \delta'\right] \leq 2\exp\left(-\frac{n!^2|\Omega_n|\delta'^2}{4(2\bar{\gamma}Nt)^{2n}}\right) \equiv p_1 \tag{D.8}$$

provided that $\delta' \leq (2\bar{\gamma}Nt)^n/n!$, and where we have set $|V_n| = t^n/n!$.

Now, we show that the second term in the right hand side of Eq (D.2) can be bounded for all Ω_n. From the definition of $\tilde{\epsilon}_{[\vec{\omega},\vec{t}]}$, we note that

$$\begin{aligned}\mathbb{E}\left[\frac{N^n|V_n|}{|\Omega_n|}\tilde{\epsilon}_{[\vec{\omega},\vec{t}]}\right] &= \frac{N^n|V_n|}{|\Omega_n|}\sum_i \tilde{\epsilon}^i_{[\vec{\omega},\vec{t}]}p^i_{[\vec{\omega},\vec{t}]} = \\ &= \frac{N^n|V_n|}{|\Omega_n|}\left(\sum_i \tilde{A}^i_{\vec{\omega}}(\vec{t})p^i_{[\vec{\omega},\vec{t}]} - \langle A_{\vec{\omega}}(\vec{t})\rangle\right) = 0\end{aligned} \tag{D.9}$$

where $\tilde{\epsilon}^i_{[\vec{\omega},\vec{t}]}$ $(\tilde{A}^i_{\vec{\omega}}(\vec{t}))$ is a particular value that the random variable $\tilde{\epsilon}_{[\vec{\omega},\vec{t}]}$ $(\tilde{A}_{\vec{\omega}}(\vec{t}))$ can take, and $p^i_{[\vec{\omega},\vec{t}]}$ is the corresponding probability. Notice that the possible values of the random variable $\tilde{\epsilon}_{[\vec{\omega},\vec{t}]}$ depend on the Pauli decomposition of $A_{\vec{\omega}}(\vec{t})$. In fact, $A_{\vec{\omega}}(\vec{t})$ is a sum of n-time correlation functions of the Lindblad operators, and our method consists in decomposing each Lindblad operator in Pauli operators (see Appendix C), and then measuring the real and the imaginary part of the corresponding time-correlation functions. As the final result has to be real, eventually we consider only the real part of $\tilde{A}_{\vec{\omega}}(\vec{t})$, so that also $\tilde{\epsilon}_{[\vec{\omega},\vec{t}]}$ can take only real values. In the case $n = 2$, one of the terms to be measured is

$$\begin{aligned}&L^\dagger_{\omega_2}(t_2)L^\dagger_{\omega_1}(t_1)O(t)L_{\omega_1}(t_1)L_{\omega_2}(t_2) = \\ &\quad = \sum_{l=1}^{M_O}\sum_{k_1,k_2,k_1',k_2'=1}^{M} q^O_l q^{\omega_1 *}_{k_1} q^{\omega_2 *}_{k_2} q^{\omega_1}_{k_1'} q^{\omega_2}_{k_2'}\, Q^{\omega_2\dagger}_{k_2}(t_2)Q^{\omega_1\dagger}_{k_1}(t_1)Q^O_l(t)Q^{\omega_1}_{k_1'}(t_1)Q^{\omega_2}_{k_2'}(t_2),\end{aligned} \tag{D.10}$$

where we have used the Pauli decompositions $L_{\omega_i} = \sum_{k_i=1}^{M_{\omega_i}} q^{\omega_i}_{k_i} Q^{\omega_i}_{k_i}$, $O = \sum_{l=1}^{M_O} q^O_l Q^O_l$, and we have defined $M \equiv \max_i M_{\omega_i}$. We will find a bound for the case $n = 2$, and the general case will follow straightforwardly. For the term in Eq. (D.10), we have that

$$\begin{aligned}&\sum_{l=1}^{M_O}\sum_{k_1,k_2,k_1',k_2'=1}^{M} |q^O_l||\Re\, q^{\omega_1 *}_{k_1} q^{\omega_2 *}_{k_2} q^{\omega_1}_{k_1'} q^{\omega_2}_{k_2'}(\lambda^{\omega_1\omega_2}_{k_2k_1lk_1'k_2',r} + i\lambda^{\omega_1\omega_2}_{k_2k_1lk_1'k_2',im})| \leq \\ &\quad \leq 2\sum_{l=1}^{M_O}\sum_{k_1,k_2,k_1',k_2'=1}^{M} |q^O_l||q^{\omega_1 *}_{k_1} q^{\omega_2 *}_{k_2} q^{\omega_1}_{k_1'} q^{\omega_2}_{k_2'}|\, \|Q^{\omega_2\dagger}_{k_2}(t_2)Q^{\omega_1\dagger}_{k_1}(t_1)Q^O_l(t)Q^{\omega_1}_{k_1'}(t_1)Q^{\omega_2}_{k_2'}(t_2)\|_\infty \leq \\ &\quad \leq 2\sum_{l=1}^{M_O}|q^O_l| \sum_{k_1,k_2,k_1',k_2'=1}^{M} |q^{\omega_1 *}_{k_1} q^{\omega_2 *}_{k_2} q^{\omega_1}_{k_1'} q^{\omega_2}_{k_2'}| \leq 2\sqrt{M_O}\, M^2,\end{aligned} \tag{D.11}$$

where we have defined the real part ($\lambda^{\omega_1\omega_2}_{k_2k_1lk'_1k'_2,r}$) and the imaginary part ($\lambda^{\omega_1\omega_2}_{k_2k_1lk'_1k'_2,im}$) of the single-shot measurement of $Q^{\omega_2\dagger}_{k_2}(t_2)Q^{\omega_1\dagger}_{k_1}(t_1)Q^{O}_{l}(t)Q^{\omega_1}_{k'_1}(t_1)Q^{\omega_2}_{k'_2}(t_2)$, and we have used the fact that $\|Q^i_k\|_\infty = 1$, $\|Q^O_l\|_\infty = 1$, and relation (i) of Appendix C. Eq. (D.11) is a bound on the outcomes of $L^\dagger_{\omega_2}(t_2)L^\dagger_{\omega_1}(t_1)O(t)L_{\omega_1}(t_1)L_{\omega_2}(t_2)$. Notice that the bound in Eq. (D.11) neither depends on the particular order of the Pauli operators, nor on the times s_i, so it holds for a general term in the sum defining $A_{\vec{\omega}}(\vec{t})$. Thus, we find that, in the case $n = 2$, $\tilde{A}_{\vec{\omega}}(\vec{t})$ is upper bounded by $|\tilde{A}_{\vec{\omega}}(\vec{t})| \leq 2\sqrt{M_O}(2\bar{\gamma}M)^2$. In the general case of order n, it is easy to show that $|\tilde{A}_{\vec{\omega}}(\vec{t})| \leq 2\sqrt{M_O}(2\bar{\gamma}M)^n$. It follows that

$$\begin{aligned}\left|\frac{N^n|V_n|}{|\Omega_n|}\tilde{\epsilon}_{[\vec{\omega},\vec{t}]}\right| &= \frac{N^n|V_n|}{|\Omega_n|}\left|\tilde{A}_{\vec{\omega}}(\vec{t}) - \langle A_{\vec{\omega}}(\vec{t})\rangle\right| \leq \\ &\leq \frac{(2\bar{\gamma}N)^n|V_n|}{|\Omega_n|}(1 + 2\sqrt{M_O}M^n) \leq \\ &\leq \frac{3\sqrt{M_O}(2\bar{\gamma}MN)^n|V_n|}{|\Omega_n|}. \end{aligned} \tag{D.12}$$

Regarding the bound on the variance, we have that

$$\begin{aligned}\mathbb{E}\left[\left(\frac{N^n|V_n|}{|\Omega_n|}\tilde{\epsilon}_{[\vec{\omega},\vec{t}]}\right)^2\right] &= \sum_i \left(\frac{N^n|V_n|}{|\Omega_n|}\tilde{\epsilon}^i_{[\vec{\omega},\vec{t}]}\right)^2 p^i_{[\vec{\omega},\vec{t}]} \leq \\ &\leq \frac{N^{2n}|V_n|^2}{|\Omega_n|^2}\sum_i \tilde{A}^{i\,2}_{\vec{\omega}}(\vec{t})p^i_{[\vec{\omega},\vec{t}]} \leq \\ &\leq \frac{N^{2n}|V_n|^2}{|\Omega_n|^2}\max_i \tilde{A}^{i\,2}_{\vec{\omega}}(\vec{t}) = \\ &= \frac{N^{2n}|V_n|^2}{|\Omega_n|^2}\left(\max_i |\tilde{A}^i_{\vec{\omega}}(\vec{t})|\right)^2 \leq \\ &\leq \frac{4M_O(2\bar{\gamma}MN)^{2n}|V_n|^2}{|\Omega_n|^2}, \end{aligned} \tag{D.13}$$

Using Bernstein inequality, we obtain

$$\Pr\left[\left|\frac{N^n|V_n|}{|\Omega_n|}\sum_{\Omega_n}\tilde{\epsilon}_{[\vec{\omega},\vec{t}]}\right| > \delta''\right] \leq 2\exp\left(-\frac{n!^2|\Omega_n|\delta''^2}{16M_O^2(2\bar{\gamma}MNt)^{2n}}\right) \equiv p_2, \tag{D.14}$$

provided that $\delta'' \leq \frac{8}{3}\sqrt{M_O}(2\bar{\gamma}MNt)^n/n!$, where we have set, as before, $|V_n| = t^n/n!$. Now, choosing $\delta' = \frac{1}{2M^n+1}\delta_n$, $\delta'' = \frac{2M^n}{2M^n+1}\delta_n$, $|\Omega_n| > \frac{36M_O^2(2+\beta)}{\delta_n^2}\frac{(2\bar{\gamma}MNt)^{2n}}{n!^2}$, we have that $p_1, p_2 \leq \frac{e^{-\beta}}{2}$. Notice that $\delta_n \leq (2\bar{\gamma}Nt)^n/n!$ always holds, so the conditions on δ', δ'' are satisfied. By using the union bound, we conclude that

$$\Pr\left[\left|\sum_{[i_1,\ldots,i_n]=1}^{N}\int dV_n\,\langle A_{[i_1,\cdots,i_n]}(\vec{s})\rangle - \frac{(Nt)^n}{n!|\Omega_n|}\sum_{\Omega_n}\tilde{A}_{\vec{\omega}}(\vec{t})\right| > \delta_n\right] \leq p_1 + p_2 \leq e^{-\beta}. \tag{D.15}$$

Appendix E

Simulation of dissipative processes: error bounds and efficiency

In this Appendix, we provide several technical proofs of the results in Chapter 5, which describe the efficiency of the proposed method.

E.1 Error bounds

In this section, we provide the proof for the bound in Eq. (5.15)

$$D_1(\rho(t), \tilde{\rho}_0(t)) \leq \frac{1}{2}\int_0^t ds\ \|\mathcal{L}_D^s\|_{1\to 1}\|\rho(s)\|_1 \leq \sum_{i=1}^{N} |\gamma_i(\epsilon_i)|\|L_i\|_\infty^2 t,$$

and the general bound in Eq. (5.16) of the main text

$$D_1(\rho(t), \tilde{\rho}_n(t)) \leq \prod_{k=0}^{n}\left[2\sum_{i_k=1}^{N}|\gamma_{i_k}(\epsilon_{i_k})|\right]\frac{t^{n+1}}{2(n+1)!} \leq \frac{(2\bar{\gamma}Nt)^{n+1}}{2(n+1)!},$$

with $\bar{\gamma} = \max_{i,s\in[0,t]}|\gamma_i(s)|$. We note that

$$\begin{aligned} D_1(\rho(t), \tilde{\rho}_0(t)) &\leq \frac{1}{2}\int_0^t ds\ \|\mathcal{L}_D^s\|_{1\to 1}\|\rho(s)\|_1 = \\ &= \frac{1}{2}\int_0^t ds\ \|\mathcal{L}_D^s\|_{1\to 1}, \end{aligned} \tag{E.1}$$

where we have introduced the induced superoperator norm $\|\mathcal{A}\|_{1\to 1} \equiv \sup_\sigma \frac{\|\mathcal{A}\sigma\|_1}{\|\sigma\|_1}$. Moreover, the following bound holds

$$\begin{aligned}\|\mathcal{L}_D^t\sigma\|_1 &= \left\|\sum_{i=1}^N \gamma_i(t)\left(L_i\sigma L_i^\dagger - \frac{1}{2}L_i^\dagger L_i\sigma - \frac{1}{2}\sigma L_i^\dagger L_i\right)\right\|_1 \leq \\ &\leq \sum_{i=1}^N |\gamma_i(t)|\left(\|L_i\sigma L_i^\dagger\|_1 + \frac{1}{2}\|L_i^\dagger L_i\sigma\|_1 + \frac{1}{2}\|\sigma L_i^\dagger L_i\|_1\right) \leq \\ &\leq 2\sum_{i=1}^N |\gamma_i(t)|\|L_i\|_\infty^2\|\sigma\|_1, \end{aligned} \tag{E.2}$$

where we have used the triangle inequality and the inequality $\|AB\|_1 \leq \|A\|_\infty\|B\|_1$. Eq. (E.2) implies that $\|\mathcal{L}_D^t\|_{1\to 1} \leq 2\sum_{i=1}^N |\gamma_i(t)|\|L_i\|_\infty^2$. Inserting it into Eq. (E.1), it is found that

$$\begin{aligned}D_1(\rho(t),\tilde{\rho}_0(t)) &\leq \sum_{i=1}^N \|L_i\|_\infty^2 \int_0^t ds\ |\gamma_i(s)| = \\ &= \sum_{i=1}^N |\gamma_i(\epsilon_i)|\|L_i\|_\infty^2 t, \end{aligned} \tag{E.3}$$

where we have assumed that $\gamma_i(t)$ are continuous functions in order to use the mean-value theorem ($0 \leq \epsilon_i \leq t$). Indeed, $|\gamma_i(\epsilon_i)| = \frac{1}{t}\int_0^t ds\ |\gamma_i(s)|$, that can be directly calculated or estimated.

The bound in Eq. (5.16) has to been proved by induction. Let us assume that Eq.(5.16) holds for the order $n-1$. We have that

$$\begin{aligned}D_1(\rho(t),\tilde{\rho}_n(t)) &\leq \int_0^t ds\ \|\mathcal{L}_D\|_{1\to 1} D_1(\rho(s),\tilde{\rho}_{n-1}(s)) \leq \\ &\leq \prod_{k=0}^{n-1}\left[2\sum_{i_k=1}^N |\gamma_{i_k}(\epsilon_{i_k})|\|L_{i_k}\|_\infty^2\right]\sum_{i=1}^N \|L_i\|_\infty^2 \frac{1}{n!}\int_0^t ds\ |\gamma_i(s)|s^n, \end{aligned} \tag{E.4}$$

where we need to evaluate the quantities $\int_0^t ds\ |\gamma_i(s)|s^n$. By using the mean-value theorem, we have $\int_0^t ds\ \gamma_i(s)s^n = |\gamma_i(\epsilon_i)|\int_0^t ds\ s^n$, with $0 \leq \epsilon_i \leq t$, and Eq. (5.16) follows straightforwardly. In any case, we can evaluate $\int_0^t ds\ |\gamma_i(s)|s^n$ by solving directly the integral or we can estimate it by using Hölder's inequalities:

$$\int_0^t ds\ |\gamma_i(s)|s^n \leq \left\{\sqrt{\int_0^t ds\ \gamma_i(s)^2}\sqrt{\frac{t^{2n+1}}{2n+1}}\ ,\ \max_{s\in[0,t]}|\gamma_i(s)|\ \frac{t^{n+1}}{n+1}\right\}. \tag{E.5}$$

E.2 Error bounds for the expectation value of an observable

In this section, we find an error bound for the expectation value of a particular observable O. As figure of merit, we choose $D_O(\rho_1,\rho_2) \equiv |\mathrm{Tr}\left(O(\rho_1-\rho_2)\right)|/(2\|O\|_\infty)$. The quantity $D_O(\rho_1,\rho_2)$ tells us how close the expectation value of O on ρ_1 is to the expectation value of O on ρ_2, and it is always bounded by the trace distance, i.e. $D_O(\rho_1,\rho_2) \leq D_1(\rho_1,\rho_2)$. Recall Eq. 5.13 of the main text:

$$\tilde{\rho}_n(t) = e^{t\mathcal{L}_H}\rho(0) + \int_0^t ds\; e^{(t-s)\mathcal{L}_H}\mathcal{L}_D^s\,\tilde{\rho}_{n-1}(s). \tag{E.6}$$

By taking the expectation value of O in both sides, we find that

$$\begin{aligned} D_O(\rho(t),\tilde{\rho}_n(t)) &= \frac{1}{2\|O\|_\infty}\left|\int_0^t ds\;\mathrm{Tr}\left(e^{(t-s)\mathcal{L}_H}\mathcal{L}_D^s(\rho(s)-\tilde{\rho}_{n-1}(s))O\right)\right| = \\ &= \frac{1}{2\|O\|_\infty}\left|\int_0^t ds\;\mathrm{Tr}\left(\mathcal{L}_D^{s\dagger}O(\rho(s)-\tilde{\rho}_{n-1}(s))\right)\right| \leq \\ &\leq \frac{1}{\|O\|_\infty}\int_0^t ds\;\|\mathcal{L}_D^{s\dagger}O\|_\infty D_1(\rho(s),\tilde{\rho}_{n-1}(s)) \leq \\ &\leq \frac{\|\mathcal{L}_D^{s\dagger}O\|_\infty}{\|O\|_\infty}(2\bar{\gamma}N)^n\,\frac{t^{n+1}}{2(n+1)!}, \end{aligned} \tag{E.7}$$

where $\mathcal{L}_D^{s\dagger}O = \sum_{i=1}^N \gamma_i(s)\left(L_i^\dagger O L_i - \frac{1}{2}\{L_i^\dagger L_i, O\}\right)$. The bound in Eq. (E.7) is particularly useful when L_i and O have a tensor product structure. In fact, in this case, the quantity $\|\mathcal{L}_D^{s\dagger}O\|_\infty$ can be easily calculated or bounded. For example, consider a 2-qubit system with $L_1 = \sigma^-\otimes\mathbb{I}$, $L_2 = \mathbb{I}\otimes\sigma^-$, $\gamma_i(s) = \gamma > 0$ and the observable $O = \sigma_z\otimes\mathbb{I}$. Simple algebra leads to $\|\mathcal{L}_D^{s\dagger}O\|_\infty = \gamma\|(\mathbb{I}+\sigma_z)\otimes\mathbb{I}\|_\infty = \gamma\|\mathbb{I}+\sigma_z\|_\infty\|\mathbb{I}\|_\infty = 2\gamma$, where we have used the identity $\|A\otimes B\|_\infty = \|A\|_\infty\|B\|_\infty$.

E.3 Total number of measurements

In this section, we provide a magnitude for the scaling of the number of measurements needed to simulate a certain dynamics with a given error ε and for a time t. We have proved in section E.1 that

$$\varepsilon' \equiv D_1(\rho(t),\tilde{\rho}_n(t)) \leq \frac{(2\bar{\gamma}Nt)^{n+1}}{2(n+1)!}, \tag{E.8}$$

where $\bar{\gamma} \equiv \max_i|\gamma_i|$. We want to establish at which order K we have to truncate in order to have an error ε' in the trace distance. We have that, if $n \geq ex + \log\frac{1}{\bar{\varepsilon}}$, with

$x \geq 0$ and $\tilde{\varepsilon} \leq 1$, then $\frac{x^n}{n!} \leq \tilde{\varepsilon}$. In fact

$$\frac{x^n}{n!} \leq \left(\frac{ex}{n}\right)^n \leq \left(1 + \frac{\log \frac{1}{\tilde{\varepsilon}}}{ex}\right)^{-ex-\log \frac{1}{\tilde{\varepsilon}}} \leq \left(1 + \frac{\log \frac{1}{\tilde{\varepsilon}}}{ex}\right)^{-ex} \leq e^{-\log \frac{1}{\tilde{\varepsilon}}} = \tilde{\varepsilon}, \tag{E.9}$$

where we have used the Stirling inequality $n! \geq \sqrt{2\pi n}\,(n/e)^n \geq (n/e)^n$. This implies that, if we truncate at the order $K \geq 2e\bar{\gamma}Nt + \log \frac{1}{2\varepsilon'} - 1 = O(2e\bar{\gamma}Nt + \log \frac{1}{\varepsilon'})$, then we have an error lower than ε' in the trace distance. The total number of measurements in order to apply the protocol up to an error $\varepsilon' + \sum_{n=0}^{K} \delta_n$ is bounded by $\sum_{n=0}^{K} 3^n |\Omega_n|$. If we choose $\varepsilon' = c\varepsilon$, $\delta_n = (1-c)\frac{\varepsilon}{(K+1)}$ $(0 < c < 1)$, we have that the total number of measurements to simulate the dynamics at time t up to an error ε is bounded by

$$\begin{aligned}
\sum_{n=0}^{K} 3^n |\Omega_n| &= \frac{36 M_O^2 (2+\beta)(1+K)^2}{(1-c)^2\varepsilon^2} \sum_{n=0}^{K} \frac{(6\bar{\gamma}NMt)^{2n}}{n!^2} \leq \\
&\leq \frac{36 M_O^2 (2+\beta)(1+K)^2}{(1-c)^2\varepsilon^2} e^{12\gamma NMt} = \\
&= O\left(\left(6\bar{t} + \log \frac{1}{\varepsilon}\right)^2 \frac{e^{12M\bar{t}}}{\varepsilon^2}\right),
\end{aligned} \tag{E.10}$$

where we have defined $\bar{t} = \bar{\gamma}Nt$.

Appendix F

Quantum simulation of non-Hermitian Hamiltonians: error bounds

In this Appendix, we show how to apply the bounds found in Chapter 5 and in Appendix E to the simulation of a non-Hermitian Hamiltonian $J = H - i\Gamma$, with H and Γ Hermitian operators. In this case, the Schrödinger equation reads

$$\frac{d\rho}{dt} = -i[H, \rho] - \{\Gamma, \rho\} = (\mathcal{L}_H + \mathcal{L}_\Gamma)\rho, \tag{F.1}$$

where $\mathcal{L}_\Gamma$ is defined by $\mathcal{L}_\Gamma \sigma \equiv -\{\Gamma, \sigma\}$. Our method consists in considering $\mathcal{L}_\Gamma$ as a perturbative term. To ascertain the reliability of the method, we have to show that bounds similar to those in Eqs. (5.15)-(5.16) of the main text hold. Indeed, after finding a bound for $\|\rho(t)\|_1$ and $\|\mathcal{L}_\Gamma\|_{1\to 1}$, the result follows by induction, as in the previous case.

For a pure state, the Schrödinger equation for the projected wavefuntion reads [138]

$$\frac{dP\psi(t)}{dt} = -iP\mathbf{H}P\psi(t) - \int_0^t ds P\mathbf{H}Qe^{-iQ\mathbf{H}Qs}Q\mathbf{H}P\psi(t-s), \tag{F.2}$$

where $P + Q = \mathbb{I}$ and $\mathbf{H}$ is the Hamiltonian of the total system. One can expand $\psi(t-s)$ in powers of s, i.e. $\psi(t-s) = \sum_{n=0}^{\infty} \frac{(-s)^n}{n!}\psi^{(n)}(t)$, and then truncate the series to a certain order, depending on how fast $e^{-iQ\mathbf{H}Qs}$ changes. Finally one can find, by iterative substitution, an equation of the kind $dP\psi(t)/dt = JP\psi(t)$, and generalise it to the density matrix case, achieving the equation (F.1), where ρ is the density matrix of the projected system. If the truncation is appropriately done, then we always have $\|\rho(t)\|_1 \leq 1\ \forall t \geq 0$ by construction. For instance, in the Markovian limit, the integral

in Eq. (F.2) has a contribution only for $s = 0$, and we reach an effective Hamiltonian $J = P\mathbf{H}P - \frac{i}{2}P\mathbf{H}Q\mathbf{H}P \equiv H - i\Gamma$. Here, Γ is positive semidefinite, and $\|\rho(t)\|_1$ can only decrease in time.

Now, one can easily find that

$$\|\mathcal{L}_\Gamma \sigma\|_1 \leq 2\|\Gamma\|_\infty \|\sigma\|_1. \tag{F.3}$$

Hence, $\|\mathcal{L}_\Gamma\|_{1\to 1} \leq 2\|\Gamma\|_\infty$. With these two bounds, it follows that

$$D_1(\rho(t), \tilde{\rho}_0(t)) \leq \frac{1}{2}\int_0^t ds\, \|\mathcal{L}_\Gamma\|_{1\to 1}\|\rho(s)\|_1 \leq \frac{1}{2}\int_0^t ds\, \|\mathcal{L}_\Gamma\|_{1\to 1} \leq \|\Gamma\|_\infty t. \tag{F.4}$$

One can find bounds for an arbitrary perturbative order by induction, as in the dissipative case.

Bibliography

[1] S. Lloyd, Science **273**, 1073 (1996).

[2] I. M. Georgescu, S. Ashhab, and F. Nori, *Rev. Mod. Phys.* **86**, 153 (2014).

[3] R. P. Feynman, Int. J. Theor. Phys. **21**, 467 (1982).

[4] P. Hauke, F. M. Cucchietti, L. Tagliacozzo, I. Deutsch, and M. Lewenstein, Rep. Prog. Phys. **75**, 082401 (2012).

[5] A. Aspuru-Guzik and P. Walther, Nature Phys. **8**, 285 (2012).

[6] R. Blatt and C. F. Roos, Nature Phys. **8**, 277 (2012).

[7] I. Bloch, J. Dalibard, and S. Nascimbene, Nature Phys. **8**, 267 (2012).

[8] R. Barends, L. Lamata, J. Kelly, L. Garcia-Alvarez, A. G. Fowler, A. Megrant, E. Jeffrey, T. C. White, D. Sank, J. T. Mutus, B. Campbell, Y. Chen, Z. Chen, B. Chiaro, A. Dunsworth, I.-C. Hoi, C. Neill, P. J. J. O'Malley, C. Quintana, P. Roushan, A. Vainsencher, J. Wenner, E. Solano, and J. Martinis, arXiv:1501.07703 (2015).

[9] L. J. Garay, J. R. Anglin, J. I. Cirac, and P. Zoller, Phys. Rev. Lett. **85**, 4643 (2000).

[10] N. Goldman, A. Kubasiak, A. Bermudez, P. Gaspard, M. Lewenstein, and M. A. Martin-Delgado, Phys. Rev. Lett. **103**, 035301 (2009).

[11] J. I. Cirac, P. Maraner, and J. K. Pachos, Phys. Rev. Lett. **105**, 190403 (2010).

[12] M. Greiner, O. Mandel, T. Esslinger, T. W. Hänsch, and I. Bloch, Nature **415**, 39 (2002).

[13] H. Weimer, M. Müller, I. Lesanovsky, P. Zoller, and H. P. Büchler, Nat. Phys. **6**, 382 (2010).

[14] D. Ballester, G. Romero, J. J. García-Ripoll, F. Deppe, and E. Solano, Phys. Rev. X. **2**, 021007 (2012).

[15] J. S. Pedernales, R. Di Candia, D. Ballester, and E. Solano, New J. Phys. **15**, 055008 (2013).

[16] E. Jané, G. Vidal, W. Dür, P. Zoller, and J. I. Cirac, Quant. Inf. and Comput. **3**, 15 (2003).

[17] D. Porras and J. I. Cirac, Phys. Rev. Lett. **92**, 207901 (2004).

[18] A. Friedenauer, H. Schmitz, J. T. Glueckert, D. Porras, and T. Schätz, Nat. Phys. **4**, 757 (2008).

[19] K. Kim, M.-S. Chang, S. Korenblit, R. Islam, E. E. Edwards, J. K. Freericks, G.-D. Lin, L.-M. Duan, and C. Monroe, Nature **465**, 590 (2010).

[20] B. P. Lanyon, C. Hempel, D. Nigg, M. Müller, R. Gerritsma, F. Zähringer, P. Schindler, J. T. Barreiro, M. Rambach, G. Kirchmair, M. Hennrich, P. Zoller, R. Blatt, and C. F. Roos, Science **334**, 57 (2011).

[21] L. Lamata, J. León, T. Schätz, and E. Solano, Phys. Rev. Lett. **98**, 253005 (2007).

[22] R. Gerritsma, G. Kirchmair, F. Zähringer, E. Solano, R. Blatt, and C. F. Roos, Nature **463**, 68 (2010).

[23] J. Casanova, J. J. García-Ripoll, R. Gerritsma, C. F. Roos, and E. Solano, Phys. Rev. A **82**, 020101 (2010).

[24] R. Gerritsma, B. P. Lanyon, G. Kirchmair, F. Zähringer, C. Hempel, J. Casanova, J. J. García-Ripoll, E. Solano, R. Blatt, and C. F. Roos, Phys. Rev. Lett. **106**, 060503 (2011).

[25] J. Casanova, C. Sabín, J. León, I. L. Egusquiza, R. Gerritsma, C. F. Roos, J. J. García-Ripoll, and E. Solano, Phys. Rev. X **1**, 021018 (2011).

[26] L. Lamata, J. Casanova, R. Gerritsma, C. F. Roos, J. J. García-Ripoll, and E. Solano, New J. Phys. **13**, 095003 (2011).

[27] J. Casanova, L. Lamata, I. L. Egusquiza, R. Gerritsma, C. F. Roos, J. J. García-Ripoll, and E. Solano, Phys. Rev. Lett. **107**, 260501 (2011).

[28] J. Casanova, A. Mezzacapo, L. Lamata, and E. Solano, Phys. Rev. Lett. **108**, 190502 (2012).

[29] A. Mezzacapo, J. Casanova, L. Lamata, and E. Solano, Phys. Rev. Lett. **109**, 200501 (2012).

[30] M. -H. Yung, J. Casanova, A. Mezzacapo, J. McClean, L. Lamata, A. Aspuru-Guzik, and E. Solano, Sci. Rep. **4**, 3589 (2014).

[31] D. S. Abrams and S. Lloyd, Phys. Rev. Lett. **79**, 2586 (1997).

[32] N. J. Ward, I. Kassal, and A. Aspuru-Guzik, J. Chem. Phys. **130**, 194105 (2009)

[33] K. R. Brown, R. J. Clark, and I. L. Chuang, Phys. Rev. Lett. **97**0, 050504 (2006).

[34] M. Cramer, M. B. Plenio, S. T. Flammia, D. Gross, S. D. Bartlett, R. Somma, O. Landon-Cardinal, Y.-K. Liu, and D. Poulin, Nature Communication **1**, 149 (2010).

[35] G. Toth, W. Wieczorek, D. Gross, R. Krischek, C. Schwemmer, and H. Weinfurter, Phys. Rev. Lett. **105**, 210404 (2011).

[36] R. Di Candia, B. Mejia, H. Castillo, J. S. Pedernales, J. Casanova, and E. Solano, Phys. Rev. Lett. **111**, 240502 (2013).

[37] J. S. Pedernales, R. Di Candia, P. Schindler, T. Monz, M. Hennrich, J. Casanova, and E. Solano, Phys. Rev. A **90**, 012327 (2014).

[38] J. S. Pedernales, R. Di Candia, I. L. Egusquiza, J. Casanova, and E. Solano, Phys. Rev. Lett. **113**, 020505 (2014).

[39] R. Di Candia, J. S. Pedernales, A. del Campo, E. Solano, and J. Casanova, arXiv:1406.2592 (2014),*accepted in Scientific Reports*

[40] M. A. Nielsen and I. L. Chuang, *Quantum Computation and Quantum Information* (Cambridge University press, Cambridge, 2000).

[41] R. Horodecki, P. Horodecki, M. Horodecki, and K. Horodecki, Rev. Mod. Phys. **81**, 865 (2009).

[42] E. Einstein, B. Podolsky, and N. Rosen, Phys. Rev. **47**, 777 (1935).

[43] A. K. Ekert, Phys. Rev. Lett. **67**, 661 (1991).

[44] C. H. Bennett, G. Brassard, C. Crépeau, R. Jozsa, A. Peres, and W. K. Wootters, Phys. Rev. Lett. **70**, 1895 (1993).

[45] P. W. Shor, Phys. Rev. A **52**, 2493 (1995).

[46] D. Gottesman and I. Chuang, Nature **402**, 390 (1999).

[47] H. Häffner, W. Hänsel, C. F. Roos, J. Benhelm, D. Chek-al-kar, M. Chwalla, T. Körber, U. D. Rapol, M. Riebe, P. O. Schmidt, C. Becher, O. Gühne, W. Dür, and R. Blatt, Nature **438**, 643 (2005).

[48] T. Monz, P. Schindler, J. T. Barreiro, M. Chwalla, D. Nigg, W. A. Coish, M. Harlander, W. Hänsel, M. Hennrich, and R. Blatt, Phys. Rev. Lett. **106**, 130506 (2011).

[49] M. Mariantoni, H. Wang, T. Yamamoto, M. Neeley, R. C. Bialczak, Y. Chen, M. Lenander, E. Lucero, A. D. O'Connell, D. Shank, M. Weides, J. Wenner, Y. Yin, J. Zhao, A. N. Korotkov, A. N. Cleland, and J. M. Martinis, Science **334**, 61 (2011).

[50] E. P. Menzel, R. Di Candia, F. Deppe, P. Eder, L. Zhong, M. Ihmig, M. Haeberlein, A. Baust, E. Hoffmann, D. Ballester, K. Inomata, T. Yamamoto, Y. Nakamura, E. Solano, A. Marx, and R. Gross, Phys. Rev. Lett. **109**, 250502 (2012).

[51] W.-B. Gao, C.-Y. Lu, X.-C. Yao, P. Xu, O. Gühne, A. Goebel, Y.-A. Chen, C.-Z. Peng, Z.-B. Chen, and J.-W. Pan, Nat. Phys. **6**, 331 (2010).

[52] A. Wong and N. Christensen, Phys. Rev. A **63**, 044301 (2001).

[53] H. Barnum, E. Knill, G. Ortiz, R. Somma, and L. Viola, Phys. Rev. Lett. **92**, 107902 (2004).

[54] G. Vidal, Journal of Mod. Opt. Vol. **47**, Iss. 2-3 (2000).

[55] W. K. Wootters, Phys. Rev. Lett. **80**, 2245 (1998).

[56] O. Gühne, M. Reimpell, and R. F. Werner, Phys. Rev. Lett. **98**, 110502 (2007).

[57] T. Rudolph, and L. Grover, arXiv:quant-ph/0210187 (2002).

[58] L. M. Fernandez, and W. A. Schneeberger, arXiv:quant-ph/0307017 (2003).

[59] M. McKague, M. Mosca, and N. Gisin, Phys. Rev. Lett. **102**, 020505 (2009).

[60] W. Dür, G. Vidal, and J. I. Cirac, Phys. Rev. A. **62**, 062314 (2000).

[61] A. Uhlmann, Phys. Rev. A **62**, 032307 (2000).

[62] A. Osterloh, and J. Siewert, Phys. Rev. A **72**, 012337 (2005).

[63] J. Casanova, C. Sabín, J. León, I. L. Egusquiza, R. Gerritsma, C. F. Roos, J. J. García-Ripoll, and E. Solano, Phys. Rev. X **1**, 021018 (2011).

[64] M. H. Devoret and R. J. Schoelkopf, Science **339**, 1169 (2013).

[65] L. Gurvits, *Proceedings of the thirty-fifth ACM Symposium on the Theory of Computing* (ACM Press, New York, 2003).

[66] S. Gharibian, Quantum Information and Computation, Vol. **10**, No. 3-4, pp. 343-360 (2010).

[67] B. Röthlisberger, Jörg Lehmann, and D. Loss, Phys. Rev. A **80**, 042301 (2009).

[68] B. Röthlisberger, Jörg Lehmann, and D. Loss, Computer Physics Communications Vol. **183**, Issue 1, pp. 155 (2012).

[69] H. Häffner, C. F. Roos, and R. Blatt, Physics Reports **469**, 155 (2008).

[70] P. Schindler, D. Nigg, T. Monz, J. T. Barreiro, E. Martinez, S. X. Wang, S. Quint, M. F Brandl, V. Nebendahl, C. F. Roos, M. Chwalla, M. Hennrich and R. Blatt, New J. Phys. **15** 123012 (2013).

[71] K. Mølmer and A. Sørensen, Phys. Rev. Lett. **82**, 1835 (1999).

[72] A. Mezzacapo, L. Lamata, S. Filipp, and E. Solano, arXiv:1403.3652

[73] J. L. O'Brien, A. Furusawa, and J. Vučković, Nat. Phot. **3**, 687 (2009).

[74] W. K. Wootters, Phys. Rev. Lett. **80**, 2245 (1998).

[75] H. F. Trotter, Proc. Am. Math. Soc. **10**, 545 (1959).

[76] M. Müller, K. Hammerer, Y. L. Zhou, C. F. Roos, and P. Zoller, New J. Phys. **13**, 085007 (2011).

[77] P. Schindler, M. Moller, D. Nigg, J. T. Barreiro, E. A. Martinez, M. Hennrich, T. Monz, S. Diehl, P. Zoller, and R. Blatt, Nat. Phys. **9** 361 (2013).

[78] N. Navon, N. Akerman, S. Kotler, Y. Glickman, and R. Ozeri, e-print: arXiv:quant-ph/1309.4502.

[79] C. F. Roos, G. P. T. Lancaster, M. Riebe, H. Häffner, W. Hänsel, S. Gulde, C. Becher, J. Eschner, F. Schmidt-Kaler, and R. Blatt, Phys. Rev. Lett. **92**, 220402 (2004).

[80] A. Yu. Kitaev, arXiv:9511026

[81] D. S. Abrams and S. Lloyd, Phys. Rev. Lett. **83**, 5162 (1999).

[82] R. Kubo, J. Phys. Soc. Jpn. **12**, 570 (1957).

[83] R. Zwanzig, Annu. Rev. Phys. Chem. **16**, 67 (1965).

[84] D. Forster, *Hydrodynamic Fluctuations, Broken Symmetry, and Correlation Functions*, Advanced book classics (Perseus Books, 1990).

[85] A. L. Fetter and J. D. Walecka, *Quantum Theory of Many-Particle Systems* (McGraw-Hill, New York, 1971).

[86] L. Mandel and E. Wolf, *Optical coherence and quantum optics* (Cambridge university press, 1995).

[87] D. Bozyigit, C. Lang, L. Steffen, J. M. Fink, C. Eichler, M. Baur, R. Bianchetti, P. J. Leek, S. Filipp, M. P. da Silva, A. Blais, and A. Wallraff, Nat. Phys. **7**, 154 (2011).

[88] R. Di Candia, E. P. Menzel, L. Zhong, F. Deppe, A. Marx, R. Gross, and E. Solano, New J. Phys. **16**, 015001 (2014).

[89] M. Knap, A. Kantian, T. Giamarchi, I. Bloch, M. D. Lukin, and E. Demler, Phys. Rev. Lett. **111**, 147205 (2013).

[90] F. Buscemi, M. Dall'Arno, M. Ozawa, and V. Vedral, arXiv:1312.4240.

[91] H. Buhrman, R. Cleve, J. Watrous, and R. de Wolf, Phys. Rev. Lett. **87**, 167902 (2001).

[92] C. M. Wilmott and P. R. Wild, Int. J. Quantum Inform. **10**, 1250034 (2012).

[93] R. Somma, G. Ortiz, J. E. Gubernatis, E. Knill, and R. Laflamme Phys. Rev. A **65**, 042323 (2002).

[94] A. Sørensen and K. Mølmer, Phys. Rev. Lett. **82**, 1971 (1999).

[95] P. Jordan and E. Wigner, Z. Phys. **47**, 631 (1928).

[96] L. Lamata, A. Mezzacapo, J. Casanova, and E. Solano, arXiv:1312.2849.

[97] M.-H. Yung, J. Casanova, A. Mezzacapo, J. McClean, L. Lamata, A. Aspuru-Guzik, and E. Solano, Sci. Rep. **4**, 3589 (2014).

[98] P. Lougovski, H. Walther, and E. Solano, Eur. Phys. J. D **38**, 423 (2006).

[99] J. Casanova, C. E. López, J. J. García-Ripoll, C. F. Roos, and E. Solano, Eur. Phys. J. D **66**, 222 (2012).

[100] F. Zähringer, G. Kirchmair, R. Gerritsma, E. Solano, R. Blatt, and C. F. Roos, Phys. Rev. Lett. **104**, 100503 (2010).

[101] P. Richerme, C. Senko, S. Korenblit, J. Smith, A. Lee, R. Islam, W. C. Campbell, and C. Monroe, Phys. Rev. Lett. **111**, 100506 (2013).

[102] J. W. Britton, B. C. Sawyer, A. C. Keith, C.-C. J. Wang, J. K. Freericks, H. Uys, M. J. Biercuk, and J. J. Bollinger, Nature **484**, 489 (2012).

[103] K. Kim, M.-S. Chang, R. Islam, S. Korenblit, L.-M. Duan, and C. Monroe, Phys. Rev. Lett. **103**, 120502 (2009).

[104] J. J. García-Ripoll, M. A. Martin-Delgado, and J. I. Cirac, Phys. Rev. Lett. **93**, 250405 (2004).

[105] J. Simon, W. S. Bakr, R. Ma, M. E. Tai, P. M. Preiss, and M. Greiner, Nature **472**, 307 (2011).

[106] J. J. García-Ripoll, E. Solano, and M. A. Martin-Delgado, Phys. Rev. B **77**, 024522 (2008).

[107] L. Tian, Phys. Rev. Lett. **105**, 167001 (2010).

[108] Y. Zhang, L. Yu, J.-Q. Liang, G. Chen, S. Jia, and F. Nori, arXiv: 1308.3948 (2013).

[109] O. Viehmann, J. von Delft, and F. Marquardt, Phys. Rev. Lett. **110**, 030601 (2013).

[110] H. P. Breuer and F. Petruccione, *The Theory of Open Quantum Systems*, (Oxford University Press, New York 2002).

[111] Á. Rivas and S. F. Huelga, *Open Quantum Systems. An Introduction*, (Springer, Heidelberg, 2011).

[112] D. Leibfried, R. Blatt, C. Monroe, and D. Wineland, Rev. Mod. Phys. **75**, 281 (2003).

[113] I. Bloch, Nature Phys. **1**, 23 (2005).

[114] J. I. Cirac and P. Zoller, Nature Phys. **8**, 264 (2012).

[115] C. Schneider, D. Porras, and T. Schaetz, Rep. Prog. Phys. **75**, 024401 (2012).

[116] I. Bloch, J. Dalibard and S. Nascimbéne, Nature Phys. **8**, 267 (2012).

[117] A. A. Houck, H. E. Türeci, and J. Koch, Nature Phys. **8**, 292 (2012).

[118] S . F. Huelga, M. B. Plenio, Contemp. Phys. **54**, 181 (2013).

[119] S. Mostame, P. Rebentrost, A. Eisfeld, A. J. Kerman, D. I. Tsomokos, and and A. Aspuru-Guzik, New J. Phys. **14**, 105013 (2012).

[120] M. O. Scully, K. R. Chapin, K. E. Dorfman, M. Barnabas Kim, and A. Svidzinsky, PNAS **108**, 15097 (2011).

[121] K. E. Dorfman, D. V. Voronine, S. Mukamel, and M. O. Scully, PNAS **110**, 2746 (2011).

[122] C. Creatore, M. A. Parker, S. Emmott, and A. W. Chin, Phys. Rev. Lett. **111**, 253601 (2013).

[123] W. H. Zurek, Rev. Mod. Phys. **75**, 715 (2003).

[124] H.-P. Breuer, E.-M. Laine, and J. Piilo, Phys. Rev. Lett. **103**, 210401 (2009).

[125] Á. Rivas, S. F. Huelga, and M. B. Plenio, Phys. Rev. Lett. **105**, 050403 (2010).

[126] Bi-Heng Liu, Li Li, Yun-Feng Huang, Chuan-Feng Li, Guang-Can Guo, Elsi-Mari Laine, Heinz-Peter Breuer, ad Jyrki Piilo, Nature Phys. **7**, 931 (2011).

[127] S. Boixo, T. Albash, F. M. Spedalieri, N. Chancellor, and D. A. Lidar, Nat. Commun. **4**, 3067 (2013).

[128] S. Boixo, T. F. Rønnow, S. V. Isakov, Z. Wang, D. Wecker, D. A. Lidar, J. M. Martinis, and M. Troyer, Nature Phys. **10**, 218 (2014).

[129] F. Verstraete, M. M. Wolf, and J. I. Cirac, Nature Phys. **5**, 633 (2009).

[130] S. Lloyd and L. Viola, Phys. Rev. A **65**, 010101 (R) (2001).

[131] M. Kliesch, T. Barthel, C. Gogolin, M. Kastoryano, and J. Eisert, Phys. Rev. Lett. **107** 120501 (2011).

[132] H. Wang, S. Ashhab, and F. Nori, Phys. Rev. A **83**, 062317 (2011).

[133] J. T. Barreiro, M. Müller, P. Schindler, D. Nigg, T. Monz, M. Chwalla, M. Hennrich, C. F. Roos, P. Zoller, and R. Blatt, Nature **470**, 486 (2011).

[134] R. Alicki, D. A. Lidar, and P. Zanardi, Phys. Rev. A **73**, 052311 (2006).

[135] G. Lindblad, Commun. Math. Phys. **48**, 119 (1976).

[136] Á. Rivas, S. F. Huelga, and M. B. Plenio, Rep. Prog. Phys. **77**, 094001 (2014).

[137] R. Bellman, *Introduction to matrix analysis*, (McGraw-Hill, New York 1970).

[138] J. G. Muga, J. P. Palao, B. Navarro, and I. L. Egusquiza, Phys. Rep. **395**, 6 (2004).

[139] N. Moiseyev, Phys. Rep. **302**, 212 (1998).

[140] M. B. Plenio and P. L. Knight, Rev. Mod. Phys. **70**, 101 (1998).

[141] C. M. Bender, Rep. Prog. Phys. **70**, 947 (2007).

[142] J. Loreto, M. de Almeida, R. Di Candia, J. S. Pedernales, J. Casanova, E. Solano, and A. G. White, *in preparation*.

[143] J.-W. Pan, *private communication*.

[144] U. Alvarez-Rodriguez, R. Di Candia, J. Casanova, M. Sanz, and E. Solano, *in preparation*

[145] D. W. Berry, A. M. Child, R. Cleve, R. Kothari, and R. Somma, Phys. Rev. Lett. **114**, 090502 (2015).

[146] R. Sweke, I. Sinayskiy, D. Bernard, and F. Petruccione, arXiv:1503:05028 (2015).

[147] W. Hoeffding, J. Amer. Statist. Assoc., **58**, 13-30 (1963)

[148] J. Watrous, arXiv:0411077 (2004).